National University of Lesotho

Energy Research Centre

Adaptive, robust, and fault-tolerant control strategies for grid-connected Renewable Energy Systems: A condition monitoring approach

Tsitso Nkhabu (201000096)

A dissertation submitted in partial fulfilment
of the requirements for the degree of

Master of Science in Sustainable Energy

Offered by the

Energy Research Centre
Faculty of Science & Technology

July 2024

Abstract

Lesotho is currently facing a power generation-demand imbalance. The 2023/24 annual report by the Lesotho Electricity and Water Authority highlights a peak demand of 222.12 MW, which is nearly three times the country's installed generation capacity of 74.7 MW. Consequently, the nation relies on costly power imports from Mozambique and South Africa to cover the shortfall. To address this issue, Lesotho plans to integrate renewable energy sources, specifically wind and solar, into its national grid. However, integrating these low-inertia and intermittent renewable power sources introduces grid stability challenges, as they are vulnerable to disturbances like load changes or grid faults.

This research focused on designing control strategies capable of not only adjusting system voltage to accommodate uncertainties from power system dynamics, internal changes, and external disturbances but also stabilizing the system under small disturbances. The analysis was conducted on a grid-connected 38 MW wind power plant, using five control strategies: Constant Voltage (Const. V), Constant Reactive Power (Const. Q), Constant Power Factor (Const. cosϕ), Voltage Droop based on Reactive Power (voltage Q-droop), and voltage droop based on reactive power in the q-axis (voltage Iq-droop). These strategies were evaluated for their adaptability, robustness, and fault tolerance under two operational scenarios: variations in wind speed and fluctuations in the Point of Connection (POC) bus voltage.

With a three-phase short circuit created and cleared on the high voltage (HV) bus bar, all control strategies are within a 5 % voltage deviation upon service restoration and fault clearance within a period of 0.015 seconds. A Supervisory Control and Data Acquisition (SCADA) system was designed for the monitoring and control of the wind power plant. Determined from the closeness of the HV bus voltage to the POC voltage, the most adaptive control strategy is used for each operation scenario, taking into account the wind speed as well as the POC voltage. It was observed that the evaluation by the SCADA system is consistent with the result obtained from the DIgSILENT PowerFactory software. For further exploration, research is recommended for the implementation of Artificial Neural Networks (ANNs) in machine learning to accommodate any wind speed and POC voltage levels for the control strategies under investigation.

Acknowledgments

A heartfelt gratitude to my research supervisors, Dr. Molefe Makhele and Mr. Sebota Mokeke. Their suggestions and comments have played a crucial part to the fulfilment of my research work. I also wish to thank the Energy Research Centre at the National University of Lesotho for granting me an opportunity to further my studies. My supportive family and friends have been a pillar of strength for me during difficult encounters in my life, and for that I will forever be grateful.

A special thanks to my supportive colleagues, in particular Mr. Thabang Mokhele who was always willing to swap his work shifts to accommodate my studies, Mr. Thabo Nkakala for always availing his personal resources for me to conduct my research, my dear friend Lebohang Sakoane who always stood by my side even through the toughest moments at work, and Ms Nthati Maduna for always trying to make my studies as conducive as possible.

I dedicate this research work to my son Mahlohonolo. I have missed some of your school assignments while focusing on my research. I hope one day you may be able to use your father's work as a reference in your studies.

Contents

List of Figures

Nomenclature

This nomenclature list the acronyms and abbreviations used throughout the report. For easy reference, the list is organised as per their order of appearance along the report.

SDGs: Sustainable Development Goals

RETs: Renewable Energy Technologies

PCC: Point of Common Coupling

DA&DC: Decentralized Actors and Distributed Critic

PV: Photovoltaic

dq0: Direct-Quadrature-Zero transformation

PWM: Pulse-Width Modulation

SVPWM: Space Vector Pulse Width Modulation

ANNs: Artificial Neural Networks

UPQC: Unified Power Quality Conditioners

STATCOM: Static Synchronous Compensators

D-STATCOM: Dynamic Static Synchronous Compensator

IBRs: Inverter-Based Resources

POC: Point of Connection

SCADA: Supervisory Control and Data Acquisition

PDF: Probability Density Function

CDF: Cumulative Distribution Function

WRSG: Wound Rotor Synchronous Generator

PMSG: Permanent Magnet Synchronous Generator

WRIG: Wound Rotor Induction Generator

DFIG: Doubly-Fed Induction Generator

WECS: Wind Energy Conversion System

VSD: Variable Speed Drive

DFC: Design for Cost

CPU: Power Conditioning Unit

PVMFGCI: Multi-Functional Grid-Connected Inverter

T&D: Transmission and Distribution

RTU: Remote Terminal Unit

MTU: Master Terminal Unit

HMI: Human Machine Interface

AVR: Automatic Voltage Regulator

SVC: Static VAR Compensators

RoCof: Rate of Change of Frequency

WTG: Wind Turbine Generator

WECC: Western Electricity Coordinating Council

p.u.: per-unit

1. Introduction

1.1. Background

In nearly all the important challenges and opportunities faced by the world, energy plays a central role [1]. Its usage at several scales towards satisfying human beings' needs and countries' development [2] makes it a stimulant to the three pillars of sustainable development being social, economic, and environmental [3] that transform life, the economy, and the environment [1]. SDG 7 is one of the Sustainable Development Goals (SDGs) released in 2015, which aims to achieve "universal access to affordable, reliable and sustainable energy for all" by 2030 [3]. Moreover, it is worth highlighting that all other SDGs can be achieved by accessing sustainable electricity, as Nyarko et al. [3] pointed out. However, 73% of global greenhouse gas emissions originate from the energy sector [4], driving interest in renewable energy development and sustainable energy supply [5]. Incorporating Renewable Energy Technologies (RETs) into the energy portfolios is beneficial as they offer clean energy solutions to the market [6]. It has been demonstrated over the years that RETs such as hydropower, biomass, wind power, and solar photovoltaic can be integrated into the grid [7]. The increase in renewable energy fraction is evidenced in Figure 1.

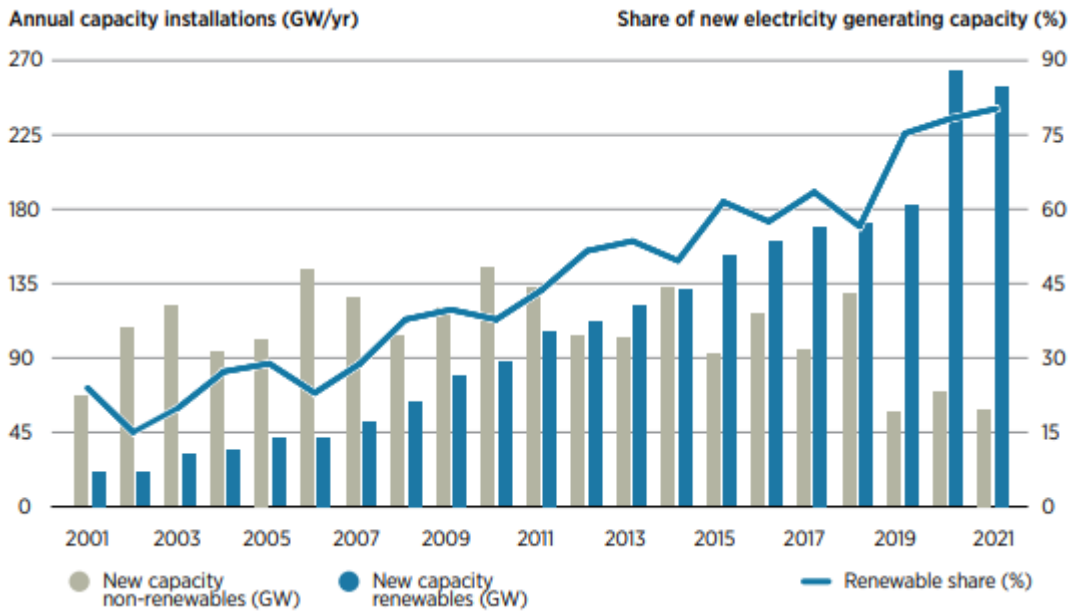

Figure 1: Share of new electricity capacity, 2001 – 2021 [8]

Figure 1 illustrates the current global trend of increased renewable electrification, and in comparison to non-renewables, the penetration rate for renewables is far greater. In contrast, the integration of the most prominent RETs, solar photovoltaics (PVs) and wind, has adverse effects on Point of Common Coupling (PCC) parameters, especially voltage, as a result of their stochastic and intermittent nature [9], [10]. Several parameters are considered when defining power quality benchmarks, including voltage, frequency, Harmonic Distortion, and reactive power imbalance [11]. Previous work has been

performed to maintain the power quality of these systems in the distribution network by maintaining the power system stability [10], [12-15]. In their work, Martínez-Lavín et al have aimed at controlling these parameters to satisfy the requirements of compliance of generation facilities in a particular national network to ensure network safety, security, and reliability as per countries' grid code requirements [12]. In ensuring compliance of generation facilities, strict constraints are applied on the connection of energy systems to the grid [13], which must be met to retain operational stability during transient disturbances and faults conditions [12].

Different control strategies have been applied for the stability of grid-connected systems. For instance, Rehman et al. [16] proposed to use the Decentralized Actors and Distributed Critic (DA&DC) architecture for multi-agents to achieve the optimal control and coordination of the PV-inverters incorporated into the distribution. Using their results, the analysis of the impact of seasonal fluctuations on voltage variation, power losses, and the active and reactive power of the PV systems and buses was achieved [16]. In an attempt to optimize the frequency control of the wind power integrated system by Zheng et al. [17], parameter identification was used to eliminate the nadir and second dip of the frequency trajectory. After each disturbance, the inertia and damp coefficient were then identified by the extended Kalman smoother algorithm and the shape of the transfer function for their wind power integrated system was achieved [17]. Several previous studies on this subject have included methods such as detecting the Direct-Quadrature-Zero transformation (dq0) and utilizing Space Vector Pulse Width Modulation (SVPWM) [18], developing an ANN Controller to control Unified Power Quality Conditioners (UPQCs) [19], and developing a Distribution-Static Compensator (D-STATCOM) [11].

1.2. Problem Statement

Lesotho has an electricity access rate of approximately 40%, with the installed generation capacity and peak demands of 74.7 MW and 222.12 MW, respectively, as of 2023 [20]. It is, however, important to note that Lesotho's electricity generation remained below 80 MW since 1998 [21-22]; an additional baseload requirement and peak demand requirement imported from Mozambique and South Africa [22]. On the other hand, numerous studies conducted recently have shown how much potential there is for solar and wind energy in Lesotho [21-26], with estimates of 2300 MW renewables technical capacity that can account towards 5900 GWh of energy per year [26]. Nonetheless, the country's installed capacity has remained the same over the years, with a capacity deficit reaching 63 % in the year 2021/22, as shown in Figure 2.

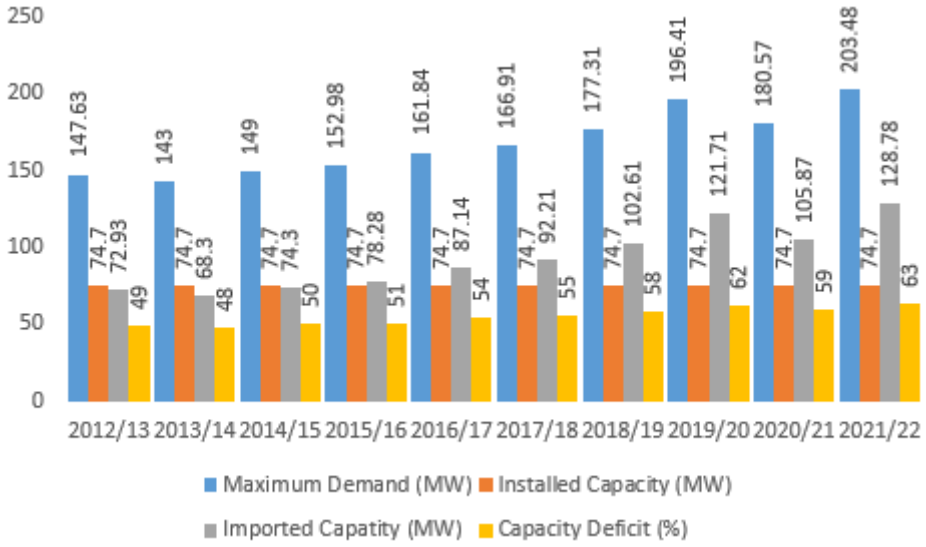

Figure 2: Lesotho Maximum Demand Profile for Period 2012/13 - 2021/22, adapted from [27]

It is important to realize that successful grid integration of various renewables is possible. With the country on the verge of integrating wind and solar power generation systems into the national grid to mitigate the energy deficit, it is crucial to come up with control strategies for the already anticipated grid instabilities. It has been observed that with the increase in variable renewable energy generation, maintaining a balance between generation and load demand becomes increasingly challenging for grid operators. Therefore, there is often a need to support the frequency instability of grids with a high penetration of utility-scale Inverter-Based Resources (IBRs) such as wind, solar, and batteries [28]. The challenge comes as a result of the loss in the power system inertia levels resulting from the increasing penetration of these converter-based renewables [28], [29]. The reason here is that an RE power system's inertia can take many different forms and exhibit a variety of response characteristics; following a disturbance, the system's inertia is influenced by the operating conditions, the controller parameters as well as other factors, exhibiting nonlinear and time-varying characteristics [30]. Contrary to RE systems, the system inertia of a conventional power system depends on the synchronous inertia of the synchronous generator, which is both constant and sufficient, hence able to withstand a voltage disturbance [30]. It is therefore deemed necessary to employ control strategies for these systems to attain frequency stability. It declines when demand exceeds generation, and vice versa [10].

Another issue of concern in grid-connected systems is voltage stability; it is defined as “the ability to regain steady-state voltage after being subjected to a large contingency event such as a sudden increase in a load or grid fault” [10]. It has been emphasized that power systems with inadequate reactive power support are susceptible to unstable voltage, which poses a significant challenge for maintaining the bus voltages [31] since the grid's failure to provide the necessary reactive power is

the main cause of voltage collapse [32]. Since fault occurrences can also trigger a power network's voltage instability [31], it is worth mentioning that the proposed control strategies must be tolerant to short-circuit faults.

1.3. Research Question and Objectives

The research question of the study is as follows:

What adaptive control strategies can be implemented for grid-connected wind energy systems to enhance the resilience and performance of the generation systems in the presence of dynamic variations such as wind speeds fluctuations and Point of Connection voltage changes?

The objective of this work is to design an adaptive control strategy that will automatically adjust the characteristics of the power generation system controller to maintain the overall power system performance by compensating for variations in the dynamics of the power system. It should be capable of adjusting system voltage to account for uncertainties arising from power system dynamics, internal changes, and external disturbances. Additionally, the system must be robust, with resilience needed to stabilize its behaviour in the presence of minor disturbances and external dynamics. In the design of the power system control, the following objectives are prioritized:

- Power system modeling and simulation, incorporating RE systems into the existing LEC network and performing load flow analysis using DIgSILENT PowerFactory 2024 Preview software.
- Evaluating control strategies for their adaptability, robustness, and fault tolerance under two operational scenarios: variations in wind speed and fluctuations in the Point of Connection (POC) bus voltage.
- Descriptive statistical analysis for robustness under varying wind speeds using IBM SPSS Statistics 22 software.
- Designing and implementing a SCADA system for wind power plant monitoring and control using Apache Netbeans IDE 22.

1.4. Justification of the study

With a 25-year Power Purchase Agreement signed between Lesotho Electricity Company (LEC) and Neo 1 SPV (Pty) Ltd, for the nation's first public-private utility-scale power plant with a Capital Expenditure (Capex) of M430 million [33], a 20 MW solar PV Electricity generation license at Ha Ramarothole in the Mafeteng district has been issued to this Independent Power Producer (IPP) [27]. Hirundo Energy has planned to integrate another renewable energy source into Lesotho's grid by using wind farms to supply rated power of 110 MW [34]. It is therefore, worth the effort to focus on the control of grid-connected renewable energy systems for Lesotho's energy future ahead. The main

challenge of increasing RE penetration is grid instability as a result of the low inertia of the system. The intermittency of these renewables also affects the reliability of the system. Efforts have been made to deal with the problem of grid instability, but optimization of the power system remains a challenge. The government of Lesotho has been tasked with an RE grid integration study by the African Development Fund (ADF), and with the country aiming to reach 375 MW of renewable electricity by 2030 [35], it is necessary to design control strategies for these power systems that are fault-tolerant to maintain the stability of the grid.

1.5. Synopsis of the report

The structure of the report's subsequent chapters is as follows:

Chapter 2. Literature review: This chapter defines the concepts of adaptive control, robust control, fault-tolerance control, and condition-monitoring. Renewable grid-integrated systems are then explored, with a focus on electrical power systems' transmission and generation, as well as SCADA. Voltage and frequency stability are then reviewed, as well as the involved control theory concepts

Chapter 3. Methodology: This chapter presents the system design, the controller configuration, and the design of the wind farm substation. Case studies and operation scenarios for different control strategies are implemented at different wind speeds and changing voltages at the point of connection (POC). Service restoration is analysed for each control strategy after a created fault is cleared. A SCADA system is then designed for the monitoring and control of the power plant.

Chapter 4. Results and Interpretation: A response analysis is conducted for steady as well as varying wind speeds for both dynamic and steady-state responses. A case of fault-tolerance and service restoration is monitored, and the chapter concludes by presenting the designed SCADA system for monitoring and control.

Chapter 5. Conclusion and recommendations: Conclusions are drawn from the research results, and recommendations for further research are made.

2. Literature Review

2.1. Conceptualization

This section defines the key terms as they are contextually used in the research. From the research title “Adaptive, robust, and fault-tolerant strategies for grid-connected renewable energy systems: a condition-monitoring approach”, the main control phenomena lie in the adaptation, robustness, and fault-tolerance of the system, in a condition-monitoring approach. It is therefore deemed necessary to first define the key terms being: adaptive control, robust control, fault-tolerance control, and condition-monitoring as per their contextual meaning.

2.1.1. Adaptive Control

Adaptive control is a control mechanism whereby a feedback control system’s intelligence enables it to adjust its characteristics in a changing environment to satisfy some pre-defined criteria [36]. The control system adjusts the controller characteristics for the overall system to remain stable, or rather optimized, by automatically compensating for variations in system dynamics, while taking into account any time-variant performance degradation [37]. The main reason for the use of adaptive controllers, which require a deep mathematical formulation to understand their development, is the inaccuracy of the models for disturbances [38]. Hence, it is regarded as a promising technology that can enhance the control system performance in the presence of uncertainties arising from factors such as degradation and modeling uncertainty [39]. The adaptive control schemes, which can either be model reference or self-tuning [38], include elements to measure the process dynamics and other elements to alter the characteristics of the controller accordingly, thus maintaining the overall system performance [37]. Gupta and Yan [37] outline three essentials of an adaptive system:

1. Identification of system dynamics
2. Decision, and
3. Modification

In their work further emphasizing of the operation of the decision function upon system identification should activate the modification function for the alteration of the particular parameter of the process for optimization of the process [37].

2.1.2. Robust Control

Robust control refers to the design of a controller whose model incorporates a pre-assumed uncertainty or error between the actual plant and its mathematical model in the design process [40]. The controller design method emphasizes the reliability of its algorithm to meet the minimum requirements necessary for practical application [38]. Its optimization approach, grounded in a decision-making philosophy that seeks feasible solutions across all possible variations of uncertain

parameters, serves as a robust and powerful modelling framework [41]. The key advantage of robust control lies in its ability to create control was that not only shapes the system response to achieve the desired behaviour but also maintains this performance despite operational fluctuations [42].

2.1.3. Fault-tolerance Control

Real-world systems are often subject to uncertainties such as disturbances and faults [43], which can negatively impact the controller's performance by altering system dynamics and constraints [44], or even leading to significant performance degradation and instability [43], [45]. To address these challenges, model matching and fault-tolerant control strategies have been widely researched in the context of dynamic corrective control [46]. Fault tolerance, as defined by Zhao et al. [47], is *"the ability of a functional unit or system to continue performing a required function despite faults and errors."* While aknowledging that any physical component will eventually fail [48], the design of a fault-tolerant system must account for various failure scenarios while ensuring continuous operation [47]. Failures, whether caused by age, wear, manufacturing defects, or random events, can be mitigated by incorporating fault-tolerant designs [48].

2.1.4. Condition-monitoring

More often than not, renewable energy plants, especially wind plants, are situated in remote regions such as rural areas or aislands where environments are tough. These harsh conditions can cause the failure of system components such as fans, bearings, and generators, which results in increased operating expenses and maintenance costs, as well as prolonged downtimes [49]. Therefore, condition monitoring is essential for fault diagnosis and predictive maintenance [50], which contributes to improving system efficiency [51]. It is an essential component of predictive maintenance and process equipment, involving real-time data analysis to facilitate the timely triggering of maintenance activities [52]. Used to monitor equipment conditions to give an advanced warning of failure, the operational principle of condition-monitoring is to select a physical measurement at regular intervals and identify anomalies indicating the existence of a problem [53]. Not only is condition monitoring a reliability measure, but it has also become a legislative requirement formulated for protection from unscrupulous application of technology in many countries [54]. In its technologies, including infrared thermography, ultrasound scanning, oil analysis, vibration analysis, and motor circuit analysis, some of the outstanding benefits of condition monitoring are [55]:

- The plethora of information about the nature of defects offered by condition-monitoring technologies enables the significant enhancement of root cause analysis processes and eliminates the re-occurrence possibilities of the fault.
- Early fault detection helps in planning and scheduling outages and, therefore, reduces the surprise of unexpected equipment failure.

- The amount of specific information from technological data provides information about the problem and, therefore, allows specific defect identification instead of general fault indication.

2.2. Renewable grid-integrated power systems

Among mankind's most complex systems is an electricity network known as an electric grid [56]. An electric grid is an interconnected network consisting of power stations, substations, transmission and distribution systems to deliver electricity from the source to the consumers [57]. This deliverance is via a high-voltage transmission network and a low-voltage distribution network consisting of transformers, switches, and other electrical hardware [56]. The interconnection of the main elements of the electrical power system is to attain power generation in the most suitable locations while sufficiently meeting customers' demands by generating a sufficient quantity of good-quality electricity to load centers at competitive prices [58]. The ever-increasing energy demand has emphasized the importance of renewable-dominated power systems, which are replenished over time, as opposed to conventional grids, which rely on depleting fossil fuels [59], [60]. As a result, not only will there be an increase in the overall power supply, thus leading to a cost-effective and environmentally friendly grid, but the depleting fossil fuel resources will also be progressively replaced. With less mismatching between the generation and demand of electricity and the integration of renewable energy technologies, the maintenance of power grid safety and reliability with electricity flow regulations is a requirement for increasing power consumption in this new energy landscape [61]. A typical example of an RE highly-penetrated electrical power grid is illustrated in Figure 3.

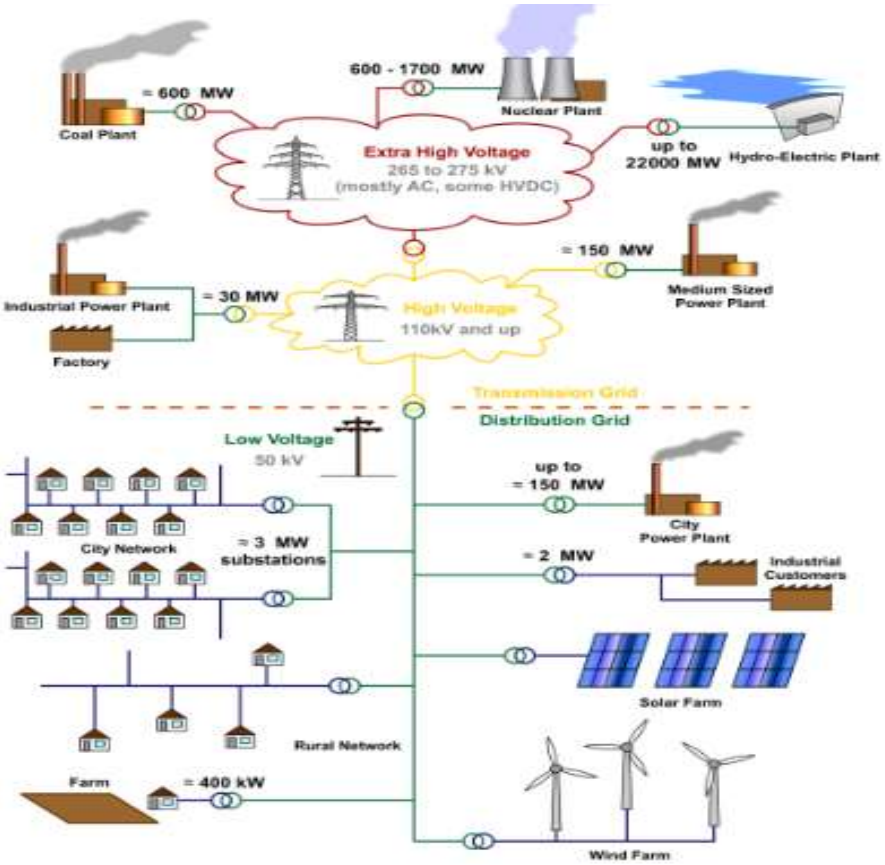

Figure 3: Electrical Grid with renewable penetration [62]

From the electrical grid in Figure 3, the electrical power system can be divided into three main sub-systems: generation system, transmission system, and distribution system. These three sub-systems of the power system are discussed in detail in section 2.3 (Electrical Power Grid System) of this document.

2.3. Electrical Power Grid System

Credit for the first electric power grid is given to Thomas A. Edison for his work on the electric light in 1878, the formulation of distributed lighting services from a centrally located power station, and the opening of New York's historic Pearl Station on September 4, 1879 [63]. Defined as "a framework of electrical components that are used to supply and transmit electric power according to the consumer demand [64]", this interrelated network consists of a generation station, power transmission system, power distribution system, and the end user [64], [65] as illustrated in Figure 4.

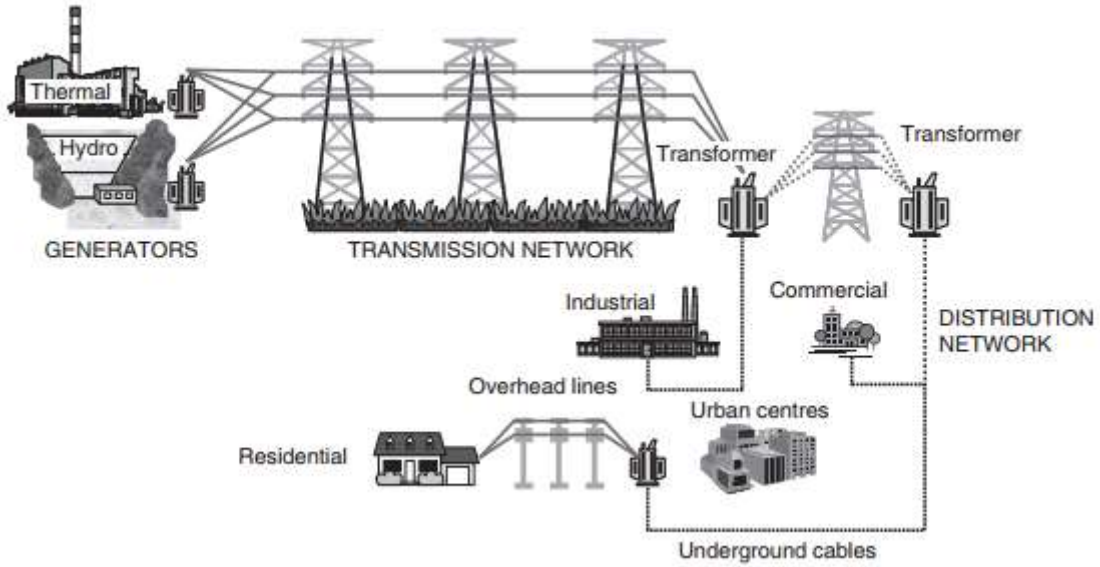

Figure 4: Illustration of the basic components of an electric grid power system [66]

The energy yielded from the generation station is converted to high power for transmission and distribution [67]. It is at this juncture that the sub-systems of the electrical power grid system are explicitly elaborated.

2.3.1. Electrical Power Generation System

Initiated at the point of generation, generators are at the start of an electrical network [66], [68]. By converting certain materials' available potential energy into electrical energy [68], these generators that produce electricity at an electrical power station [65] do so either through direct conversion (such as in the case of solar and wind) or through some driving mechanism (example being hydro plants and nuclear boilers) [68]. The two main electrical machines are generators and transformers [69].

2.3.1.1. Wind power generation technology

As the second largest renewable energy resource after hydropower, wind power is one of the fastest-growing power sources [70]. Of the 1.74×10^{17} W of energy emitted from the sun to the earth's surface, about 1-2 % of this energy is transformed into wind energy. The generation of this wind is a result of air's natural flow as a result of the earth's rotation and uneven heating and cooling of the earth's surface that causes a temperature difference, ultimately causing winds to blow [71]. The total capacity installation of wind energy has experienced a rapid rise since the beginning of the 21st century [72]. Nonetheless, the growth in wind power utilization is not evenly distributed in the world's entirety and varies per country as well as per region. A typical example of the varying wind power installation capacity is shown in Figure 5 [70].

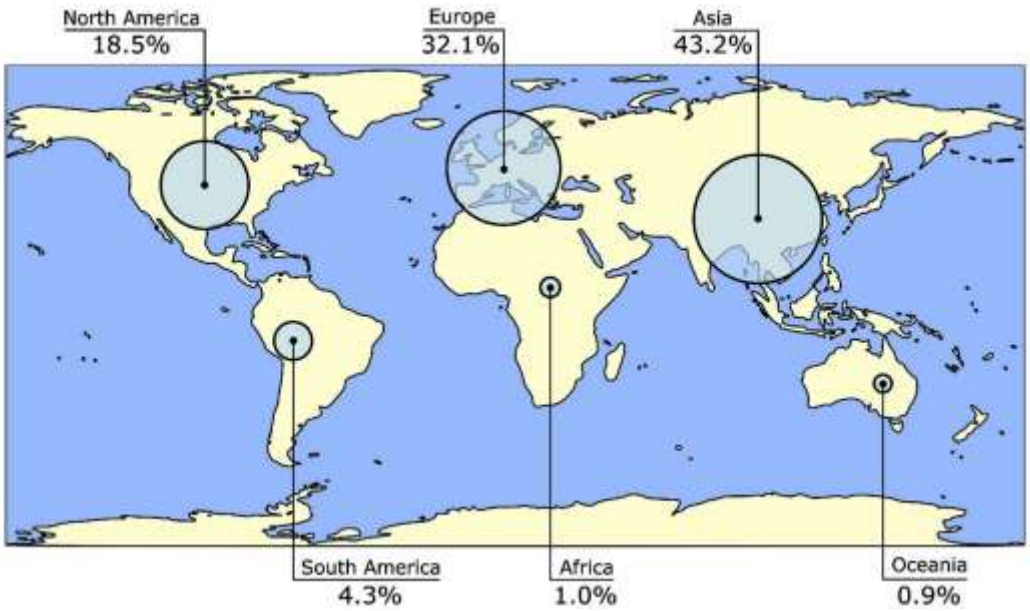

Figure 5: Wind power contribution per continent (2019) [70]

At 1.0 % of the total installation capacity as seen in Figure 5, Africa is among the less privileged regions in terms of installation capacity. In fact, not only is the continent lagging behind in terms of wind generation capacity, but studies have shown that the overall electricity capacity of the continent is the global lowest and accounts for less than 4 % of worldwide usage [73].

For the proper installation of wind turbines at a location of interest, it is essential to conduct a site-specific pre-feasibility wind resource evaluation known as Wind Resource Assessment (WRA) [74] for broad-scale wind resource preliminary estimates [75]. From the WRA, high-capacity computers are used to generate wind resource maps from meteorological models called mesoscale models [76] by analyzing wind data from meteorological agencies for broad-scale wind power distribution [75]. Figure 6 shows an example of WRA data for two different regions, India and Lesotho, taken at 100m and 80m above ground level (agl), respectively.

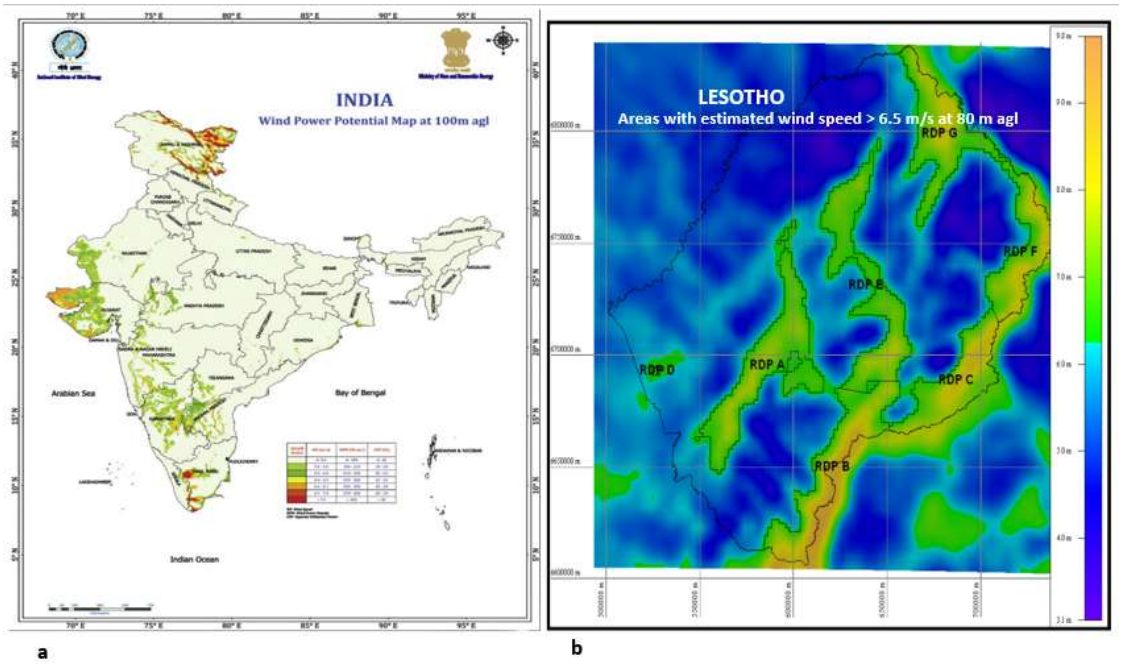

Figure 6: Wind resource assessment: (a) India at 100m agl [77], (b) Lesotho at 80m agl [78]

Taking into account the topography, local wind flow, wind velocity global distribution, and speed continuity, the speed continuity-dependent wind energy production can be estimated [74] from the correct input data whose model complexity can vary based on terrain changes such as coastlines and mountains as they influence the surface roughness [76]. The general wind speed assessment process for a site of interest is illustrated in Figure 7.

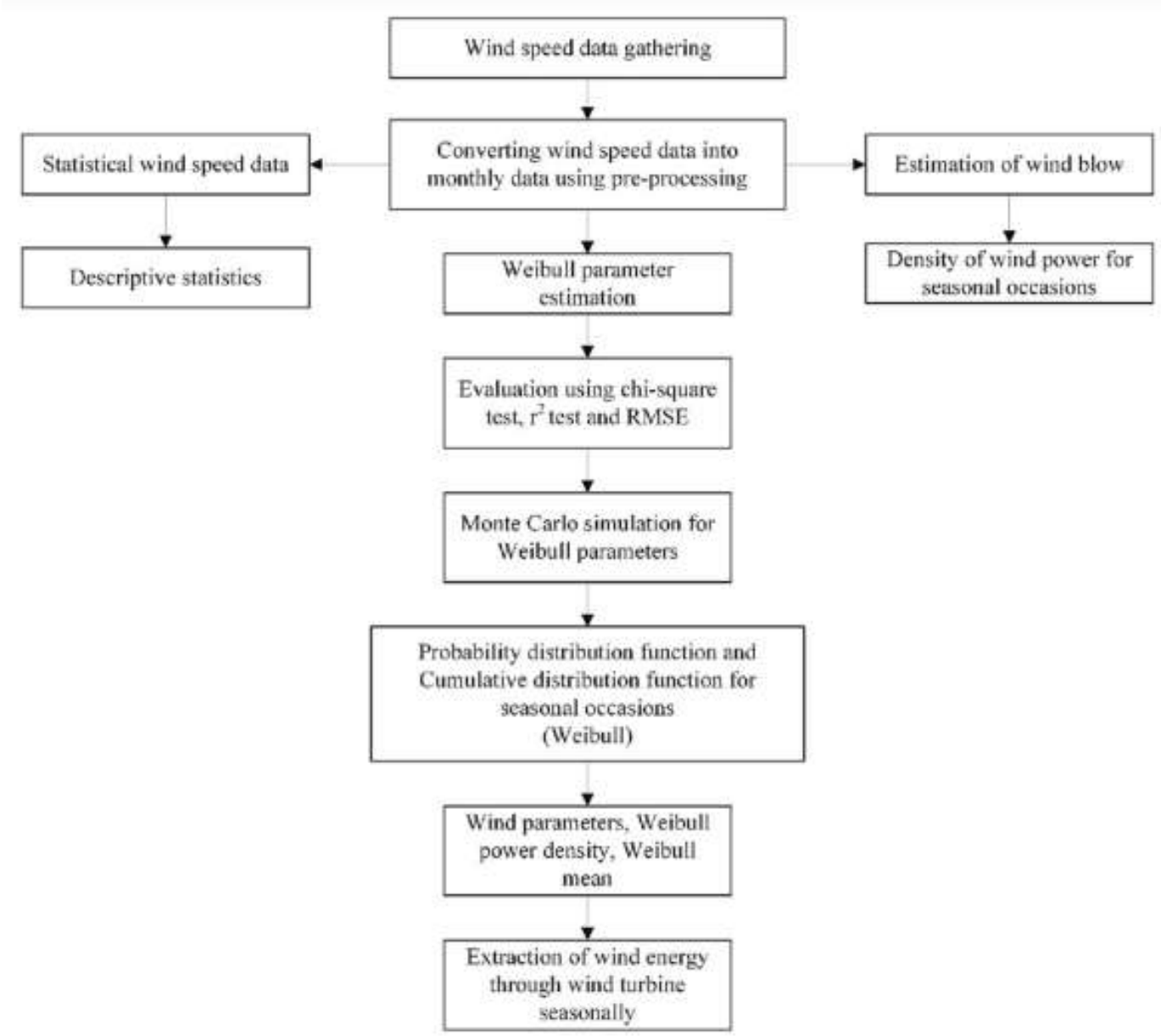

Figure 7: Wind speed assessment process [79]

One particular parameter of interest and utmost importance observed in Figure 7 is the Weibull parameter as it governs all the wind power system generation assessment procedures. The Weibull distribution function is commonly used to approximate the surface wind distribution [80]. As one of the widely used statistical methods for the analysis of wind data [81], its continuous probability distribution accounts for the wind speed variations for most areas across the world that have different wind conditions [82], despite limited observation periods resulting in under-sampling [80]. When modeling wind power generation in terms of the Weibull distribution [79]-[82], the general Probability Density Function (PDF) and Cumulative Distribution Function (CDF) are, respectively, given by:

$$f(v) = \frac{dF(v)}{dv} = (\frac{k}{c})(\frac{v}{c})^{k-1} e^{-(\frac{v}{c})^{k}} \qquad \textit{Equation 1}$$

$$F(z) = 1 - e^{-(\frac{v}{c})^{k}} \qquad \textit{Equation 2}$$

where v denotes the wind speed in m/s, k is the non-dimensional shape parameter, and c is the scale parameter. When the natural logarithm is taken on both sides of *Equation 2*, the yielded expression becomes:

$$-\ln[1 - F(v)] = k\ln(v) - k\ln(c) \qquad \textit{Equation 3}$$

which is the representation of the Weibull paper constructed such that the shape factor k becomes the gradient of a straight-line cumulative Weibull distribution.

When a linear relationship between the non-dimensional shape parameter and the scale factor is assumed, the least square method can be used for some exclusive calculation to minimize the relationship, and the expression takes the forms in *Equation 4* and *Equation 5*.

$$k = \frac{n\sum_{i=1}^{n}\ln(v)\ln\left[-\ln\left(1 - F(v)\right)\right] - \sum_{i=1}^{n}\ln(v)\sum_{i=1}^{n}\ln(v)\sum_{i=1}^{n}\ln[-\ln\{1 - F(v)\}]}{n\sum_{i=1}^{n}\ln(v^2) - \{\sum_{i=1}^{n}\ln(v)\}^2} \qquad \textit{Equation 4}$$

$$c = \exp\{\frac{k\sum_{i=1}^{n}\ln(v) - \sum_{i=1}^{n}\ln[-\ln\{1 - F(v)\}]}{nk}\} \qquad \textit{Equation 5}$$

For the least square method, *Equation 4* and *Equation 5* are commonly used in problems that are more often than not regarded as non-estimation problems.

2.3.1.2. Wind turbine components and aerodynamics

The use of wind captured by the turbine blades for shaft turning for exploitation of the resulting rotational motion to produce power is the basis upon which all stationary wind machines are based [83]. Consisting of a tower and a nacelle that contains essential components for wind energy to electrical conversion [84], the main components of a horizontal axis wind turbine, which has established itself as the standard configuration model [83] are illustrated in Figure 8.

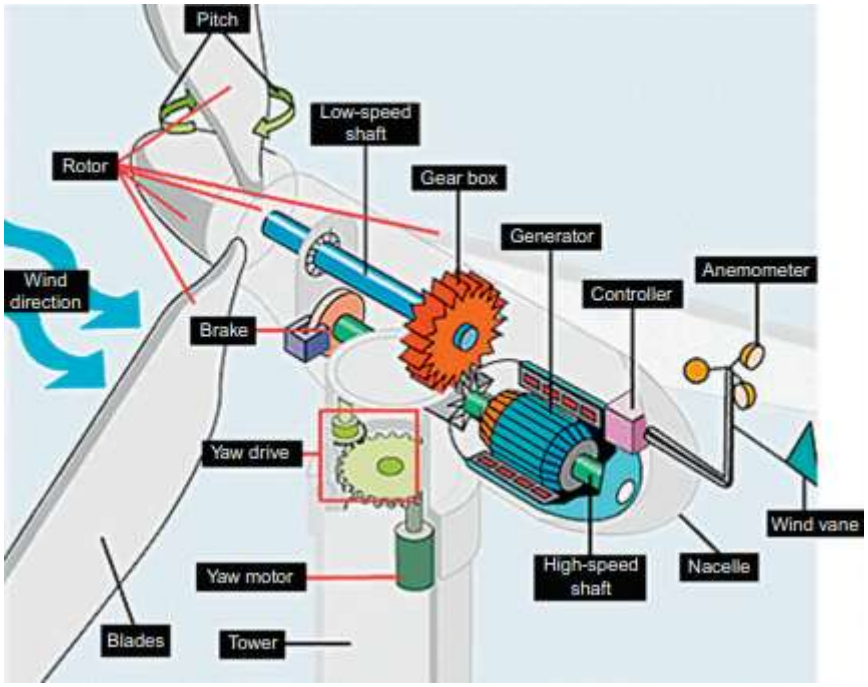

Figure 8: Wind turbine's drive drain and nacelle's principle components [83]

The main components of the turbine discussed in this section are the aerodynamic rotor, transmission system, generator, and power electronic interface.

Aerodynamic rotor:

Mainly made up of the hub and blades that are mechanically jointed to the hub at the end shaft, the function of the aerodynamic rotor, or propeller, is to capture the wind and convert wind power to kinetic mechanical power [83], [84]. In the computational flow modeling, it has been observed that the power generated by the aerodynamic rotor depends on the swept area of the blades with constant density and an approximate Reynolds number for the flow in an atmospheric boundary layer is given by [85]:

$$Re_D = \frac{\rho U_{ref} D}{\mu} \qquad \textit{Equation 6}$$

Where , U_{ref}, D, and μ denote constant air density, rated wind speed, rotor diameter, and air dynamic viscosity, respectively. By use of the actuator disk method where the turbine rotor emulated by a circular surface is mapped onto a computational mesh, the thrust force acting on the rotor is given by:

$$T_{disc} = s_{disc} \sum_{b=1}^{B} \int_0^R \int_0^{2\pi} t_b(r) d\theta dr \qquad \textit{Equation 7}$$

Where s_{disc}=1/2π represents the actuation region's effective solidarity, B denotes the number of rotor blades, R is the length of each blade, r is the local radial position, and θ denotes the azimuthal direction.

Consisting of spars, webs, ribs, and trailing and leading-edge reinforcements, the wind turbine spar system's number of components is based on the loads acting on the blade, such as [86]:

- Flap-wise and edge-wise bending that comes from the pressure forces acting on the turbine blade.
- Gravitational forces that are responsible for the edgewise bending moments and changing the blade's rotational direction.
- Torsional loading is caused by flap and edge-wise loads and causes the shear.
- Normal loading results from the blade's rotation.
- Minor loading owing to the blade's accelerations and retardations.

Transmission system:

Consisting of a rotor shaft, mechanical brakes, and a gearbox, the transmission system transmits the kinetic mechanical power from the aerodynamic rotor to the generator [84]. Supported by two-point self-aligning roller bearings for the endurance of transmission torsion and axial force from the hub to the gearbox, the rotor shaft is a critical turbine component carrying variable forces that the system transmits [87]. While enabling the coupling of the rotor's low-speed shaft to the generator's high-speed shaft [88], [89], the gearbox plays a critical role in the industry of electric power as it enhances the system efficiency by simplifying the components of the wind turbine generator [90]. In the majority of wind turbine generators with synchronous or induction generators installed for power generation, gearboxes are installed [88] to increase the rotational speed of the turbine's rotor to match the speed required by the generator [91], thus making the gearbox-based wind turbine generator system an ideal configuration in the wind power field [90].

With the gearbox being a speed-increasing device in the wind turbine, its design concept, as outlined by McFadden and Basu [88] is as follows:

Step 1: Define gear ratio according to the required input and output speed.

Step 2: Define gearbox input torque according to WTGs power and gearbox input speed.

Step 3: Design a gear stage including number of stages, gear split ratio and gear macro design.

Step 4: Select the bearing according to the chosen gear stages.

Step 5: Design the gearbox housing.

As per the steps in the gearbox concept design defining the gear ratio η_g according to the required input and output ratio relates to the rotor side's input speed as Ω_{IN} and the generator side's output speed as Ω_{OUT}:

$$\eta_g = \frac{\Omega_{OUT}}{\Omega_{IN}} \qquad \textit{Equation 8}$$

The value of the speed-up ratio η_g is always greater than 1 in all cases of speed-increasing gearboxes. As the gearbox receives power on the rotor side P_{ROTOR} and delivers it to the generator side P_{GB}, some power loss P_{LOSS} is experienced as a result of the generated heat due to the friction between relatively moving parts as well as viscous losses, resulting in the energy conservation as:

$$P_{ROTOR} = P_{GB} + P_{LOSS} \qquad \textit{Equation 9}$$

If the gearbox output power is related to the rotor power by the gearbox efficiency that depends on the gear loss and oil churning loss η_M, then the generator side's power can be written as:

$$P_{GB} = \eta_M P_{ROTOR} \qquad \textit{Equation 10}$$

When the gearbox power on the generator side and the wind power are related, the resulting equation takes the form:

$$P_{GB} = \eta_M C_p P_{WIND} \qquad \textit{Equation 11}$$

where C_p is the rotor's power coefficient that does not theoretically exceed the Betz limit [88]. This Betz limit is the upper limit of the turbine's efficiency based on the mass and momentum conservation principles as well as the actuator disk theory [92], suggesting that the maximum efficiency of an ideal wind turbine, from which it follows the conversion of an incompressible fluid into work of the kinetic energy is limited to 16/27 (59.3%) [93], thereby setting 16/27 as the maximum power coefficient known as Betz limit [94]. According to Betz [95], the equation governing the mechanical energy's power output captured by the wind turbine blades is given by:

$$P_{OUT} = \frac{1}{2}\rho A v^3 4a(1-a)^2 \qquad \textit{Equation 12}$$

where a is the axial factor of induction, and the resulting power efficiency is given by

$$C_p = 4a(1-a)^2 \qquad \textit{Equation 13}$$

It is from *Equation 13* that the maximum power efficiency is drawn and obtained when the value of a is 1/3 with the associated maximum efficiency of $C_p = \frac{16}{27}$.

Measured as a function of wind speeds, the amount of electrical output of a wind turbine is represented by a power curve [96], which plays a crucial role for several purposes such as the forecasting of wind power, turbine selection, wind turbine potential estimation, as well as turbine condition monitoring [97]. With the manufacturers' assumption of ideal meteorological and topographical conditions, it typically has three main characteristics which are illustrated in Figure 9.

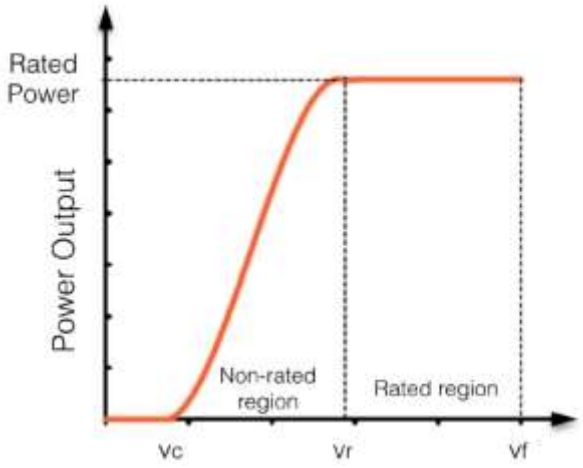

Figure 9: Typical wind turbine power curve [98]

Showing how the wind turbine's power output varies with steady wind speed in Figure 9, the three main parameters in the wind speed are shown being [96], [98]:

- v_c is the cut-in speed, the threshold speed where the turbine begins to operate. Starting to generate electricity at this speed, any speed below the cut-in speed is insufficient for any power production.
- v_r is the rated speed between the cut-in and cut-out speeds, where the turbine generates maximum power output.
- v_f refers to the cut-out speed beyond which the turbine's power generation shuts down to prevent any damage.

Generator:

Receiving the rotary motion from the turbine's rotor as input through the gearbox [99], the electric generator, normally located at the top of the tower in front of it for better passive cooling from inside the enclosure and by the ambient air on the outside [100], is an electro-mechanical component used for the conversion of mechanical input power into electricity through its stator and rotor [84]. An

illustration of an electric generator is shown in Figure 10, which is a small-scale rotating prototype model that was designed and built at Institut de Recherche d'Hydro-Québec (IREQ) and used by Dang et al. [101] in their simulations of Computational Fluid Dynamics.

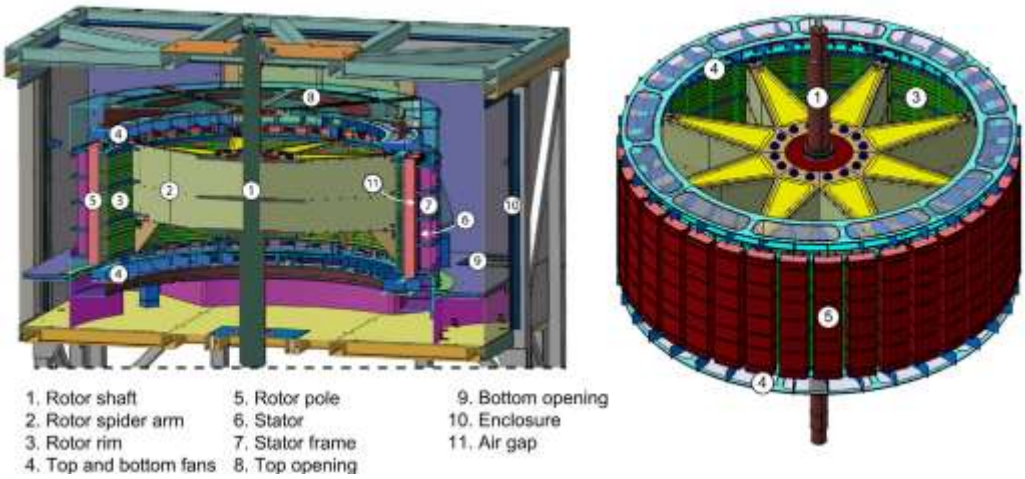

Figure 10: Electric generator scale model [101]

Consisting of a rotor and stator as in Figure 10, the magnetic induction in the form of a voltage arranged either by a magnetic field change imposed by a conducting coil or the coil moving around the magnetic field is the basis of its operation [102]. The two major industrial generator types are synchronous generators and induction (asynchronous) generators [84], with the former always rotating at the synchronous speed while the latter's speed can be varied to rotate at speeds that are different from the synchronous speed [103]. The electric generators' classifications deployed in wind turbine technology are shown in Figure 11, although the permanent magnet DC generator is beyond the scope of the research as the focus is on the AC grid connection.

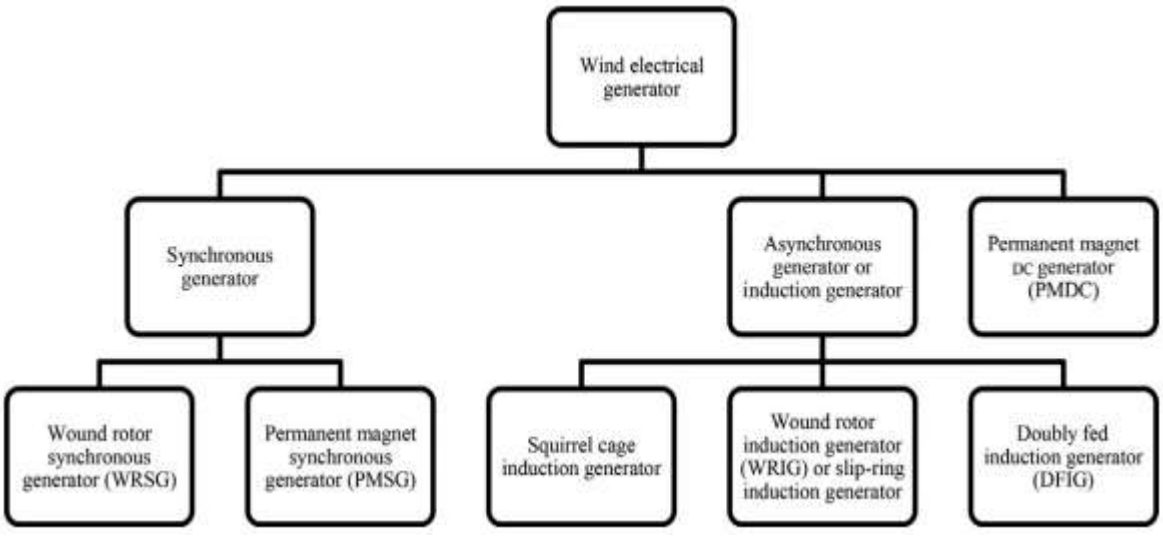

Figure 11: Classification of wind turbine electric generators [104]

Due to their ability to produce voltage at grid frequency with low rotational synchronous speeds, synchronous generators are commonly used for variable-speed wind turbine applications [105], where their synchronous speed is dictated by the grid frequency and the number of the rotor pole pairs irrespective of the applied torque magnitude [84]. Although they can produce or consume reactive power quickly depending on the excitation and this ability being utilized to address the dynamic system's volt/var control, the machine's steady-state stability and thermal limits restrict their reactive power supply and absorption capacity [106]. A typical schematic of a synchronous generator wind turbine is illustrated in Figure 12.

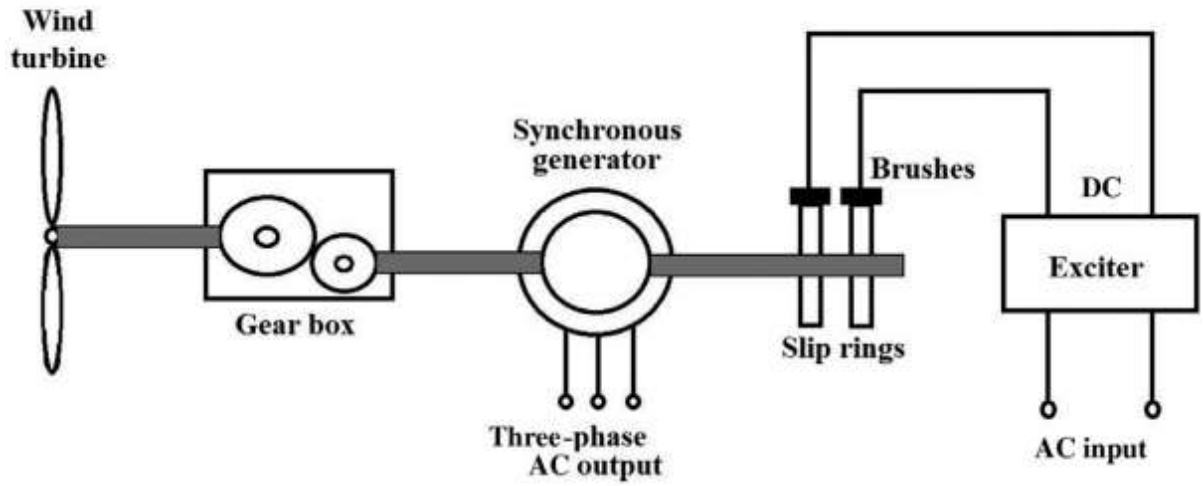

Figure 12: Schematic of a synchronous generator wind turbine [104]

In the wind turbine industry, two classical synchronous generator types often used are [84], [104]:

- **Wound Rotor Synchronous Generator (WRSG)** has directly grid-connected stator winding and therefore has a strictly fixed rotational speed enhanced by the supply grid frequency. The exciter field which rotates at the synchronous speed is generated by the rotor windings through which direct current flows.
- **Permanent Magnet Synchronous Generator (PMSG)** with a wound stator, which has its rotor installed with permanent magnets that are used for the creation of the excitation field. In its most common types such as the radial flux machine, the axial flux machine, and the traversal flux machine, the adjustment of voltage and frequency of generation and the transmission voltage and frequency requires excitation by the use of a full-scale power converter. Having a higher efficiency than their wound rotor counterparts as well as their advantage of higher output power, lower weight, lower maintenance, and machine construction simplification has led to their prominent use [107].

In Asynchronous generators, the relative motion called slip, which induces rotor windings, is the one that induces an electric field between the rotor and the rotating stator field [84], with the stator directly connected to the grid while the slip rings connect the rotor windings to a converter [98].

- **Squirrel cage induction generator**, a generator with high robustness and stability that exhibits a minute speed change as its slip varies with wind speed variations. Since it consumes reactive power, it is typically equipped with a reactive power compensation mechanism [84].
- **A Wound Rotor Induction Generator (WRIG)**, also known as a slip-ring induction generator, has its rotor windings connected through the use of brushes or slip rings by the use of power electronic equipment. Its main advantage is the outside control of its electrical characteristics, thereby allowing the impression of the rotor voltage [108].
- **A Doubly-Fed Induction Generator (DFIG)** that has its stator directly coupled to the grid and a bidirectional power converter is used to grid-link its rotor [109], [110]. Due to their flexible control, high efficiency, cleanness [111], and grid-friendliness, Wind Energy Conversion systems (WECS) based on DFIGs have become widely used for wind power generation [110]-[113]. Figure 13 illustrates a wind turbine based on a doubly-fed induction generator.

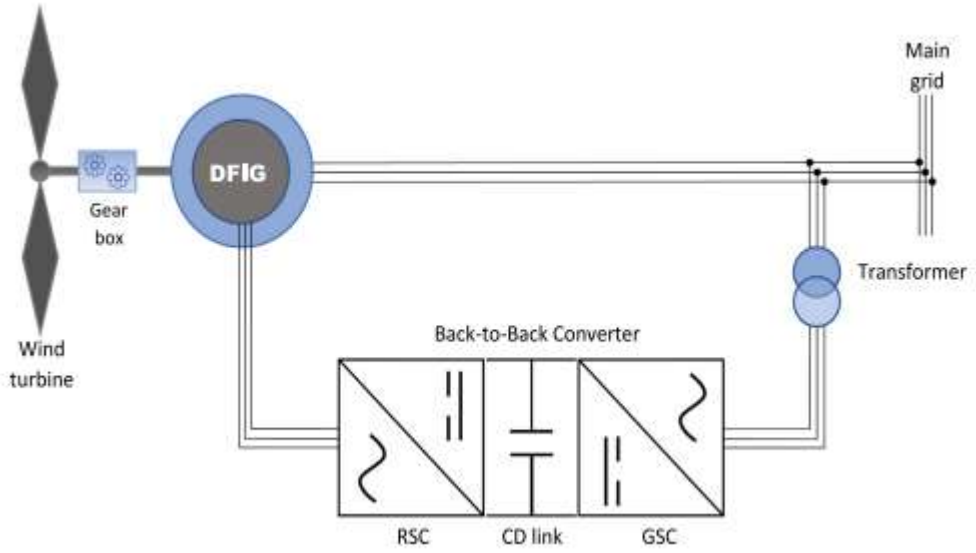

Figure 13: Schematic representation of DFIG-based wind turbine [109]

Notwithstanding their advantages, doubly-fed induction generators have their drawbacks, mainly being the inevitable requirement of slip rings [84], and the frequency stability problem in instances of high permeability of DFIGs [111].

Power electronic interface:

In satisfying both the generation and grid side requirements of the power system in a cost-effective and easily maintainable way, the power electronic interface is placed between the wind turbine

generator and the power grid [84]. Typically consisting of measurement and calculation mechanisms, loop controllers, reactors, and capacitors, among others, the general structure of the control mechanism in different power electronic devices is typically the same [114] and is generally as illustrated in Figure 14.

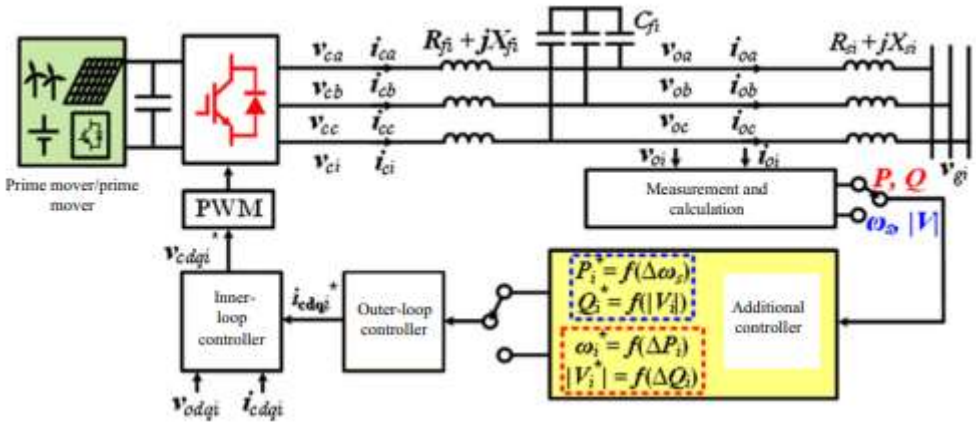

Figure 14: Control structure of power electronic interface devices [114]

The advantages of the power electronic interface include mechanical robustness, good thermal management, high power ratings, as well as the tight integration of multiple power semiconductor devices [115]. In the power electronic interface, the prominent device is the power electronic converter, whose function is to convert electrical power to meet the requirements from both sides of the generator [116]. Figure 15 shows the use of power converters as applied in wind turbines.

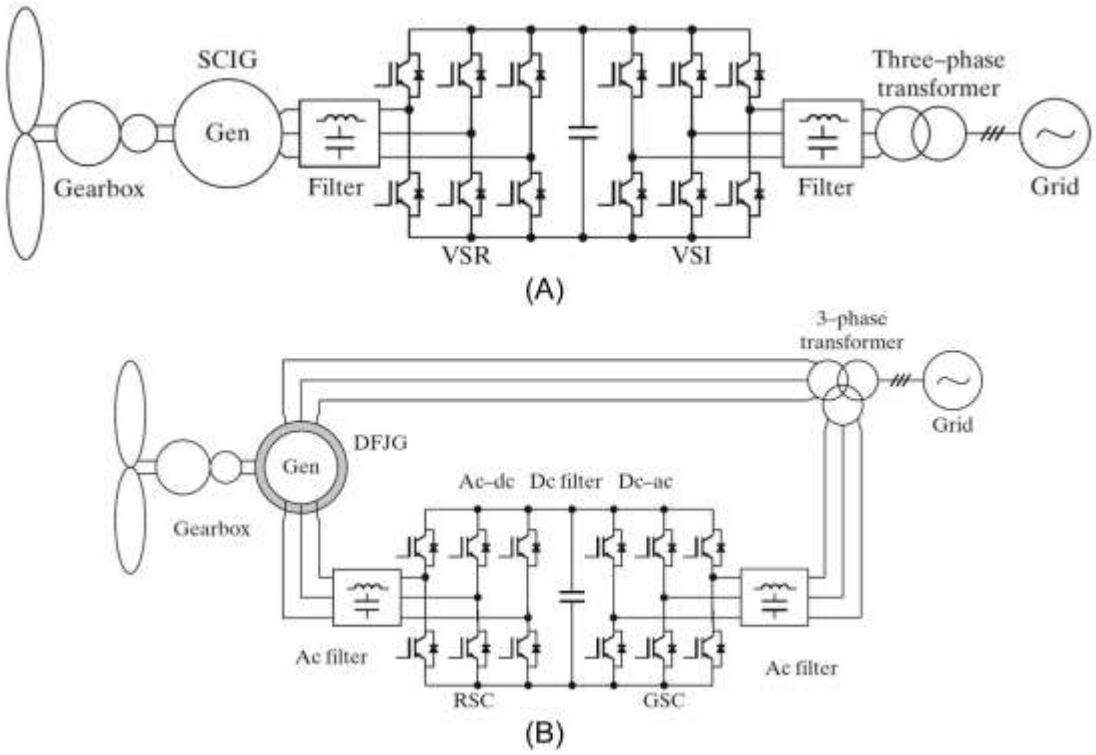

Figure 15: Power converters used in (A) Squirrel-cage induction generator wind turbine, (B) DFIG wind turbine [117]

Not only are power converters used in power systems, but they are widely applied in all industrial sectors, such as information technology, electrified transport, aeronautics, and astronautics due to their conversion efficiency advantage [116].

Two of the commonly used power electronic converters used in wind turbine technologies are:

- **Variable Speed Drive (VSD),** also known as a Variable Frequency Drive, or Frequency Converter, allows for two independent frequency electrical systems to be interconnected [84] by regulating a mechanical equipment's speed (and therefore frequency) and rotational force, or output torque [118].
- **Soft Starter,** which limits the disturbance to the grid by reducing the inrush current during the turbine's grid connection [84] and realizing a smooth starting [119]. Using a starting method such as ramp methods, phase control methods, Design for Cost (DFC) methods, and predictive control methods [120], the aim is to reduce the voltage of the induction machine, and then increase the voltage gradually until it is full [121].

2.3.1.3. Overview of Solar Photovoltaic Energy Systems

As much as it is excluded from the scope of the research, a photovoltaic (PV) energy systems overview is deemed necessary due to its potential in Lesotho. The country's location is suitable for solar systems' implementation because of the uniform solar irradiation levels distribution of 5.5 – 7.2 kWh/m^2 in its 30,355 km^2 compact size [122]. Not only is solar energy the earth's most abundant energy resource

[123], but its oriented photovoltaic systems renewable energy generation's major type [124], are one of the cleanest, most accessible, safe, inexhaustible, and durable renewable energy sources [123], [125]. Also, the continually decreasing cost of PV systems as a result of materials and processes' technical breakthroughs favors their cheap installation [125], all the more with rising oil prices due to the Ukraine war [124], therefore PV systems have become economically competitive.

PV solar energy is based on the photoelectric effect principle, transforming radiation from sunlight into electricity by photovoltaic cells. The photovoltaic panels, the fundamental element representing a photovoltaic generation system, are made up of these photovoltaic cells [123]. The PV arrays are plugged into the grid through a Power Conditioning Unit (CPU) and work together with the electricity utility grid [126].

While converting the generated direct current to alternating current that meets the grid requirements, the grid-connected inverters used must maintain consistency in power frequency, amplitude, phase, and other vital characteristics to maintain the power quality [128]. Research on the improvement of power quality for grid-tied PV systems is ever continuing. For instance, Nkambule et al. [129] addressed the challenge of partial shading and harmonics by employing a dynamic safety perimeter maximum power point tracking algorithm to develop a flexible radial movement optimization strategy to ensure optimum voltage using a fixed tilt installation configuration. In their study, Guo and Xu [130] optimized the power quality at the point of common coupling by deploying a three-layer optimization model for harmonic suppression and reactive power compensation strategy based on the photovoltaic Multi-Functional Grid-Connected Inverter (PVMFGCI).

2.3.2. Overview of Power Transmission and Distribution (T&D)

A power Transmission and Distribution (T&D) system is the section of the power system transferring power from its generation points to its consumption points, interconnecting all the disparate points of the power system, and thereby functioning as a determining factor of the power system's character to a great extent [131]. As the name suggests, the T&D system comprises the transmission system as well as the distribution network: the former, regarded as the backbone of the electric system transferring high voltage power over long distances [132], is made up of transmission networks that transfer electricity to the latter, which consists of substations, feeders, and step-down transformers for power deliverance to end users [133]. Exclusive of the generation layer, the layers of the electric power system in Figure 16: Illustration of power system layers [131] form the T&D portion of the network, with MV and LV denoting Medium Voltage and Low Voltage, respectively.

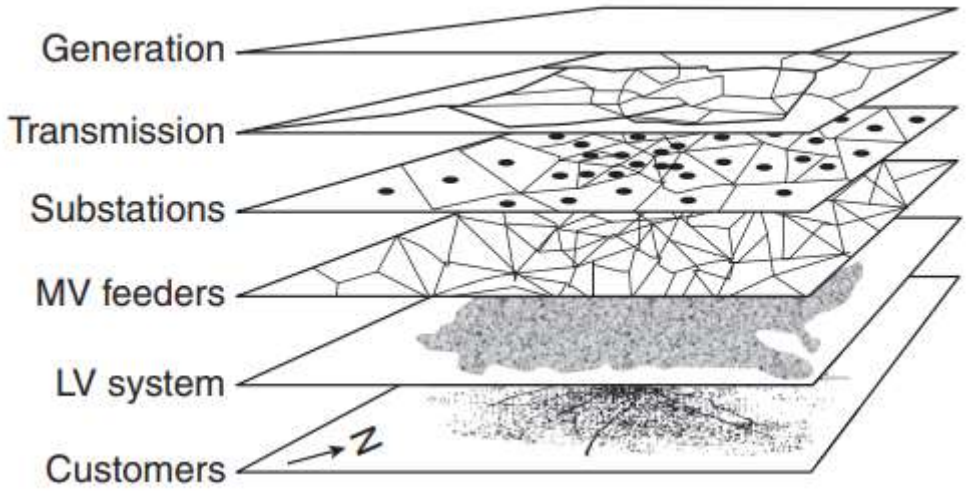

Figure 16: Illustration of power system layers [131]

The short descriptions of the layers of the T&D network are as follows:

- **Transmission:** This refers to the bulk transfer of generated power through high-voltage lines from the generation plants to the substation located close to the population centers [134].
- **Substations:** These are power network points of transmission lines and distribution feeders' interconnection [135] used for the provision of continuous grid power delivery while maintaining energy production and consumption balance [136].
- **MV feeders:** Typically, either as overhead lines mounted on wooden poles or as under-ground cables, these are lines operating at distribution voltage to route power from the substation to its different service areas [131].
- **LV system:** At a voltage's reduced magnitude from the MV feeder by the use of a step-down transformer, this is the power distribution network supplied to end users for direct consumption at prescribed standard consumption magnitudes.
- **Customers:** These refer to the end user of the electrical power. The customer is the ultimate consumer for which the power system was initially designed to service with electricity.

2.3.3. Supervisory Control and Data Acquisition

The power system's operational reliability to consistently meet performance standards is based upon a computerized tool known as SCADA [137], whose framework consists of hardware components, a Remote Terminal Unit (RTU), a Master Terminal Unit (MTU), sensors and actuators as well as software including Human Machine Interface (HMI) and a central database (Historian) that provide a hardware and software communication interface [138]. Allowing the visualization of all power system processes, they collect data from different terminal stations about the process' current status, systemically display such data in a graphical user interface, and act based on such data in case of necessary

intervention [139]. The interrelation of a SCADA system interconnection of components is shown in Figure 17.

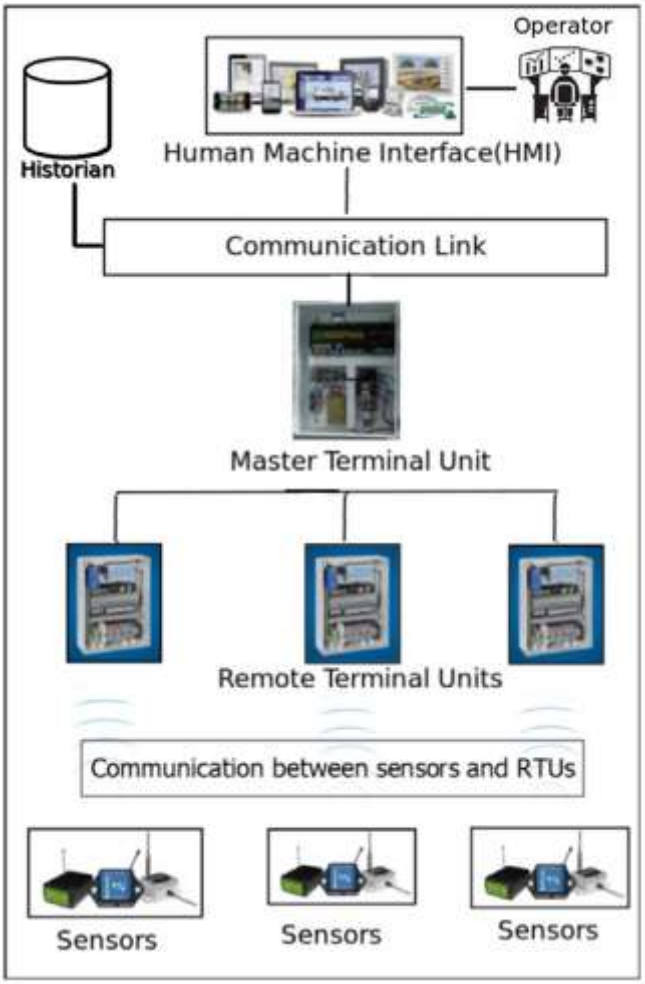

Figure 17: SCADA system components interrelation [138]

During the operation and control of complex systems, the incorporation of SCADA systems has solved many problems and has allowed better system management [140] due to its enhanced performance efficiency, having undergone a significant evolution from the typical isolated model to the highly advanced interconnected network model [141].

2.4. Stability criterion in a power system

The continuous stability between energy demand and supply is a crucial part of the power system's effectiveness, and the reason why power systems models are described by exhaustive time variations [142] to get the required quality of supply [58]. Some of the most crucial parameters considered in measuring the quality of electricity supply are [58]:

- Constant voltage magnitude
- Constant frequency

- Constant power factor
- Balanced phases
- Lack of interruptions
- Fault-tolerance and fault recovery

These parameters constitute the stability of a power system. Power system stability is defined as "*the ability to regain an equilibrium state after being subjected to a physical disturbance*" [143]. From the point of view of defining and classifying power systems' stability, quantities to consider are

(i) angles of nodal voltages, also called load angles;

(ii) frequency; and

(iii) nodal voltage magnitudes [143].

The stability of the power system can therefore be divided into:

(i) rotor angle stability;

(ii) frequency stability; and

(iii) voltage stability based on the IEEE/CIGRE Joint Task Force [144] as illustrated in Figure 18.

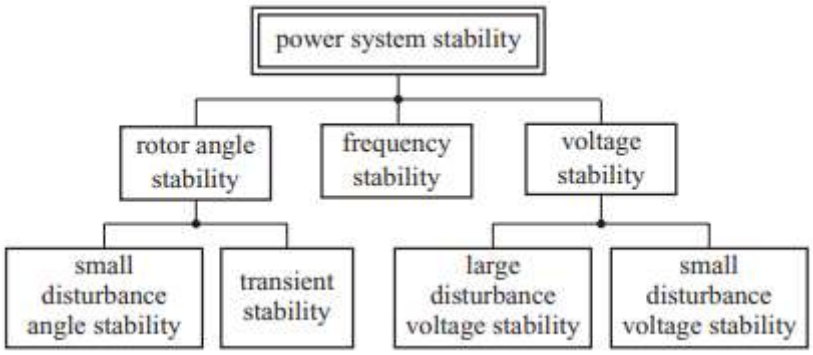

Figure 18: Classification of power system stability [143]

2.4.1. Voltage stability

When a power system is subjected to a large contingency event, such as a grid fault or sudden load increase, its ability to regain steady-state voltage defines voltage stability [10]. Nazir et al. define voltage stability as "*the ability of a power system to restore steady-state voltage of acceptable magnitude after a certain disturbance*" [145]. During normal operations, the voltage of the system will remain stable, and if the voltage turns into unstable condition, the power system experiences an intractable deterioration in voltage [144]. The main cause of voltage instability is the lack of reactive power supply from the power system. However, it can also be caused by long, weakly connected

transmission lines, low generation capacity, or even a sudden increase in the load [146]. At the generation stations, the use of Automatic Voltage Regulators (AVRs) for voltage control results in the alteration of the excitation windings of the generator and thus indirectly affects the reactive power [145]. The preferred voltage regulation closer to utility is then achieved by the installation of tap-changing transformers in transmission lines, capacitor banks, Static VAR compensators (SVCs), and Static Synchronous Compensators (STATCOMs) for reactive power compensation by use of adaptive control to make dynamic reactive power adjustments so as to maintain voltage stability [145].

Voltage stability can be classified into short-term and long-term, with short-term stability requiring the study of the power system's dynamics and employing simulations in the time domain, while long-term stability uses steady-state analysis techniques [147].

2.4.2. Frequency stability

Frequency stability refers to the ability to maintain a balance between power generation and load consumption at all times by keeping the power system frequency within acceptable limits [148]. The stability of frequency is said to be a power balancing metric between generation and demand since the system frequency declines when demand exceeds generation and vice versa; hence it must be controlled within specified operating limits around the nominal frequency [10]. The system frequency fluctuations have to be maintained within a safe range regardless of the dynamic changes that may occur in system power generation and load demand [149]. Unlike in conventional generation units, system frequency regulation is a challenge for most renewable sources as they do not provide inertia [150]. The low inertia poses an imbalance between generation and consumption. It can trip protection systems, and even lead to a blackout as a result of high-frequency deviations [150]. The power systems with low synchronous generation levels experience low system inertia levels, which in turn leads to a higher Rate of Change of Frequency (RoCof) and lower frequency nadir (minimum value of frequency reached during a transient response) [10]. Taking into account the existing reciprocity between the inertia of the system generator and the rotor's kinetic energy, and adapting the system model by Ahmed et al. [10], the generator's kinetic energy can be expressed as

$$KE = \frac{1}{2} J V^2 \qquad \textit{Equation 14}$$

where KE is the kinetic energy in watt-seconds, J is the moment of inertia in Joules, and V is the angular velocity in radians per second. With the generator constant H being equal to the kinetic energy in MW at the generator speed over the generator-rated power (S_{VA}) in MVA, it can be expressed from *Equation 14* as

$$H = \frac{1}{2}\frac{JV^2}{S_{VA}} = \frac{KE}{S_{VA}} \qquad \textit{Equation 15}$$

Applying superposition on any interconnected systems with inertia constants that depend on generator power, type, and size, the net inertia H_{SYS} from *Equation 15* becomes

$$H_{SYS} = \frac{\sum_{i=1}^{n} KE_i}{S_{SYS}} = \frac{\sum_{i=1}^{n} H_i S_{vA_i}}{S_{SYS}} \qquad \textit{Equation 16}$$

where H_{SYS} is system net inertia, S_{SYS} is the net rated power, KE_i, H_i, *and* S_{vA_i} are the stored rotating energy, inertia constant, and rotating power of the *i*-th generator for *n* online generators. From the swing equation, the system inertia and RoCof relationship can be derived as follows:

$$\frac{df}{dt} = \frac{f_0}{2H_{SYS}S_{SYS}}(P_m - P_e) = \frac{f_0 \Delta P}{2H_{SYS}S_{SYS}} \qquad \textit{Equation 17}$$

where $\frac{df}{dt} = \Delta f$ is the system RoCof, P_m is the mechanical power, P_e is the electrical power, and f_0 is the nominal frequency. For each generator R_i, the governor droop setting can be defined as:

$$R_i = \frac{(\frac{\Delta f}{f_0})}{(\frac{\Delta P_i}{S_{VA_i}})}, i = 1, \dots, n \qquad \textit{Equation 18}$$

When the system is subjected to contingency, the rate of power injection or absorption of power R_i is represented in *Equation 18* for the *i*-th generator in response to frequency deviation. A typical system response to frequency deviation is illustrated in Figure 19.

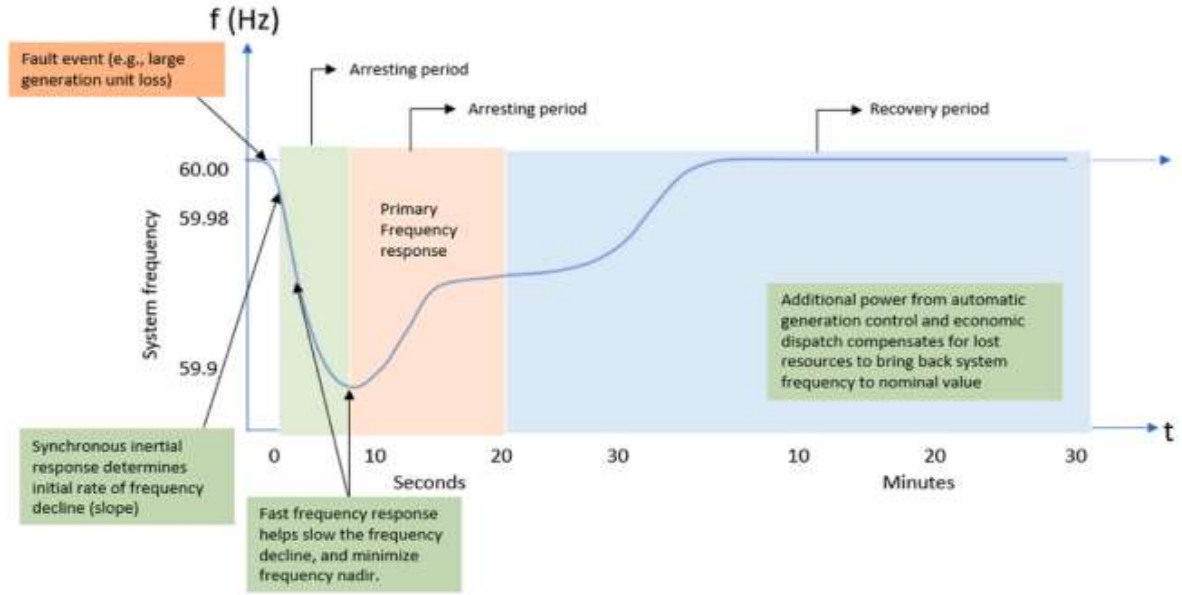

Figure 19: Typical frequency control following generation loss [10]

A detrimental impact on the system frequency nadir and RoCof comes from a growth in variable renewable energy generation, as does the retirement of synchronous machines as it results in system inertia drop [10]. It is, therefore, of utmost importance to control the system frequency and re-establish the frequency imbalance in due time to prevent the sequential trip of generators that may eventually lead to a blackout with tremendous economic and social consequences [151].

2.5. Control Theory

When electric power is injected into the grid, the use of power electronics plays a crucial role [152] because they act as an interned bridge to enable the grid system to have the role of consuming new energy sources while maintaining grid stability [153]. The limitation to the spontaneous response of renewable energy generators to voltage and frequency changes [152] is the main challenge of grid-connected systems' coordination to achieve a fast and accurate distribution of power while keeping disturbance oscillations within acceptable limits and maintaining stable voltage amplitude and frequency [153]. Improved control strategies are therefore needed for the active and reactive power of distributed generators to be automatically allocated as per the generators' power capacity ratio [154]. This section discusses some of the commonly used control strategies for grid-connected RE systems.

2.5.1. P-Q and d-q control: Clarke's transformation and Park's transformation

For a control loop system using the dual loop power flow technique, the three-phase AC currents and voltages are measured and converted into DC components through a two-stage direct quadrature transformation [155]. The procedure for the two-stage transformation uses Clarke's transformation to convert the three-phase ABC frame to *αβ* frame, which is then converted to the *dq* components by the use of Park's transformation. The following equations are adapted [155] for the complete system transformation:

$$V_{ia} = V_{amp}\sin(\omega t) \qquad \textit{Equation 19}$$

$$V_{ib} = V_{amp}(\sin \omega t - \frac{2\pi}{3}) \qquad \textit{Equation 20}$$

$$V_{ic} = V_{amp}(\sin \omega t + \frac{2\pi}{3}) \qquad \textit{Equation 21}$$

Where V_{amp} is the maximum voltage amplitude, ω is the angular frequency, and V_{ia}, V_{ib}, and V_{ic} denote the three-phase voltages. The derivation of the single-phase formula takes the form as:

$$V_i = V_L + V_R + V_g \qquad \textit{Equation 22}$$

$$V_i = L\frac{di}{dt} + I_R + V_g \qquad \textit{Equation 23}$$

$$V_g = V_i - L\frac{di}{dt} - I_R \qquad \textit{Equation 24}$$

The stationary frame can be expressed in matrix form as follows:

$$\begin{bmatrix} V_{g\alpha} \\ V_{gb} \\ V_{gc} \end{bmatrix} = \begin{bmatrix} V_{ia} - L\dfrac{dia}{dt} - I_{Ra} \\ V_{ib} - L\dfrac{dib}{dt} - I_{Rb} \\ V_{ic} - L\dfrac{dic}{dt} - I_{Rc} \end{bmatrix} \qquad \textit{Equation 25}$$

Then the transformation of the three-phase stationary ABC frame to a two-frame *αβ frame as:*

$$\begin{bmatrix} V_{g\alpha} \\ V_{g\beta} \end{bmatrix} = \frac{2}{3}\begin{bmatrix} 1 & -1/2 & -1/2 \\ 0 & \sqrt{3}/2 & -\sqrt{3}/2 \end{bmatrix}\begin{bmatrix} V_{ga} \\ V_{gb} \\ V_{gc} \end{bmatrix} \qquad \textit{Equation 26}$$

$$\begin{bmatrix} V_{g\alpha} \\ V_{g\beta} \end{bmatrix} = \frac{2}{3}\begin{bmatrix} 1 & -1/2 & -1/2 \\ 0 & \sqrt{3}/2 & -\sqrt{3}/2 \end{bmatrix}\begin{bmatrix} V_{ia} - L\dfrac{dia}{dt} - I_{Ra} \\ V_{ib} - L\dfrac{dib}{dt} - I_{Rb} \\ V_{ic} - L\dfrac{dic}{dt} - I_{Rc} \end{bmatrix} \qquad \textit{Equation 27}$$

$$\begin{bmatrix} V_{g\alpha} \\ V_{g\beta} \end{bmatrix} = \begin{bmatrix} V_{i\alpha} - L\dfrac{di\alpha}{dt} - I_{R\alpha} \\ V_{i\beta} - L\dfrac{di\beta}{dt} - I_{R\beta} \end{bmatrix} \qquad \textit{Equation 28}$$

Then the conversion of the *αβ* to *dq* components yields:

$$\begin{bmatrix} V_{gd} \\ V_{gq} \end{bmatrix} = \begin{bmatrix} cos\omega t & sin\omega t \\ -sin\omega t & cos\omega t \end{bmatrix}\begin{bmatrix} V_{g\alpha} \\ V_{g\beta} \end{bmatrix} \qquad \textit{Equation 29}$$

$$\begin{bmatrix} V_{gd} \\ V_{gq} \end{bmatrix} = \begin{bmatrix} cos\omega t & sin\omega t \\ -sin\omega t & cos\omega t \end{bmatrix}\begin{bmatrix} V_{i\alpha} - L\dfrac{di\alpha}{dt} - I_{R\alpha} \\ V_{i\beta} - L\dfrac{di\beta}{dt} - I_{R\beta} \end{bmatrix} \qquad \textit{Equation 30}$$

$$\begin{bmatrix} V_{gd} \\ V_{gq} \end{bmatrix} = \begin{bmatrix} V_{id} \\ V_{iq} \end{bmatrix} - R\begin{bmatrix} i_d \\ i_q \end{bmatrix} - L\begin{bmatrix} cos\omega t & sin\omega t \\ -sin\omega t & cos\omega t \end{bmatrix}\begin{bmatrix} \dfrac{di\alpha}{dt} \\ \dfrac{di\beta}{dt} \end{bmatrix} \qquad \textit{Equation 31}$$

For some controllers, the current references are generated at the fundamental frequency that is in phase or quadrature with the system voltage. For adaptation and robustness a phase-locked loop, the circuit continuously keeps track of the system voltages' fundamental frequency, and its design should allow proper operation even when the voltage waveform is distorted or unbalanced [156].

2.5.2. Droop Control

By controlling the output and frequency of the voltage source inverter as per the output power change, and distributing the active and reactive power to each distributed power source, droop control simulates the droop characteristics of the generator by adjusting the output voltage and frequency of each inverter [153] as it is usually applied in autonomous power sharing [157]. Droop

control imitates the distributed generators' static power frequency characteristics [158], and the control principle is illustrated in Figure 20.

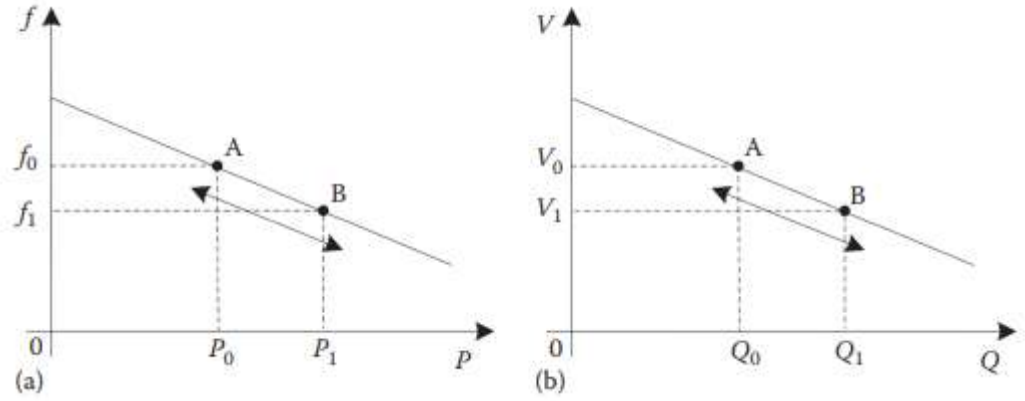

Figure 20: Droop control principle: (a) active power and frequency and (b) reactive power and voltage [158]

With the assumption of A being the initial operating point of the distributed generator in Figure 20, the active and reactive power outputs are P_0 and Q_0, and the frequency and voltage at the connection point are f_0 and V_0. The voltage magnitude decreases as a result of lacking reactive power while the frequency decreases due to a lack of active power, and vice versa. The control system output power increases according to the droop characteristics if the frequency decreases along with the active load increase [158]. An illustration of the outer loop controller based on (f-P)/(Q-V) droop control is shown in Figure 21, where the frequency and magnitude of the voltage are controlled based on the output power.

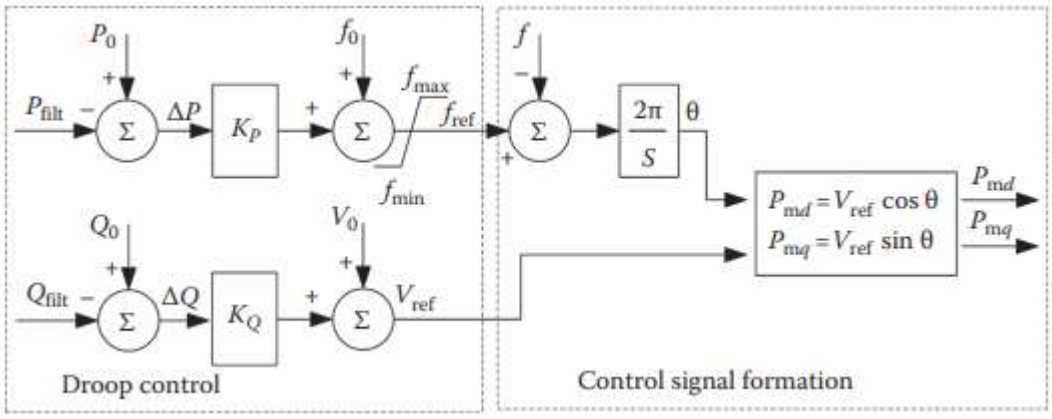

Figure 21: Droop control-based outer loop controller [158]

In the method shown in Figure 21, the regulation of the voltage phase through reference frequency integration is based on the active power, and the voltage magnitude is controlled via the output reactive power [158]. Under the unbalanced line impedance, the limitation of fixed droop control of dealing with a deviation of the output terminal voltage and parallel inverter voltage is rectified by a dynamical droop coefficient strategy. The strategy has some advantages, which are listed below [153]:

- Adjustable voltage amplitude under uneven reactive power distribution.
- A good realization ability that applies to multi-inverter paralleling scenarios with different rated powers.
- Adjustable reactive droop coefficient allows it to be relatively small upon reaching system stability and, therefore, maximizes the reduction of voltage loss.

2.5.3. DSTATCOM Control Mode

With the increasing voltage and reactive power problems as a result of the integration of renewable energy sources, reactive power compensation devices are being used for voltage regulation at points of grid connection. One such device is a Distribution Static synchronous Compensator (DSTATCOM), an IGBT-based AD-DC inverter used to maintain a constant current during low or high voltages by creating an output AC voltage controlled with Pulse-Width-Modulation (PWM) for producing leading or lagging reactive current into the grid [158]. A schematic of a DSTATCOM is represented in Figure 22.

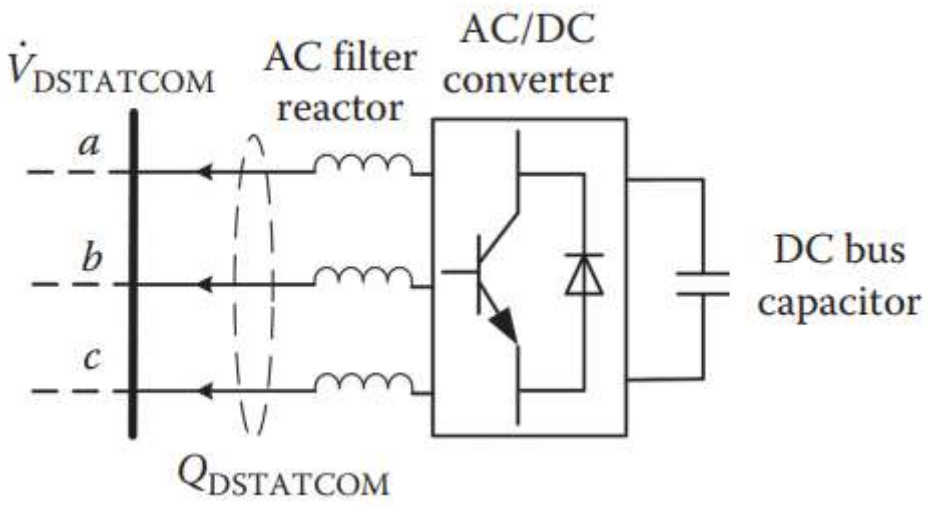

Figure 22: Schematic diagram of a DSTACOM [158]

The reactive power in the DSTATCOM is directly proportional to the voltage system. The typical control modes for a DSTATCOM are [158]:

- **V Control Mode:** where a DSTATCOM is configured for reactive power flow control at the DSTATCOM's point of connection. Here, the bus voltage is being controlled at a specified value with the bus regarded as a *PV* bus with active power output $P = 0$.
- **Q Control Mode:** where the reactive power is controlled to maintain the bus voltage at a specified value. Thus, at $P=0$, the bus can be regarded as a *PV* bus, and it is controlled at a specified value.

3. Methodology

The main objective of the study is to design an adaptive control system that will automatically adjust the characteristics of the controller to maintain the overall power system performance by compensating for variations in the dynamics of the power system. On the Lesotho electricity grid network, the Lets'eng wind farm was used as a case study for voltage control when a Renewable Energy system is connected to the electricity grid. Provided by the Lesotho Electricity Company (LEC), Lesotho's electrical grid network's Single-Line-Diagram as per the DIgSILENT PowerFactory software is shown in Figure 23.

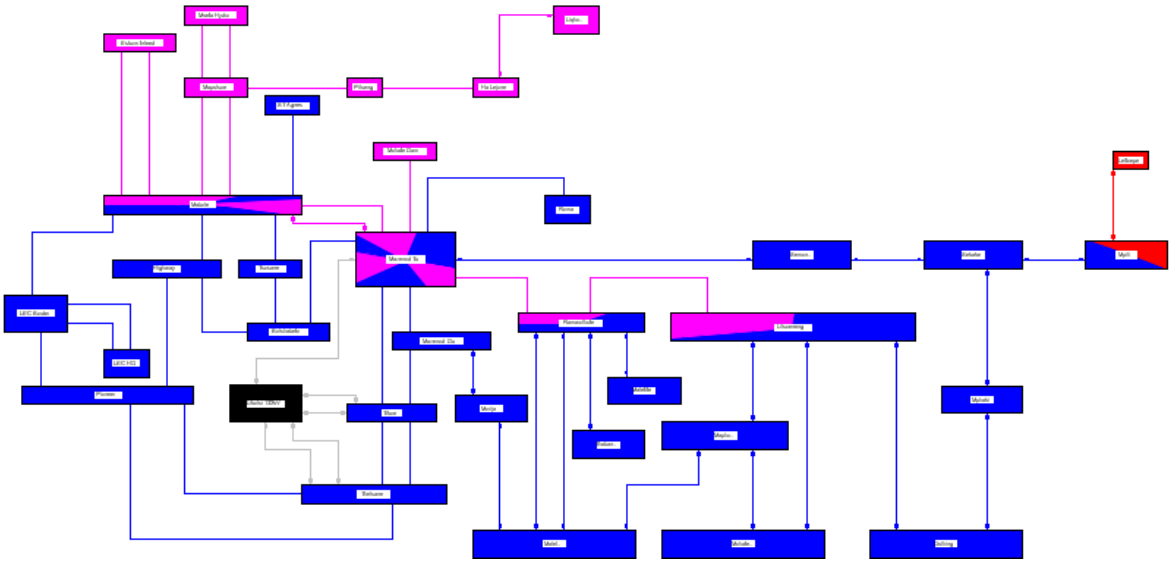

Figure 23: Lesotho Electricity grid network. The substation colour codes representing bus voltages as follows: purple for 132 kV, blue for 33 kV, red for 11 kV, and black for out of service substation

Within the network interconnections, the Lets'eng wind farm links to the 88 kV Khukhune bus bar, whose electric power is supplied the Eskom Clarens' external grid. It was therefore necessary to control the wind farm substation voltage to synchronize that of the Clarens external grid in real-time even when the wind power system is subjected to disturbances, or the external grid experiences voltage variations. For the adaptation analysis of each control method, the operational capability modification to achieve the best operational mode is determined by the closeness of the controlled bus voltages to the desired voltage value limit of 10 %. The robustness of the control strategy is measured by its ability to maintain the controlled bus voltages as close as possible when the system undergoes wind speed variations.

3.1. Wind farm system design

For the convenience of the study to accommodate the intermittency of wind energy, the Lets'eng wind farm was re-designed in the system modeling. Consisting of four 9.5 MW wind turbines, the rated capacity of the wind farm is 38 MW. The wind farm is shown in Figure 24.

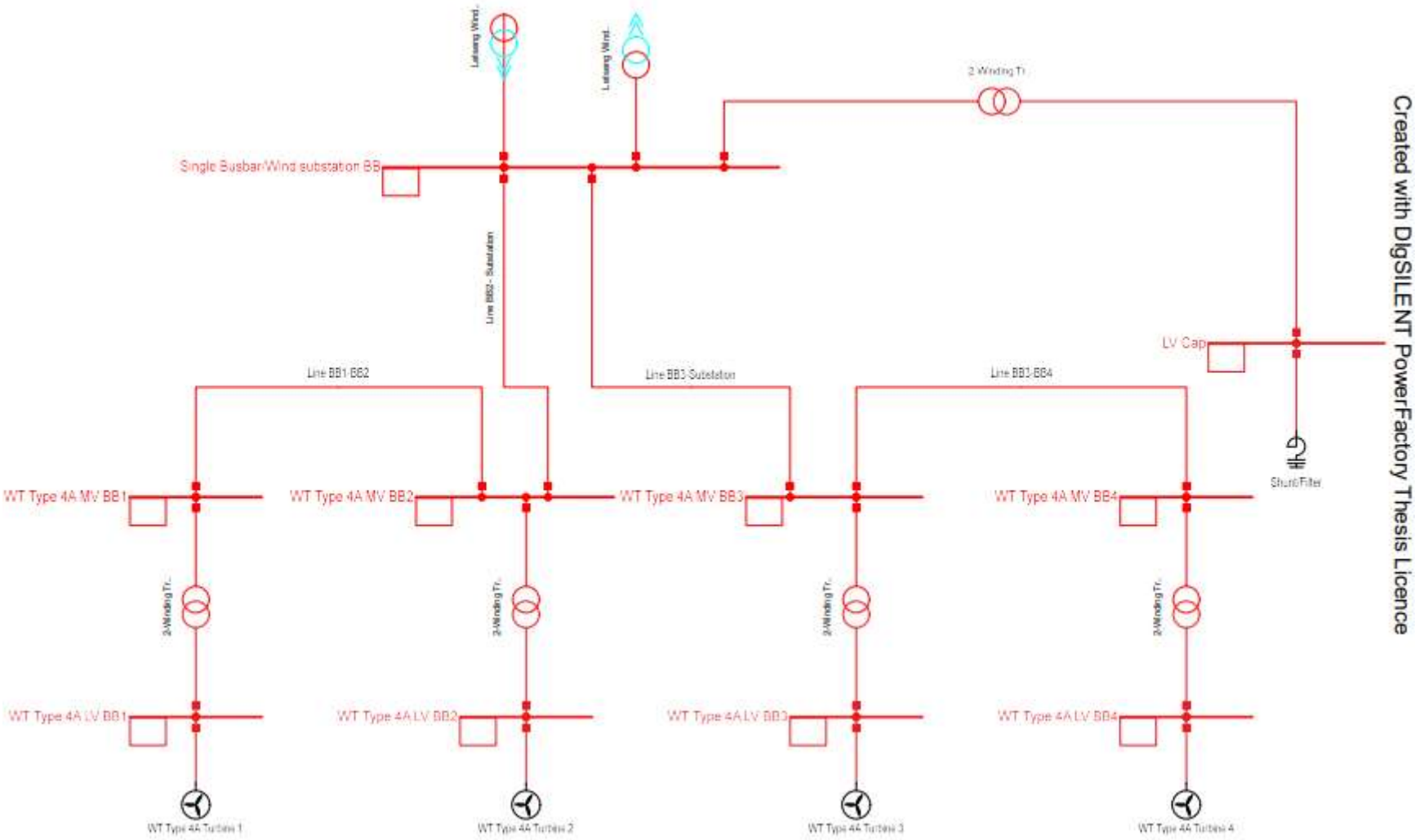

Figure 24: Lets'eng wind farm

Each wind generator is connected to a three-phase 380V LV bus bar, which in turn connects to a 0.38/11 kV step-up transformer that feeds the MV bus bar. With future growth anticipated, the transformer rating was chosen to be 10 MVA to provide sufficient headroom. The four MV bus bars are then connected to a single substation bus bar of the wind farm.

3.1.1. Wind turbine design

The Wind Turbine Generator (WTG) model used in the system is the Western Electricity Coordinating Council (WECC) Type 4A WTG connected through a full power scale converter. The capacity of each WTG was set at 10 MVA with a power factor of 0.95. The selected turbine input mode is the wind speed as well as the power factor. The power curve of the selected WTG is shown in Figure 25.

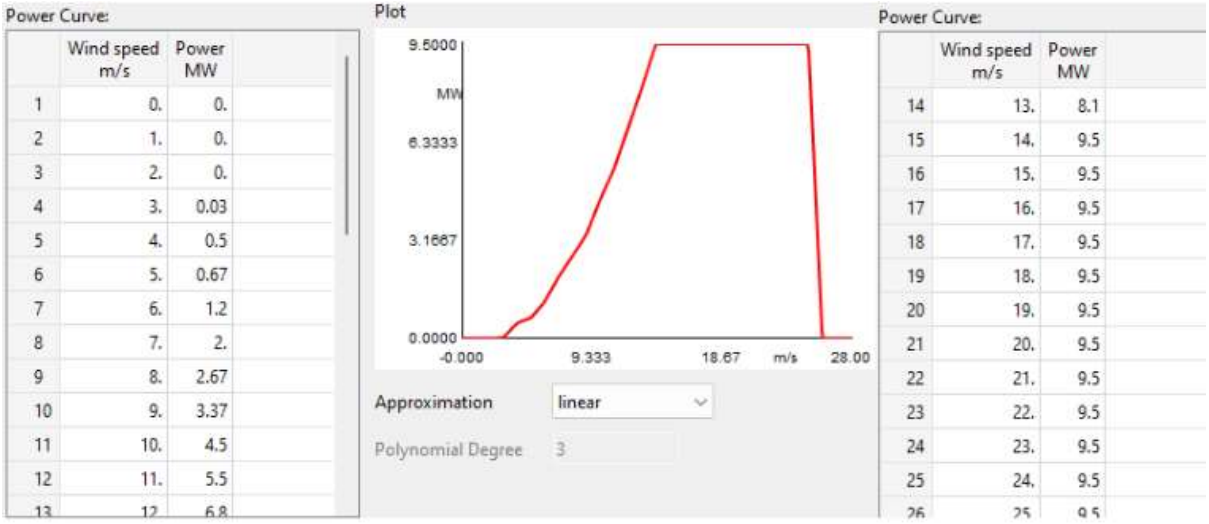

Figure 25: 9.5 MW WTG power curve

As illustrated in Figure 25, the cut-in speed of the WTG is 3.0 m/s. It is from this minimum wind speed that the WTG, with a hub height of 100m, starts to generate power. From the same speed, the generated power increases linearly with an increase in wind speed, reaching a maximum power output of 9.5 MW at the speed of 14.0 m/s. The constant maximum power output is then retained from 14.0 m/s wind speed to the cut-out speed of 25 m/s, beyond which the power output drops to zero.

3.1.2. Turbine Controller Configuration

The control of the WTG lies in the WECC type 4A control system Composite Frame Model. Having configured the rated power of the static generator, the nominal power and the power factor are the parameters used for the calculation of the rated active power. Through model aggregation, the total active power output is the product of each active power dispatch and the number of parallel paths. Figure 26 shows the composite frame model of the used WTG control system.

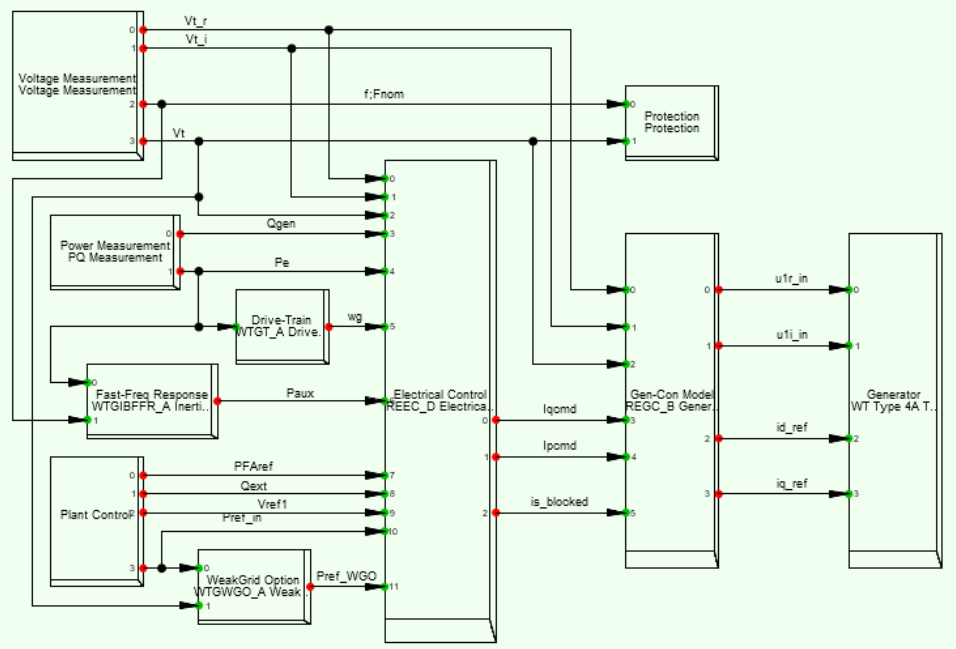

Figure 26: WECC type 4A wind turbine Composite Frame Model

In this composite frame model, the main contents of the control systems, as well as their descriptions, are [159]:

- Generator: This represents the wind turbine generator in the network model
- WTGT_A: It is used for the implementation of WTG torsional mode oscillations' behavior
- WTGAR_A: To implement the aero-dynamics linear model of the WTG
- WTGTRQ_A: Based on the speed or power error to compute the power command, it implements the corresponding operation mode
- WTGIBFFR_A: For cases of under-frequency events and system frequency decrease, it initiates the auxiliary inertial-based fast frequency response
- WTGWGO_A: In the event of a weak grid, it implements a supplemental option control
- REEC_D: Its function is to implement the electrical control mode via the control of reactive power injections
- REGC_B: It acts to interface the generator and converter, and implements the fast converter controllers
- Protection: For disconnection of the system from the grid in cases of frequency and voltage limit violations
- Plant Control: For determination of commanded active and reactive currents, it implements the plant controller
- Voltage and power measurement: To measure the voltages and power within the network elements of control

3.1.3. Wind farm Substation design

The wind farm substation design is illustrated in Figure 27. It shows the main bus bar that connects the wind farm elements and the interface with external elements.

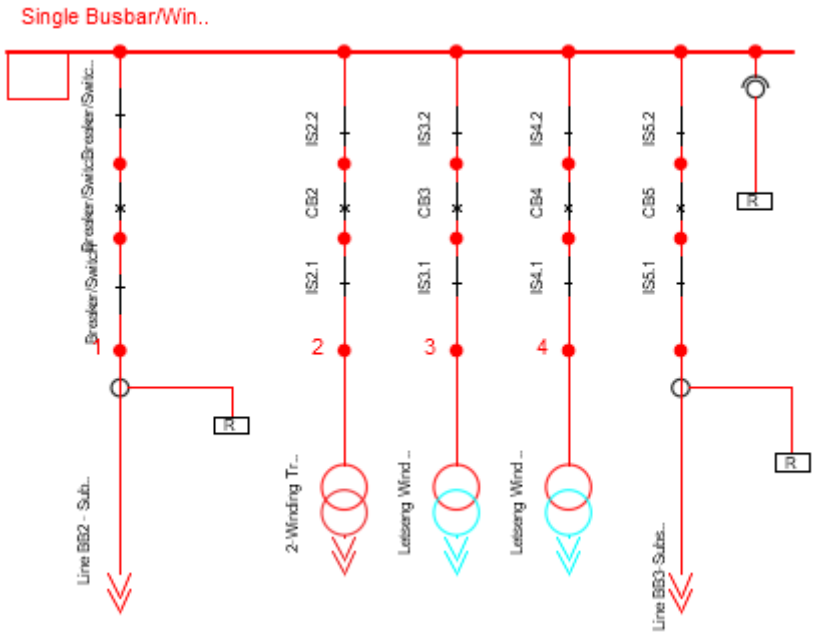

Figure 27: Wind farm 11 kV substation

The wind farm contains the following critical elements:

- Two 11/88 kV 2-windings transformers connect the MV bus bar to two 88 kV HV bus bars that feed the external grid with power from the wind farm.
- 11/0.38 2-windings transformer that is connected to the LV cap of the capacitor bank for reactive power compensation.
- Two current transformers are used for overcurrent protection of the lines that connect the 11 kV MV bus bars to the substation bus bar.
- A voltage transformer that regulates the bus voltage of the substation bus bar.
- Circuit breakers and switches for additional overcurrent protection.

3.2. Study cases and operation scenarios

Different study cases are considered to study the behavior of the controller under different Reactive Power/Voltage Controls. Figure 28 shows the study cases under analysis as well as different studied scenarios of operation as configured in PowerFactory DIgSILENT.

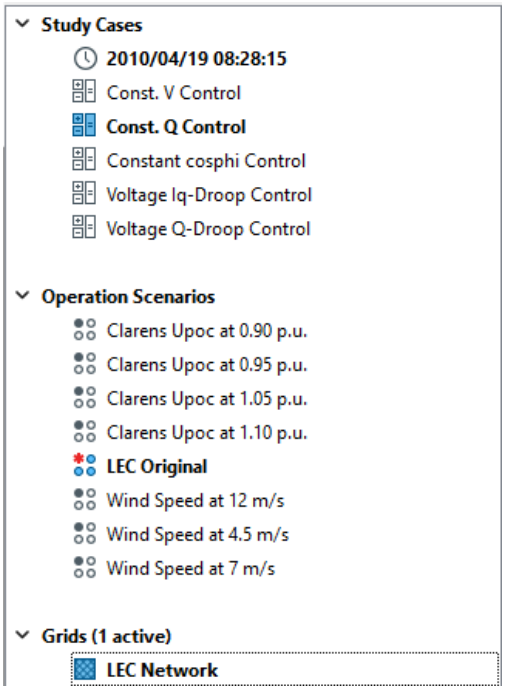

Figure 28: Study cases and operation scenarios in DIgSILENT

3.2.1. Constant voltage control

The synchronous generators at power stations operating in voltage control mode are utilized to directly manage the voltage at their terminals. The voltage at these terminals serves as the reference for the controlled per-unit (p.u.) value. The designated station controller regulates the voltage at a remote bus bar and coordinates bus bar voltages supplied by multiple WTGs.

The equation governing the addition of an offset to the generator-specified reactive power operating point is:

$$Q = Q_0 + K.\Delta Q_{SCO} \qquad \textit{Equation 32}$$

For this study case, the controller response is analyzed for different operating scenarios.

3.2.2. Voltage Q-Droop Control

Corresponding to the proportional control, the amount of reactive power injected varies as the voltage set-point deviation. A droop value is entered when the system is set to q-droop control. Voltage Q-Droop control is illustrated in Figure 29.

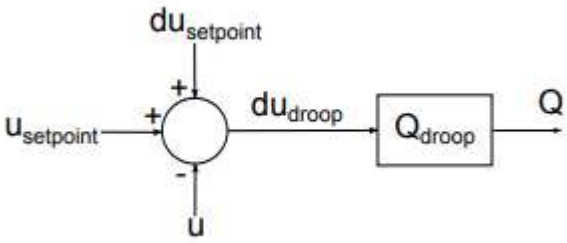

Figure 29: Voltage Q-Droop Control

For control of the local bus bar, the following set of equations applies:

$$u' = u_{setpoint} + du_{setpoint} - \Delta u_{droop} \qquad \textit{Equation 33}$$

$$u = \begin{cases} usp_{max}, & if\ u > usp_{max} \\ usp_{min}, & if\ u < usp_{min} \\ u', & if\ u \geq usp_{min}\ and\ u_s \leq usp_{max} \end{cases} \qquad \textit{Equation 34}$$

$$\Delta u_{droop} = \frac{Q - Q_{setpoint}}{Q_{droop}} \qquad \textit{Equation 35}$$

$$\mathrm{Q_{droop}} = \frac{100\ \mathrm{S_r}}{\mathrm{d_{droop}}} \qquad \textit{Equation 36}$$

where:

- u is the actual terminal voltage value
- $u_{setpoint}$ is the specified voltage set point
- usp_{max} and usp_{min} are the maximum and minimum voltage set-points
- Δu_{droop} is the voltage deviation
- $du_{setpoint}$ is the voltage coming from the Voltage Set-point Adaptation Station Controller
- Q is the reactive power output
- $Q_{setpoint}$ is the reactive power dispatch
- Q_{droop} is the voltage droop additional reactive power
- S_r is the rated apparent power
- d_{droop} is the percentage value of the voltage droop value

For usp_{max} and usp_{min} to be considered, the load option “Consider reactive power limits” is enabled.

3.2.3. Voltage IQ-Droop Control

In this study case, the reactive current calculation is based on the element voltage set-point deviation.

The system control block diagram of this study case is illustrated in Figure 30.

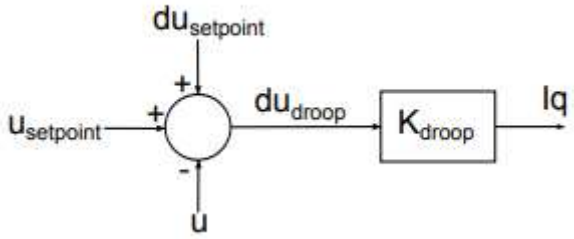

Figure 30: Voltage IQ-Droop Control

For the control of the local bus bar, the voltage IQ-Droop Control is governed by *Equation 33* and *Equation 34*, with all symbols retaining their meaning as in Q-Droop Control. Additional equations for the IQ-Droop control study case are:

$$\Delta \mathrm{u}_{\mathrm{droop}} = \frac{\mathrm{Iq} - \mathrm{Iq}_{\mathrm{setpoint}}}{\mathrm{K}_{\mathrm{droop}}.\,\mathrm{Ip}_{\mathrm{r}}} \qquad \textit{Equation 37}$$

with the reactive current set-point as:

$$\mathrm{Iq}_{\mathrm{setpoint}} = \frac{\mathrm{qgini.\,ngnum}}{\sqrt{3}\mathrm{U}_{\mathrm{nom}}} \qquad \textit{Equation 38}$$

and the rated active being:

$$\mathrm{Ip}_{\mathrm{r}} = \frac{\mathrm{sgn.\,ngnum.\,cosn}}{\sqrt{3}\mathrm{U}_{\mathrm{r}}} \qquad \textit{Equation 39}$$

where:

- Iq is the machine's reactive current output in kA
- $Iq_{setpoint}$ is the machine reactive current set-point in kA
- K_{droop} is the controller gain
- $qgini$ is the set-point of the reactive power in MVA
- $ngnum$ is the number of parallel WTGs
- U_{nom} is the corresponding connected bus bar nominal voltage in kV
- U_r is the machine-rated voltage in kV
- Ip_r is the rated active current in kA
- sgn is the rated power in MVA
- $cosn$ is the rated power factor

In this study case, instead of the machine's rated voltage, the nominal voltage of the connected bus bar is referenced in the calculation of the dispatched reactive current.

3.2.4. Constant power factor Control (Const. cosϕ)

The study case makes use of the local controller to act as a reactive power controller. To keep the power factor constant, the reactive power set-point is adapted per the WTG's active power output. Under normal circumstances, the mode acts as a constant reactive power control, thereby enabling the specification of the active and reactive power dispatch of the generator. Upon the activation of the secondary controller, or when the load flow balancing by the generator is based on the slack distribution, the constant reactive power mode is deactivated, and the constant power factor mode is enabled to accommodate the varying active power output.

3.2.5. Point of Connection Voltage (Upoc) Operation Scenarios

In these operation scenarios, the wind farm WTGs control is investigated under different voltages of the Khukhune 88kV bus bar that is connected directly to the external Clarens grid. From the load flow of the external grid, the voltage set-point is set to different per-unit values concerning the 88 kV Khukhune grid. The voltage set-points per unit under investigation are 0.90, 0.95, 1.00, 1.05, and 1.10, thus corresponding to the bus voltages of 79.2 kV, 83.6 kV, 88 kV, 92.4 kV, and 96.8 kV, respectively, and for each operation scenario, comparisons are made for the control study cases. The adaptation and robustness of each control method are measured from the bus voltages for a change in the external grid voltage set-point. The voltage levels under investigation are of the following bus bars:

- Khukhune 88 kV
- WT Type 4A LV (BB1, BB2, BB3, BB4)
- WT Type 4A MV (BB1, BB2, BB3, BB4)
- Wind substation (11 kV)
- Letseng Wind 88 kV (BB1, BB2)

3.2.6. Wind Speed Variations Operation Scenarios

The control strategies are evaluated and compared for adaptation and robustness of each voltage set-point per unit value for the Khukhune 88 kV bus bar, in parallel with the operation scenarios in section 3.2.2. The voltage response is tested at wind speeds of 4.5 m/s, 7.0 m/s, 12.0 m/s, and 14.0 m/s. For each wind speed, the performance of each control strategy at different voltage set-points is analyzed and ranked when voltage variations are applied to the Clarens external grid.

3.3. Fault-tolerance and Service Restoration

For a fault case created at a wind speed of 14.0 m/s and a POC voltage of 1.00 p.u., the system response is determined for each control strategy. A three-phase short circuit is created at 3.2 seconds and cleared at 3.4 seconds. Upon a short-circuit encounter, the system automatically isolates from the HV bus bar and the respionse time of each control strategy is evaluated. The restoration after a fault clearance is also analysed for each control strategy when the fault has been cleared.

3.4. Condition Monitoring and Instrumentation

Assuming the presence of field instruments for measuring wind speeds and voltage at the point of connection, a SCADA system is designed to monitor wind speeds at various bus voltages for the POC bus bar. The SCADA system is developed using Apache NetBeans IDE 22, with its graphical user interface programmed in Java. The control strategy that best adapts to each operating scenario is selected by the determination algorithm integrated into the SCADA system design.

4. Results and Interpretation

The previous chapter provided an in-depth model of the grid-connected renewable energy system. Five study cases were implemented, each introducing a distinct control strategy focused on self-adaptation and robustness. This chapter assesses the outcomes of these control strategies and ranks them based on their performance across different operational scenarios. Adaptation analysis is centered on the voltage deviation from the (POC) bus voltage, while robustness is evaluated by the system's ability to maintain stable operation under both normal and disturbed conditions. Additionally, robustness is assessed by examining voltage deviations at various wind speeds for each POC voltage set-point. The power system analysis methods used include electromechanical transient time-domain simulations and load flow analysis.

4.1. Results discussion for steady wind speeds

This section discusses the system response for each control strategy for both transient and steady states. Comparisons are made for different wind speed scenarios and unique conclusions are drawn independentlybfor each wind speed scenario. A correlation analysis method is also used to validate the results for each study case's control strategy and performance evaluation is made.

4.1.1. Voltage control at 14.0 m/s wind speed

For the proposed control strategies, a 10-second RMS time domain simulation was performed at different values of the point of connection bus voltage. The result visualization simulation plot is presented in Figure 31 for all study cases under 14.0 m/s wind speed.

In Figure 31a for the point of connection voltage at 0.90 p.u., the curve with the least margin from the 0.90 p.u. Khukhune bus bar is of the voltage Iq-Droop. It is, therefore, considered to be the most adaptive to achieve the desired voltage set-point. However, in its attempt to attain the desired voltage, the voltage Iq-droop continuously ramps up and down from its settling point for this duration of 10 seconds, hence compromising its robustness to maintain a stable operation. Const. Q and Const. V display equally prominent curves and are the second-ranked adaptive controllers as they have the second least margin from the desired set-point. The difference between the two controllers is the lower robustness of Const. V, which ramps down twice from the maintained voltage, while Const. Q maintains its voltage for the whole duration. The next adaptive controllers are the Voltage Q-Droop and the Const. cosϕ which have also maintained their robustness for the simulation duration. It is therefore concluded that the Const. Q, Voltage Q-Droop, and Const. cosϕ are the most robust controllers, followed by Const. V, and lastly, Const. Q for 0.90 p.u. voltage of the POC when the wind speed is 14.0 m/s. The results, therefore, indicate a trade-off between adaptation and robustness for this operation scenario since the most adaptive control strategy is not the most robust.

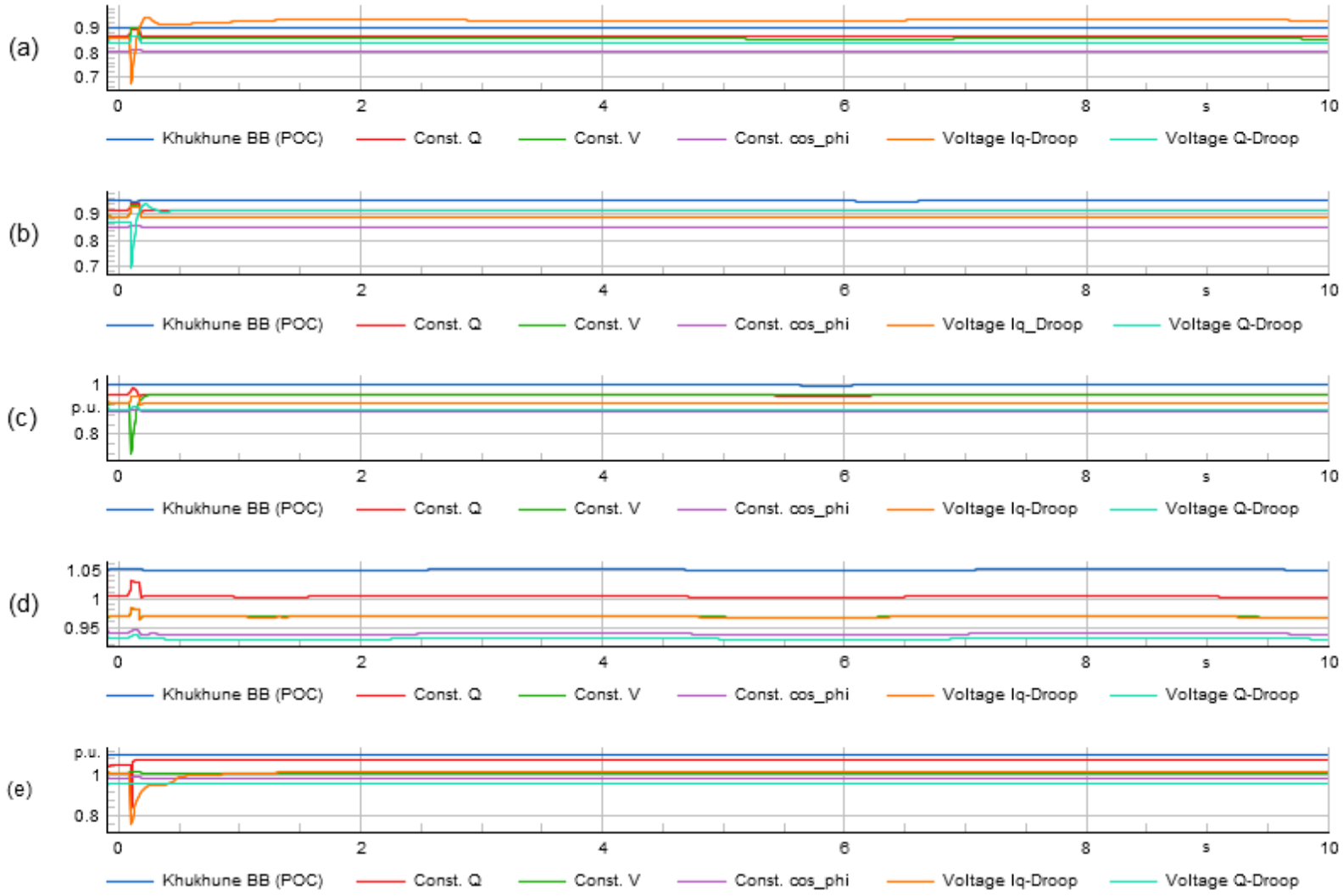

Figure 31: RMS simulation for control strategies at wind speed = 14 m/s: (a) Upoc=0.90 p.u. (b) Upoc=0.95 p.u. (c) Upoc=1.00 p.u. (d) Upoc=1.05 p.u. (e) Upoc=1.10 p.u.

Applying the same evaluation criteria for POC voltage at 0.90. p.u., conclusions drawn from the other four operation scenarios in Figure 31 for dynamic state simulation at the wind speed of 14.0 m/s are as follows:

- In Figure 31b when the point of the connection voltage set-point is 0.95 p.u., the order of the controller adaptation is Const. Q and Voltage Q-Droop, Const. V, Voltage Iq-Droop, and lastly, Const. cosϕ. A similar extent of robustness is portrayed by all control strategies. For this particular scenario, the best-performing control strategies are the Const. Q and Voltage Q-Droop by being the most adaptive when all controller strategies are equally robust.
- From Figure 31c,at 1.00 p.u. set-point of the POC voltage, the adaptation order is first Const. Q and Const. V, followed by Voltage Iq-Droop, and lastly Const. cosϕ and Voltage Q-Droop. With most controllers equally robust, the difference between the Const. Q and Const. V is the ramp-down in Const. Q at around t=5s, thus Const. V is the best control strategy in this scenario. It is worth noting that during the ramp-down period of Const. Q, the POC voltage experiences a short ramp down. This can in no way be regarded as an adaptation of Const. Q responding to a change in POC voltage. It is evident that the Const. Q deviated before the voltage drop of the set-point voltage.
- The most adaptive controller at 1.05 p.u. POC voltage shown in Figure 31d is the Const. Q, followed by Const. V and voltage Iq-Droop, Const. cosϕ, and lastly, the Voltage Q-Droop. Determined by the least voltage ramps, the most robust controllers are the Const. V and Const. cosϕ, and the three other controllers are equally and least robust. Therefore, the Const. V is the best control strategy for this scenario.
- At 1.10 p.u. POC voltage set-point in Figure 31e, the Const. Q is the most adaptive controller. It is followed by the Voltage Iq-Droop. Const. V precedes Const. cosϕ, while Voltage Q-Droop is the least adaptive controller. Although all controllers demonstrate a highly robust response, there is a slight voltage ramp down in the Voltage Iq-Droop, which is categorized below all the other controllers. The operation scenario concludes that the Const. Q is the strategy of choice.

Still, at the wind speed of 14.0 m/s, the steady-state load flow analysis was performed to analyze the response of each control strategy under steady-state conditions. As with the dynamic analysis, each control strategy study case in this operation scenario was analyzed for different values of the point of connection voltage set-point. The voltage match of the system high voltage (HV) bus bar to the point of connection voltage is benchmarked against the desired ±5 % limit as well as against the SANS 10142-3:2012 and IEC TS 62749:2020 standards. The steady-state system bus voltages as per the load flow at a wind speed of 14.0 m/s are presented in Table A2 of Appendix A.

The last three columns in Table A2 are used for the analysis of voltage compliance to the grid voltage desired deviation set-point. The aim is to limit the HV supply voltage to ±5 % fluctuations of the POC bus voltage.

When the POC voltage is set to 0.90 p.u., the voltage matches for Const. V, Const. cosϕ, Voltage Iq-Droop, Voltage Q-Droop, and Const. Q is 0.996338, 0.911742, 1.03548, 0.994697, and 1.01553, respectively, therefore corresponding to -0.37 %, -8.83 %, +3.55 %, -0.53 %, and +1.55 % voltage fluctuations. Thus, for the set ±5 % set margin, all control strategies but Const. cosϕ meets the set voltage match with Const. V as the controller with the best voltage match. However, since the wind power generation station connects to the Clarens Eskom grid from South Africa, the Const. cosϕ still meets the South African set standard, SANS 10142-3:2012, as well as the international standard, IEC TS 62749:2020. The requirement of these two standards is for the exclusion of interruption periods, the power supplier should comply with the voltage percentiles in the boundary of 10 % under normal operating conditions [160]. The compliance of the two standards is being met by the Const. cosϕ, operation continues under this control strategy, but mitigation measures should take place to meet the local plant compliance of 5 % margin regarded as a key performance indicator (KPI). This can be achieved by autonomously switching to a locally compliant strategy as programmed in the control system design.

At 0.95 p.u. POC voltage set-point, the best voltage match is achieved by the Voltage Iq-Droop at -0.25 %, followed by Const. Q at 1.03 %, Const. V, Voltage Iq-Droop, and Const. Cosϕ at -3.82 %, -4.01 %, and -9.03 % respectively. Besides the Const. cosϕ which only meets the requirements of the two standards, all other control strategies are within the locally set voltage margin.

Setting the POC voltage to 1.00 p.u. allows all but the Voltage Q-Droop to attain local generation compliance, although it still meets the standards at -7.38 % voltage deviation. It is worth highlighting that for the Const. cosϕ and Const. Q, the two best scenario controllers at +0.5 % deviation, have identical values for all bus voltages. Equally important to note, the Const. Cosϕ acts as Const. Q control thereby enabling the specification of the active and reactive power dispatch of the generator with no activation of the secondary controller, hence the two controllers are practically identical for this scenario. With Voltage Iq-Droop and Const. V at -3.72 % and -3.82 %, respectively, it is only the Voltage Q-Droop that meets the requirements of the two standards at -7.38 .

Interestingly, at 1.05 p.u. POC voltage, when the Const. Q achieves a 100 % voltage match to the POC voltage, none of the other control strategies meets the local deviation threshold. Furthermore, the Const. V and Voltage Q-droop at -10.40 % and -10.44 %, respectively, do not even comply with the HV standards. Although they do not meet the local voltage KPIs, the Const. cosϕ and Voltage Q-Droop at

-9.38 % and -6.50 %, respectively, are within the HV fluctuations limit and can therefore still be used for power supply to the grid. However, for system optimization, switching the control mode to Const. Q would yield an optimal performance for this particular scenario.

When the POC voltage is set to 1.10 p.u., it is only the Const. Q that complies with the 5 % local voltage boundary limit at -0.48 %. At -7.66% and -9.50 %, the Voltage Iq-Droop and Const. cosϕ only comply with the South African and International standards, whereas- the Const. V is completely non-compliant at a deviation of -13.38 %. Therefore, the Const. V should not be considered for voltage control in this scenario.

4.1.2. Voltage control at 12.0 m/s wind speed

At a wind speed of 12.0 m/s, a 10-second RMS time domain simulation run for different values of the point of connection bus voltage is presented in Figure 32. The simulation curves' results are interpreted as follows:

When the POC bus voltage is set to 0.90 p.u. as shown in Figure 32a, the most adaptive controller is the Const. V with the least margin from the Khukhune bus voltage. It is, however, the controller with the least robustness degree, having the most voltage ramps for the 10-second time domain simulation. While the Const. Q and Voltage Iq-Droop are the next adaptive controllers, followed by Voltage Q-Droop and lastly Const. cosϕ, these controllers are equally robust with no ramps along the propagation.

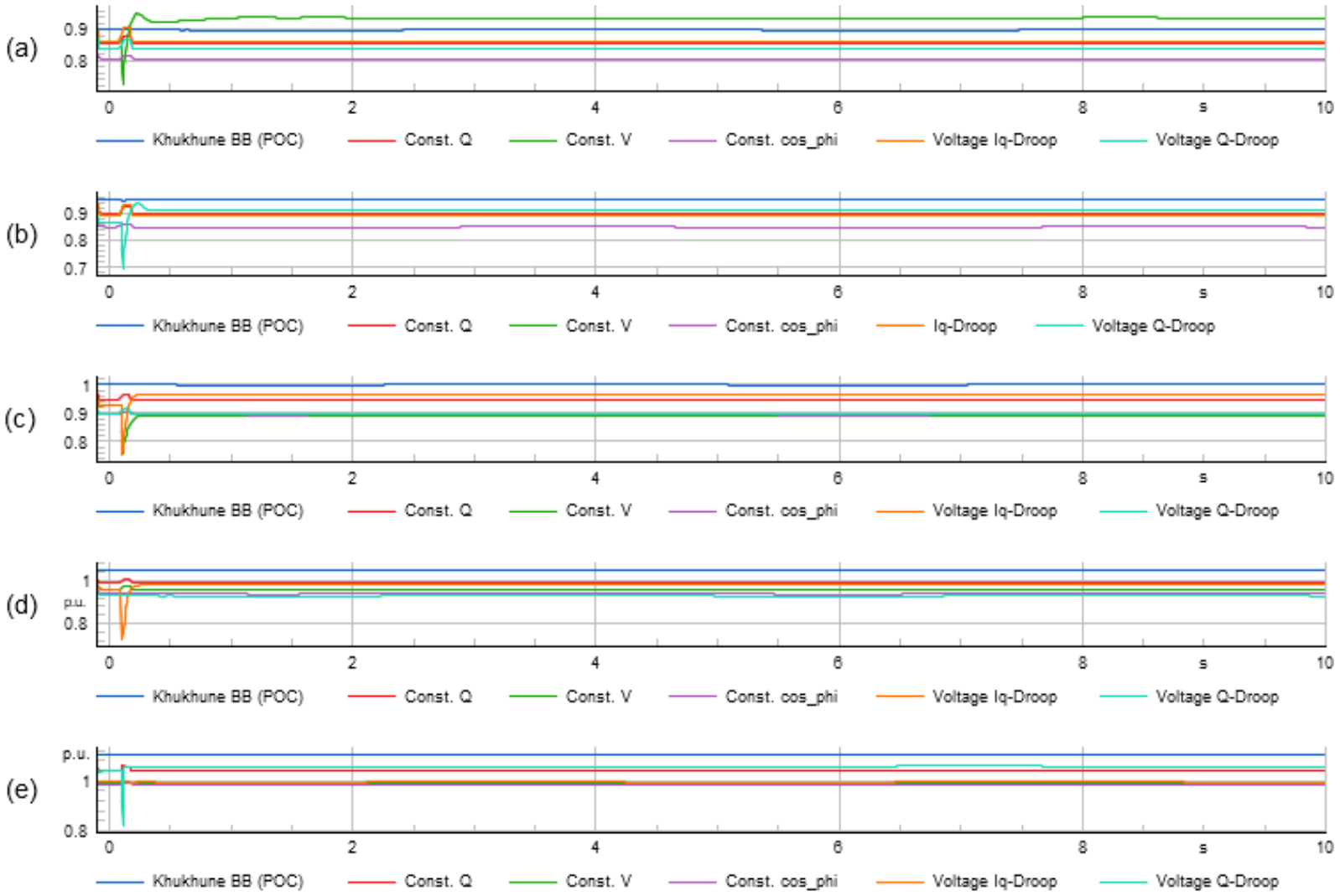

Figure 32: RMS simulation for control strategies at wind speed = 12 m/s: (a) Upoc=0.90 p.u. (b) Upoc=0.95 p.u. (c) Upoc=1.00 p.u. (d) Upoc=1.05 p.u. (e) Upoc=1.10 p.u.

Setting the POC voltage at 0.95 p.u. in Figure 32b when the wind speed is 12.0 m/s favours the adaptation to the Voltage Q-Droop, which is followed by the equally adaptive Const. Q, Const. V, and Voltage Iq-Droop while the Const. cosϕ is the least adaptive control strategy. All controllers but the Const. cosϕ, the only controller with voltage ramps, are equally robust.

As observed in Figure 32c with complete robustness in all controllers beyond the overshoot settling point, the only difference in the controllers when the POC voltage is set at 1.00 p.u. is the adaptation. The most adaptive controller is the Voltage Iq-Droop followed by the Const. Q, and lastly, the Const. V, Const. cosϕ, and Voltage Q-Droop which are at equal footing.

Figure 32d at 1.05 p.u. POC voltage set-point, the adaptation prominence lies on the Const. Q followed by the Voltage Iq-Droop, and lastly, the Const. V. These three controllers portray a visually equal robustness extent with no voltage amplitude fluctuations for the entire simulation period. Not only are the Const. cosϕ and Voltage Q-Droop the least adaptive controllers, but they are also the only controllers which have fluctuating voltage amplitudes, hence experiencing a compromised robustness level.

Figure 32e for the POC voltage set-point of 1.10 p.u., the most favorable adaptive controller is the Voltage Q-Droop followed by the Const. Q. The less adaptive controllers: the Const. V, Const. cosϕ and Voltage Iq-Droop have overlapping curves with some level of voltage ramps. With the Voltage Q-Droop also showing a voltage magnitude fluctuation along a certain time period, the Const. Q is recognizable as the most robust controller with a straight line on the RMS simulation curve.

When analyzing each control strategy's steady-state response at a wind speed of 12.0 m/s, the results for the steady-state load flow analysis are presented in Table A3, where each system's HV bus bar is compared to the POC voltage and evaluated for compliance.

When the voltage set-point is 0.90 p.u., the voltage match for the HV bus bars is 1.042172 for the Const. V, 0.995328 for both the Const. cosϕ and Const. Q, 1.041035 for both the Voltage Iq-Droop and Voltage Q-Droop, corresponding to voltage deviations of +4.22 %, -0.47 %, and 4.10 %, respectively, meaning the compliance of all control strategies to the locally set voltage deviation of ±5 %, both the SANS 10142-3:2012 and IEC TS 62749:2020 standards that allow a maximum deviation of 10 %. Likewise, complete compliance for all system requirements is met by all control strategies when the POC voltage is set to 0.95 p.u., where voltage deviations of +0.26 %, -1.02 %, 0.19 %, and 0.20 % are obtained for the Const. V, Const. cosϕ as well as the Const. Q, Voltage Iq-Droop, and Voltage Q-Droop, respectively. This is also the case when the POC is at 1.00 p.u., where the voltage deviations are -3.40

%, -1.51 %, -3.35, and -1.51 for the Const. V, Const. cosϕ, Voltage Iq-Droop as well as the Voltage Q-droop, and Const. Q, respectively.

When the POC voltage set-point is increased to 1.05 p.u., the local voltage fluctuation compliance is lost in three controllers. Only the Const. cosϕ and Const. Q meet the requirement of a 5 % boundary limit at -1.97 % for both strategies. This limit is exceeded by the Const. V, Voltage Iq-Droop, and Voltage Q-Droop, although they are still well within the grid connection limits of 10 % and therefore can still be used while mitigation strategies are employed to meet the local voltage fluctuation KPI.

Still behaving as the Const. Q at 1.10 p.u. POC voltage, the Const. cosϕ meets all the system requirements as per the Const. Q's compliance, which is at -2.38 %. The other three controllers violate the local voltage obligation, yet they still comply with the set standards as they are well within the boundary limit of 10 %. The Const. V experiences -9.67 %, while the Voltage Iq-Droop and Voltage Q-Droop are at -9.43 % and -9.44 %, respectively.

4.1.3. Voltage control at 7.0 m/s wind speed

At a wind speed of 7.0 m/s, a 10-second RMS time domain simulation was again run for different values of the point of connection. The dynamic simulation results for the system bus voltages for this scenario are presented in Figure 33.

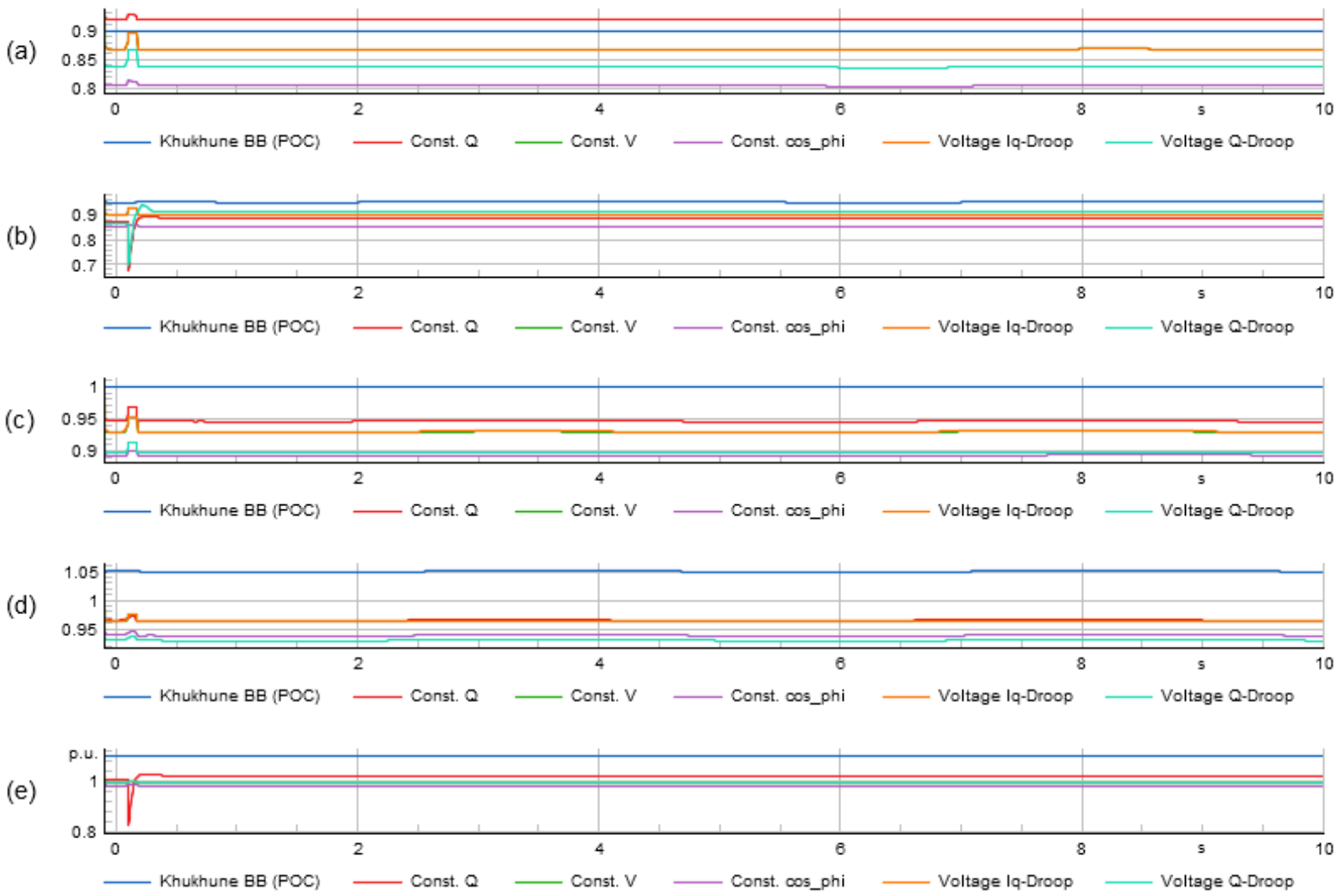

Figure 33: RMS simulation for control strategies at wind speed = 7 m/s: (a) Upoc=0.90 p.u. (b) Upoc=0.95 p.u. (c) Upoc=1.00 p.u. (d) Upoc=1.05 p.u. (e) Upoc=1.10 p.u

For the RMS simulations shown in Figure 33, the analysis of the control strategies' response at a wind speed of 7.0 m/s is as follows:

Figure 33a at 0.90 p.u. POC voltage set-point, the Const. Q is the controller whose amplitude is closest to that of the point of connection. It is then followed in marginal difference by the Voltage Iq-Droop, which is followed by the Voltage Q-Droop, Const. cosϕ, and lastly Const. V. Not only is the Const. Q the most adaptive controller, but it is also the most robust controller, followed by the Voltage Iq-Droop, Voltage Q-Droop, and lastly, the Const. cosϕ. Although a single voltage ramp exists for the three least robust controllers, the extent of the robustness loss has been categorized by the duration of each voltage deviation. Hence, the Voltage Iq-Droop is classified as more robust than the Voltage Q-Droop and Const. cosϕ because its deviation has the least duration. The invisibility of the Const. V in Figure 33 is the indication that its behavior is similar to that of one of the strategies whose curve has overlapped and overshadowed the Const. V. As a result, the response of the Const. V is inconclusive as it cannot be determined from the response curves.

Figure 33b with all visible controllers displaying equally complete robustness for the POC voltage at 0.95 p.u., the order of the strategies adaptation is first, the Voltage Q-Droop, followed by the Voltage Iq-Droop, Const. Q, and lastly, the Const. cosϕ.

Succeded by the Const. V and Voltage Iq-Droop in Figure 33c, the Const. Q is the controller demonstrating the highest voltage adaptation to the point of connection at 1.00 p.u. POC voltage. The next adaptive controller is the Voltage Q-Droop, while the Const. cosϕ is the least adaptive strategy. It is worth noting that despite its low adaptation ability, the Voltage Q-Droop is the only control strategy with complete robustness for this scenario as it is the only controller without any voltage ramps along the 10-second dynamic response analysis.

As the most robust controller without any voltage amplitude deviations at 1.05 p.u. POC voltage in Figure 33d, the Voltage Iq-Droop is the most adaptive controller along Const. Q. The other visible controllers are the Const. cosϕ and Voltage Q-Droop in descending adaptation order.

In Figure 33e there are only three visible controllers at the POC voltage of 1.00 p.u., with the Const. Q being the most adaptive, followed by Voltage Q-Droop, and lastly, the Const. cosϕ. All the controllers appear to be equally robust beyond the controllers' setting times. Therefore, the Cons. Q is the most favorable control strategy for this particular scenario.

Still at the wind speed of 7.0 m/s, a load flow was performed for the steady-state analysis of all the control strategies. The results for all system bus voltages are shown in Table A4.

At a POC voltage of 0.90 p.u., all controllers meet the South African and international grid voltage standards, with the Const. V having a voltage match of +2.73 %, the Const. cosϕ and Voltage Q-Droop at -6.27 %, while the Voltage Iq-Droop is at +2.74 %, and Const. Q is at -3.16 %. Only the Const. cosϕ and Voltage Q-Droop do not comply with the local set voltage limit as they exceed the 5 % boundary. Changing the POC voltage to 0.95 p.u. shifts the local non-compliance to the Const. cosϕ and Const. Q, both at -6.48 %, while all other strategies fully comply with the local KPIs and the two standards. A similar compliance case is observed when the POC voltage is at 1.00 p.u., with the two control strategies still not complying with the local voltage set variation of 5 % as they both have a voltage match of -6.66 %. It is interesting to observe that for both POC voltages of 1.05 p.u. and 1.10 p.u., none of the control strategies meet the local set requirement, as all HV voltages are above the 5 % margin. However, all controllers can still be utilized with precise monitoring as they are below the grid voltage standards of 10 % boundary limits.

4.1.4. Voltage control at 4.5 m/s wind speed

At a wind speed of 4.5 m/s, a 10-second RMS time domain simulation was once more run for different voltage values of the point of connection. The dynamic simulation results for the system bus voltages for this scenario are presented in Figure 34.

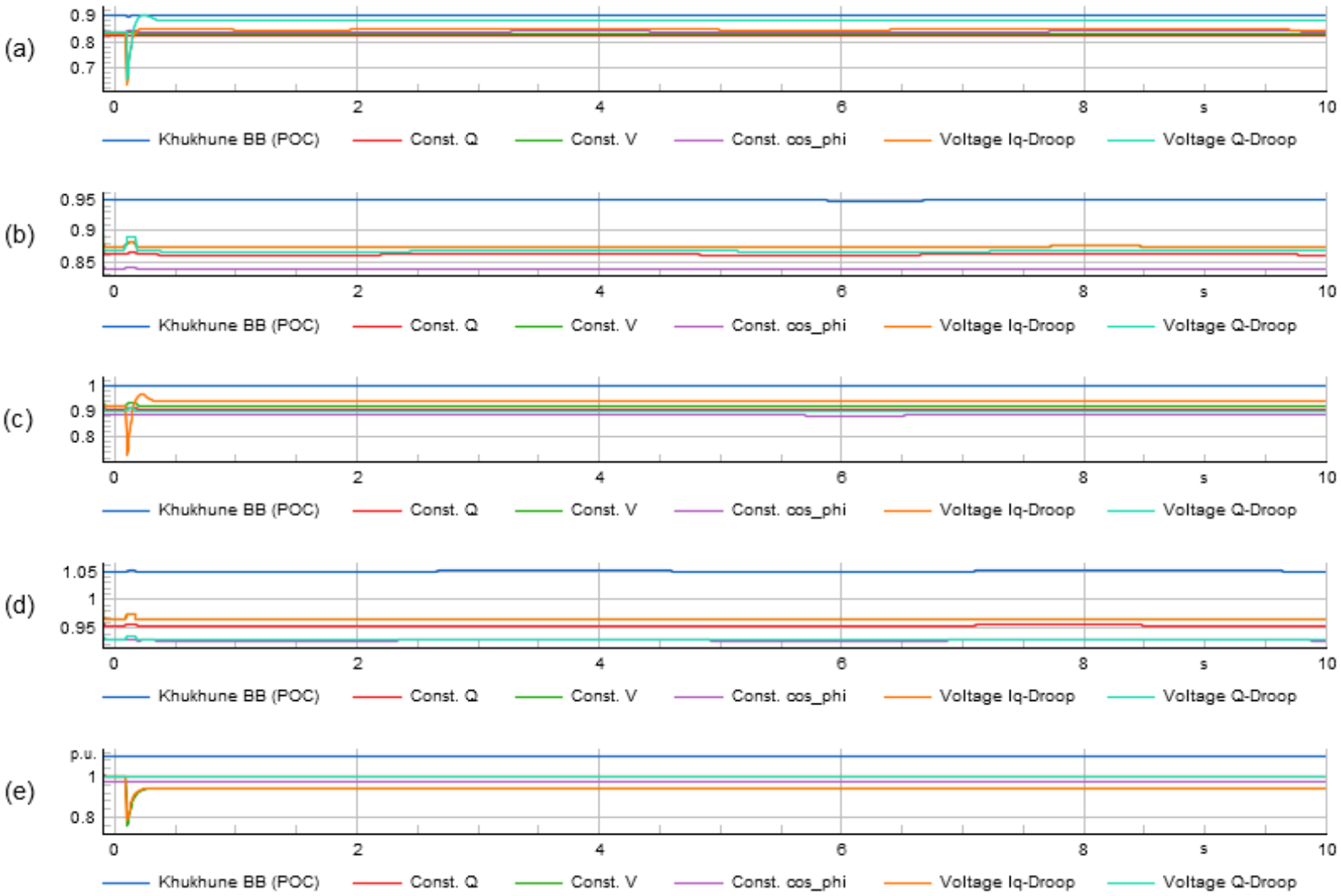

Figure 34: RMS simulation for control strategies at wind speed = 4.5 m/s: (a) Upoc=0.90 p.u. (b) Upoc=0.95 p.u. (c) Upoc=1.00 p.u. (d) Upoc=1.05 p.u. (e) Upoc=1.10 p.u.

In Figure 34a when the POC voltage is set to 0.90 p.u., the Voltage Q-Droop can clearly be recognised to be the most adaptive and robust controller from its lowest voltage margin from the POC voltage, as well as its consistent propagation without any voltage ramps. The second most adaptive Controller which is the Const. Q experiences voltage deviations and, therefore, has a compromised level of robustness. The response curves of the remaining controllers are intertwined, and the controllers cannot be distinguished with high precision. Hence, their evaluation is left inconclusive.

In Figure 34b for the visible controllers at a POC voltage of 0.95 p.u., the order of adaptation is: the Voltage Iq-Droop, Voltage Q-Droop, Const. Q, and lastly, Const. cosϕ, with the latter being the most robust control strategy without voltage fluctuations.

All controllers in Figure 34 but the Const. cosϕ portray an equally high robustness degree at a POC voltage of 1.00 p.u., with only the Const. cosϕ experiencing a fluctuation in its voltage magnitude. The order of adaptation for visible controllers in this scenario is: the Voltage Iq-Droop, Const. V, Const. Q, and lastly, Const. cosϕ.

The four controllers that can be identified in Figure 34d for the POC voltage of 1.05 p.u. by order of adaptation are the Voltage Iq-Droop, Const. Q, and equally adaptive Const. cosϕ and Voltage Q-Droop. The Voltage Iq-Droop and Voltage Q-Droop are the two controllers displaying consistent voltages for the entire simulation tim, and are accordingly considered the most robust for the POC voltage of 1.05 p.u..

Beyond the controllers' settling times, none of the controllers in Figure 34e experienced a compromised level of robustness as none of them has any fluctuation at 1.10 p.u. POC voltage. Hence all control strategies are considered to be equally robust. In this scenario, the Voltage Q-Droop comes out as the most adaptive controller, followed by the Const. cosϕ, while the level of adaptation for the Const. V and Voltage Iq-Droop are equal.

For the steady-state analysis performed through running a load flow at a wind speed of 4.5 m/s, the results for all control strategies are shown in Table A5. It is observed that all control strategies fail to meet the local voltage requirement of 5 % fluctuations in all operation scenarios. It is also observed that the controllers' response tends to be more similar than ever, with only two instances of a single controller having a unique voltage control response.

At a POC voltage of 0.90 p.u., the characteristic response of the Const. V, Voltage Iq-Droop, and Voltage Q-Droop are the same, with their HV bus voltages at a -5.87 % fluctuation, while the Const. cosϕ and Const. Q have a -8.71 % fluctuation. The similarity in the characteristic response continues

at a POC voltage of 0.95 p.u., where the former has -6.10 % fluctuation and the latter experiences a voltage fluctuation of -8.71 %.

An HV match of 0.938068 for the Const. V, Voltage Iq-Droop and Voltage Iq-Droop, and 0.913068 for the other two controllers at 1.00 p.u. POC voltage results in -6.19 % and -8.69 % voltage fluctuation, respectively. It is at 1.05 p.u. POC voltage that a unique response is observed for the Const. V. It is the only controller with a fluctuation of -6.46 %, with the Const. cosϕ and Const. Q at -8.67 %, and the Voltage Iq-Droop and Voltage Q-Droop at -6.50 % voltage fluctuation. The unique response of the Const. V continues at a POC voltage of 1.10 p.u.. Here, only this controller has a voltage fluctuation of -9.18 % from the grid voltage, while the Const. cosϕ and Const. Q are similar, and so are the Voltage Iq-Droop and Voltage Q-Droop at a voltage fluctuation of -8.64 % and -9.16 % from the grid voltage. Although all controllers do not comply to the local voltage set-point, they can all be used at the wind speed of 4.5 m/s as they all fluctuate below the 10 % boundary limit set for the SANS 10142-3:2012 and IEC TS 62749:2020 standards compliance.

4.2. Response analysis for varying wind speeds

The control strategies under study were analysed for robustness when subjected to wind speed variations so as to investigate their consistency in maintaining HV bus voltages when there are changes in wind speed. Each controller's dynamic response was evaluated for different wind speeds for a similar POC voltage. A 10-second RMS time domain simulation run for different values of wind speed for each controller at a POC voltage of 1.00 p.u. is presented in Figure 35.

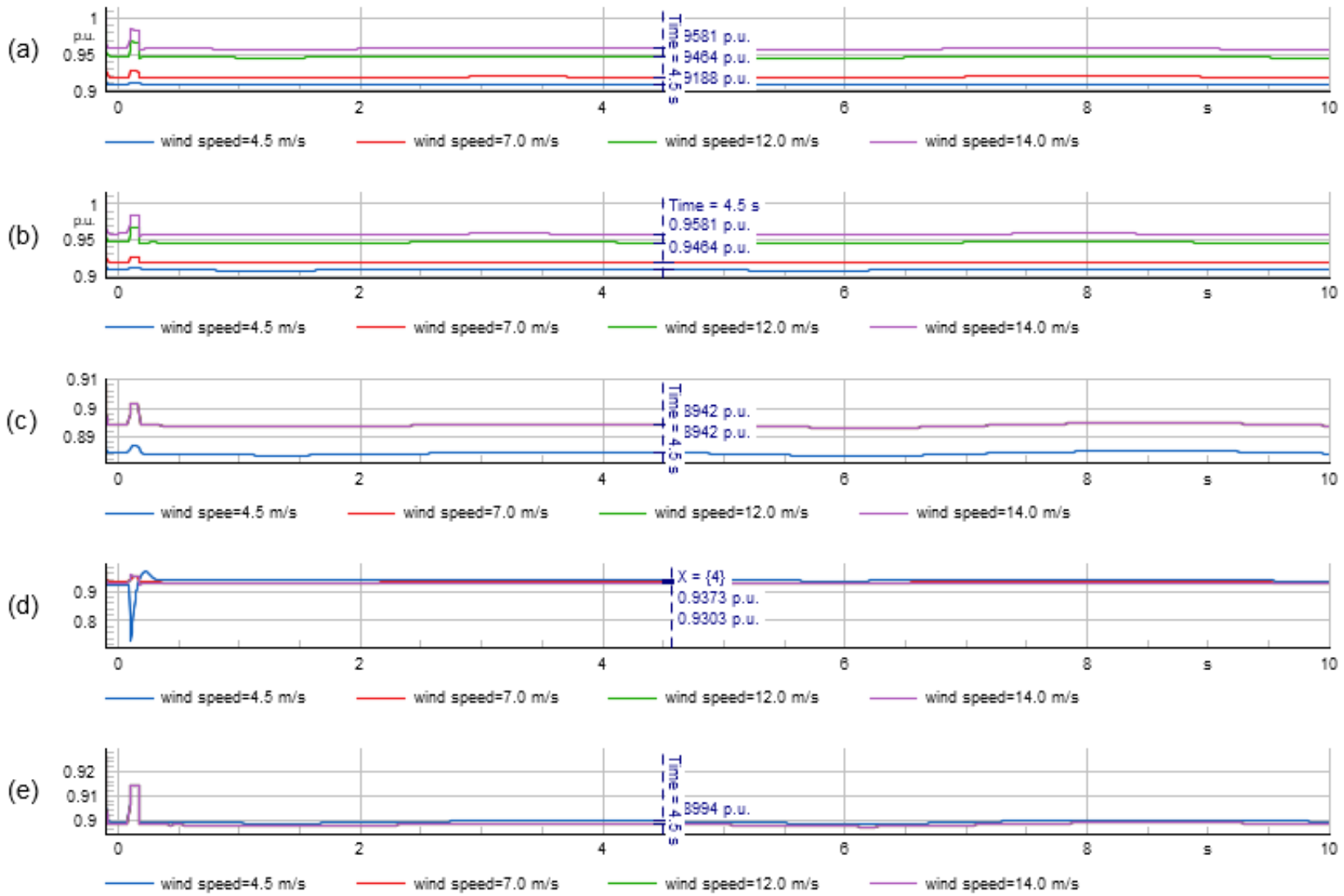

Figure 35: Control strategies' dynamic response for varying wind speeds as 1.00 p.u. POC voltage: (a) Const. Q, (b) Const. V, (c) Const. cosϕ, (d) Voltage Iq-Droop, (e) Voltage Q-Droop

For the control strategies' dynamic response under different wind speeds, an automatic intersection line was inserted on the simulation plot to observe the bus voltages at each wind speed. The observatory analysis is as follows:

For the Const. Q presented in Figure 35a, the HV bus voltages starting with the highest bus voltage in p.u. are 0.9581 for the wind speed at 14.0 m/s, 0.9464 at 12.0 m/s, 0.9188 at 7.0 m/s, and 0.9085 for 4.5 m/s. With a difference of 0.0117, 0.0276, and 0.0103 for the successive wind speed, the average fluctuation in the bus voltage is then calculated to be 0.0165 p.u., which is used as a robustness measure.

For the Const. V control illustrated in Figure 35b, the HV bus voltage is 0.9581 p.u. when the wind speed is 14.0 m/s, 0.9464 p.u. for 12.0 m/s wind speed, 0.9188 p.u. and 0.9085 p.u. for 7.0 m/s and 4.5 m/s, respectively. The average bus voltage fluctuation is, therefore, 0.0165 p.u. which is equivalent to the robustness exhibited in the Const. Q control.

In Figure 35c, complete robustness is observed for three different wind speeds in the Const. cosϕ. A bus voltage of 0.8942 p.u. exists for the wind speeds of 14.0 m/s, 12.0 m/s, and 7.0 m/s while the speed of 4.5 m/s results in a HV voltage of 0.8843. Therefore, the average voltage fluctuation accounting for all for the wind speeds is 0.0033 p.u., signifying a higher degree of robustness than the two previous control strategies.

In the voltage Iq-Droop shown in Figure 35d, the highest HV bus voltage is experienced when the wind speed is 4.5 m/s with a voltage of 0.9373 p.u.. It is followed by a wind speed of 7.0 m/s at 0.9303 p.u., 12.0 m/s at 0.9262 p.u., and lastly, 14.0 m/s at 0.9257 to give an average fluctuation of 0.0039 p.u. which indicate higher robustness than both the Const. Q and Const. V yet lower than the Const. cosϕ.

From Figure 35e, the speed of 4.5 m/s yields the highest HV bus voltage in the Voltage Q-Droop control at 0.8994 p.u. The other three controllers have a bus voltage of 0.8983 p.u., taking the average voltage fluctuation for this control strategy to 0.00037 p.u., which is the highest robustness of all control strategies at a POC voltage of 1.00 p.u.

The descriptive analysis of all control strategies for wind speed variation is presented in Table 1

Table 1: Control strategies' descriptive statistics for varying wind speeds

Descriptive Statistics

	N	Std. Deviation
Const.cos_phi	4	.00495
Voltage_QDroop	4	.00055
Voltage_IqDroop	4	.00536
Const.V	4	.02318
Const.Q	4	.02318
Valid N (listwise)	4	

Using data extracted from the dynamic simulation in Figure 35, a descriptive analysis was conducted using IBM SPSS Statistics, as shown in Table 5. The results in the table confirm the robustness criteria used to assess the control strategies at different wind speeds for a POC voltage of 1.00 p.u. Since "a smaller standard deviation indicates that data points are closer to the mean, while a larger standard deviation shows that data points are spread out over a wider range around the mean" [161], the standard deviation is used here as a measure of robustness. By ranking the control strategies based on their standard deviations, the most robust controller is Voltage Q-Droop, with a standard deviation of 0.00055, followed by Const. cosϕ at 0.00495, Voltage Iq-Droop at 0.00536, and finally, Const. V and Const. Q, both with a standard deviation of 0.02318.

4.3. Fault-tolerance and service restoration analysis

At a wind speed of 14.0 m/s, a case was established to determine the systems' response to a grid fault. With a POC voltage set at 1.00 p.u., a three-phase short circuit event was created on the HV bus bar at 3.2 seconds and cleared at 3.4 seconds. The results of the simulation event are shown in Figure 36 below.

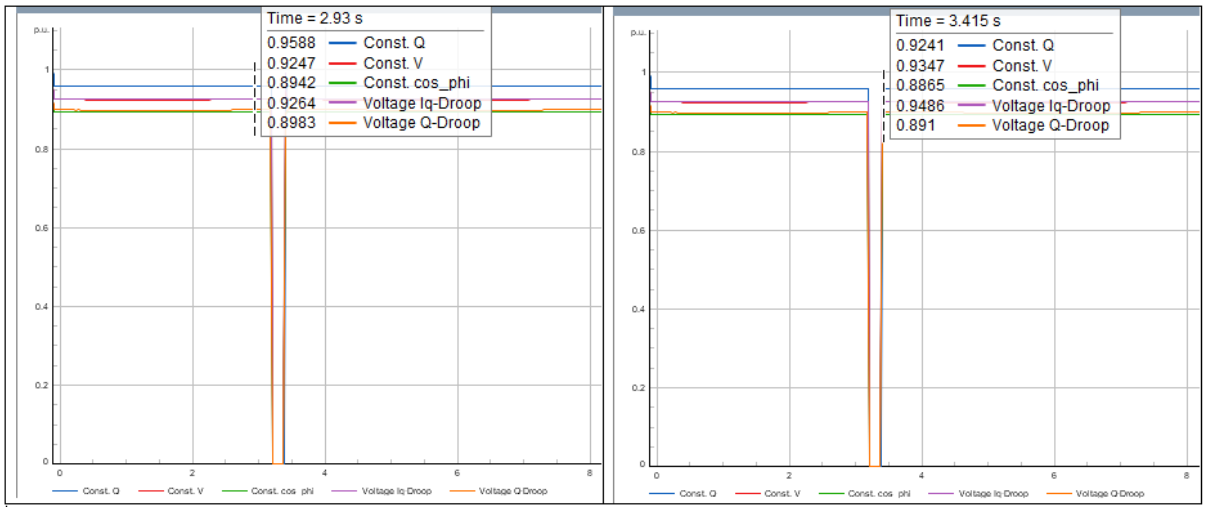

Figure 36: Control strategies' response to short-circuit fault

Considering the time points of 2.93 seconds (before the three-phase short circuit event) and 3.415 seconds (after fault clearance), the HV bus voltages for each controller are shown in Figure 38. As depicted, within 0.015 seconds after fault clearance, the Const. Q controller's bus voltage of 0.9241 p.u. at 3.415 seconds is 96% of its pre-fault voltage (0.9588 p.u.), remaining within the 5% voltage deviation range for service restoration. The post-fault clearance values for the Const. Q, Const. cosϕ, Voltage Iq-Droop, and Voltage Q-Droop controllers, relative to their initial values, are 1.0108, 0.9914, 1.0242, and 0.9919, respectively. Thus, all control strategies achieve voltage restoration within the 5% deviation range within 0.015 seconds after the fault is cleared.4.4. SCADA monitoring and control

4.4. SCADA monitoring and control

A SCADA system was designed for the control room operator to monitor the wind power plant and all wind parameters of concern. When the system is run in manual mode, the control strategy selection is at the discretion of the control room operator, but the automatic mode selects the best control strategy for each operation scenario. The best control strategy is determined as the controller whose HV bus voltage is closest to the POC bus bar voltage. Figure 37, Figure 38, and Figure 39 illustrate the SCADA operation at different wind speeds and POC voltages.

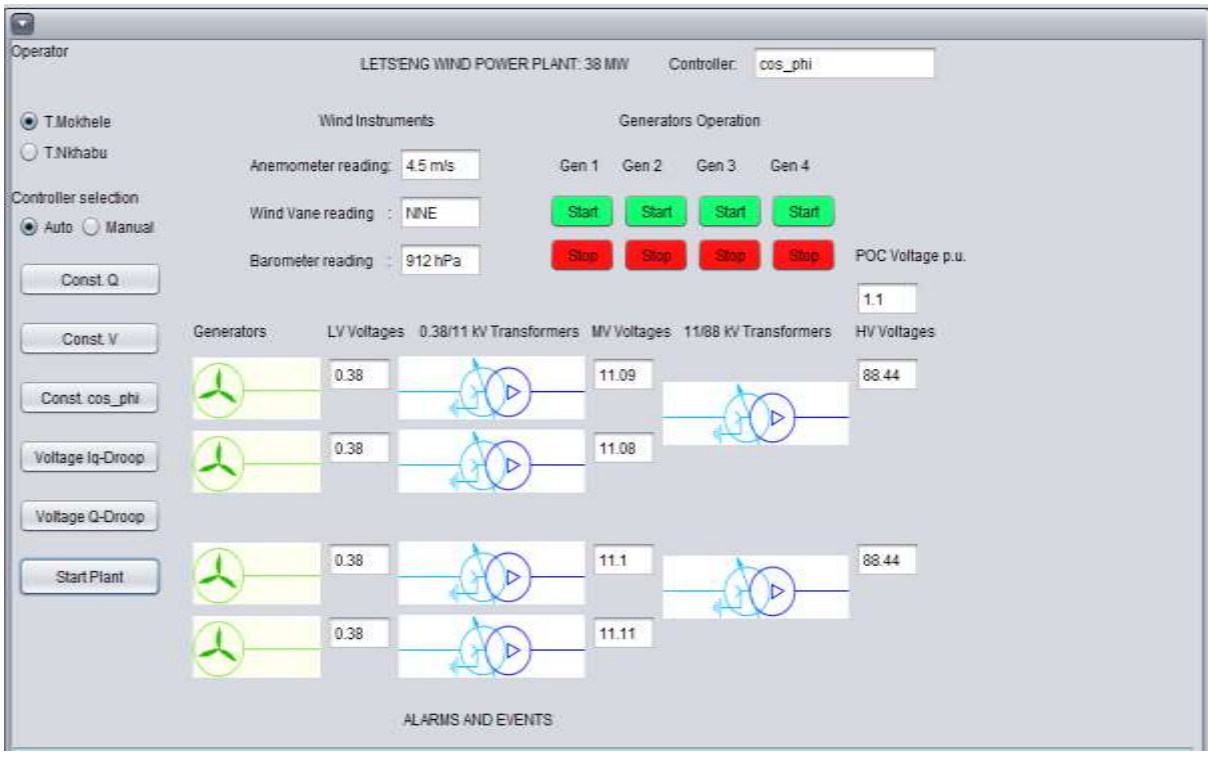

Figure 37: SCADA control at a wind speed of 4.5 m/s and POC voltage of 1.10 p.u.

Figure 39 shows that when the POC voltage is set to 1.10 p.u. at a wind speed of 4.5 m/s, the Const. cosϕ controller achieves the closest match between the HV bus voltage and the POC bus bar at 88.44V.

The SCADA system's controller selection aligns with the results in Table A5, where Const. cosϕ, along with Const. Q had the highest HV match at 0.913636.

At a wind speed of 7.0 m/s, the SCADA system automatically selects the Voltage Iq-Droop controller when the POC voltage is 0.95 p.u., producing an HV bus voltage of 83.76 V. This is consistent with Table A4, where a voltage match of 1.001914 for the Voltage Iq-Droop controller was the highest among all controllers at these wind speeds and POC voltage.

Similarly, Figure 41 aligns with Table A2 for a wind speed of 14.0 m/s. When the POC is set to 1.00 p.u., the Const. cosϕ controller achieves the highest voltage match, with an HV bus voltage of 88.44 V.

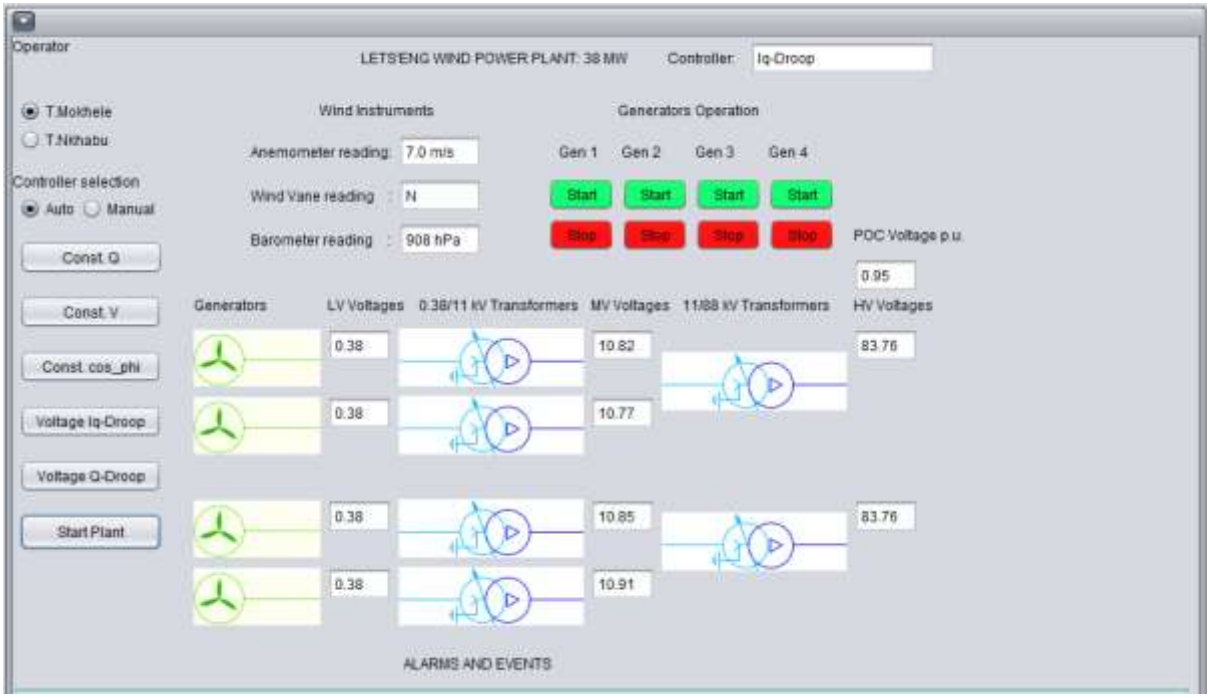

Figure 38: SCADA control at a wind speed of 7.0 m/s and POC voltage of 0.95 p.u.

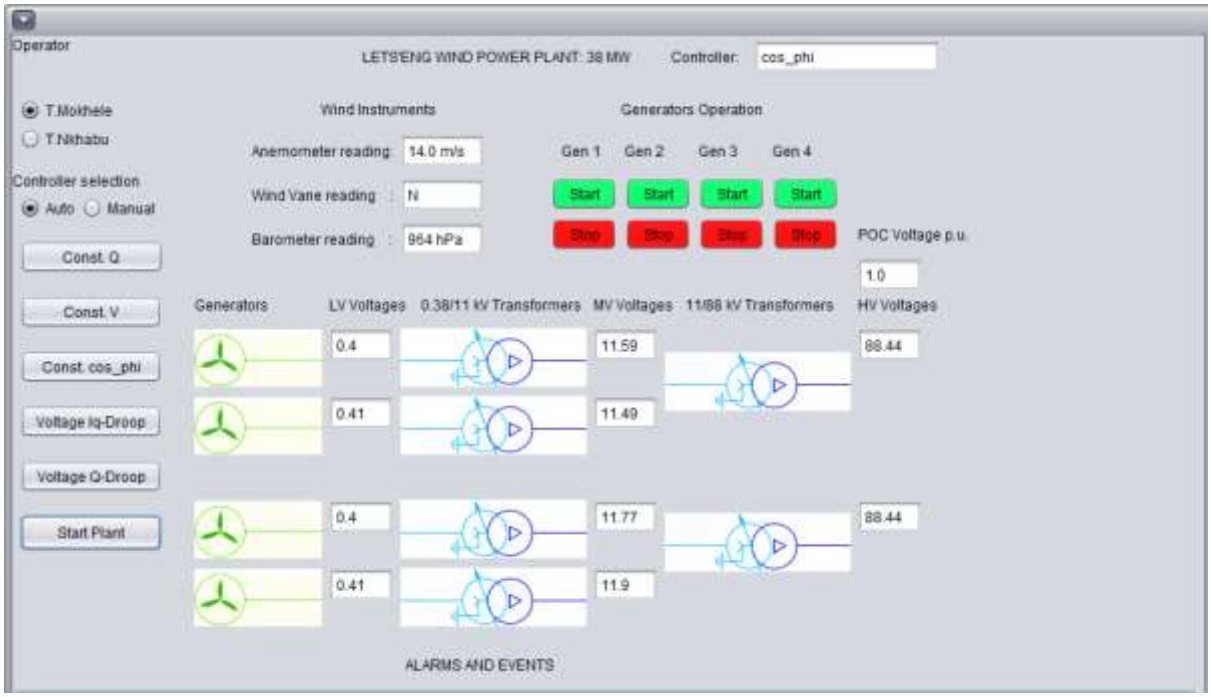

Figure 39: SCADA control at a wind speed of 14.0 m/s and POC voltage of 1.0 p.u.

The HV voltage match of 1.005 for the Const. cosϕ and Const. Q is the highest for this operation scenario, with an HV voltage of 88.44V when the wind speed is 14.0 m/s, and the POC voltage is 1.00 p.u..

5. Conclusions and Recommendations

5.1. Conclusions

The study aimed to design a control system that automatically adjusts controller characteristics to sustain overall power system performance. Five control strategies were evaluated for adaptability, robustness, and fault tolerance. The key monitored parameters for each operational scenario included wind speed and bus voltage at the point of connection. The Lets'eng wind farm, featuring four 9.5 MW turbines with a total capacity of 38 MW, was used as a case study for voltage control in a renewable energy system connected to the electricity grid. The analysis of each control strategy was conducted for both transient and steady states, with comparisons made across different wind speeds and POC voltages. For a 10-second RMS time domain simulation at a wind speed of 14.0 m/s, the voltage Iq-droop was considered to be the most adaptive controller, while the Const. Q is the most robust at a POC voltage of 0.90 p.u., the Const. Q and voltage Q-droop are the most adaptive controllers, with all controllers equally robust. The Const. Q and Const. V are the most adaptive controllers when the POC voltage is 1.00 p.u, while the Const. Q is the most adaptive control strategy for both 1.05 and 1.10 p.u. POC voltages. For a steady-state load flow analysis at a wind speed of 14.0 m/s, the Const. V is the controller with the highest voltage match to the POC voltage with -0.37 % deviation at a POC voltage of 0.90 p.u.. However, all control strategies comply to the South African standard, SANS 10142-3:2012 and the international standard, IEC TS 62749:2020. For POC voltages of 0.95 p.u, 1.00 p.u., 1.05 p.u, and 1.10 p.u, the controllers with the highest voltage match to the POC voltage are the voltage Iq-droop at -0.25 % deviation, Const. cosϕ and Const. Q at +0.5 % deviation, Const. Q at 100 % voltage match, and Const. Q at a -0.48 % deviation, respectively.

At a wind speed of 12.0 m/s, a 10-second RMS simulation resulted in the Const. V as the most adaptive controller for a POC voltage of 0.90 p.u, with all controllers but the Const. V being equally robust with no voltage ripples. The adaptation of Voltage Q-Droop is favoured when the POC voltage is 0.95 p.u., with this operation scenario resulting in an equal robustness degree for four control strategies and the Const. cosϕ as the only controller with voltage ramps for a simulation time period. All controllers have complete robustness when the POC voltage is 1.00 p.u., and the most adaptive control strategy is the voltage Iq-droop. Although the prominence of adaptation lies on the Const. Q for a POC voltage of 1.05 p.u, this controller is the most robust along with the voltage Iq-droop and Const. V. The most adaptive controller for 1.10 POC voltage is the voltage Q-droop, while the Const. Q is the most robust control strategy at this POC voltage. The steady-state response of the controllers at 0.90 p.u. shows that all controllers comply to the ±5 % locally set voltage deviation, the SANS 10142-3:2012 standard as well as the IEC TS 62749:2020 standard. Complete compliance is also achieved for 1.00 p.u. POC voltage. At 1.05 POC voltage, only the Cons. Cosϕ and Const. Q meet the 5% local boundary limit,

although all controllers are within the 10 % grid connection limits. At a -2.38 % voltage match, both the Const. Q and Const. cosϕ meet all the system requirements while the other three controllers violate the local voltage obligation, yet still comply to the set standards.

The dynamic simulation for the wind speed of 7.0 m/s resulted in the Const. Q being the most adaptive and robust controller when the POC voltage is 0.90 p.u. With complete robustness for all visible controllers at 0.95 p.u. POC voltage, the voltage Q-droop, is the most adaptive controller. While the highest adaptation lies on the Const. Q for 1.00 POC voltage, complete robustness is achieved only by the voltage Q-droop without any voltage ramps. As the most robust controller without any voltage amplitude deviations at 1.05 p.u. POC voltage, the voltage Iq-droop is the most adaptive controller together with the Const. Q. There are only three visible controllers at the POC voltage of 1.10 p.u., with the Const. Q being the most adaptive, while all the controllers appear to be equally robust beyond the setting times of the controllers. A steady-state load flow analysis at 7.0 m/s wind speed indicates that even when some controllers do not meet the local voltage requirements, all controllers can still be used as they meet the 10 % margin set for the SANS and IEC voltage margins.

For the 4.5 m/s operation scenarios, the Voltage Q-Droop is the most adaptive and robust control strategy at 0.90 p.u. POC voltage. The Voltage Iq-Droop has the highest adaptation, while the highest robustness degree is that of the Const. cosϕ when the POC voltage switches to 0.95 p.u. It is only the Const. cosϕ that experiences voltage fluctuations at 1.00 p.u. POC voltage, with the voltage Iq-Droop displaying the highest adaptation. With the voltage Iq-droop and voltage Q-droop displaying consistent voltages, it is the voltage Iq-droop that has the highest adaptation of all controllers at 1.05 p.u. POC voltage. With all the controllers equally robust at 1.10 p.u. POC voltage, the most adaptive controller is the voltage Q-droop. It is observed from the table that all control strategies fail to meet the local voltage requirement of 5 % fluctuations in all operation scenarios at a wind speed of 4.5 m/s.

When subjected to wind speed variations, a descriptive analysis was performed to evaluate the system robustness of the control strategies at a POC voltage of 1.00 p.u. showed the voltage Q-droop as the most robust controller with a standard deviation of 0.00055, followed by the Const. cosϕ at 0.00495, then the voltage Iq-droop at 0.00536, and lastly, the Const. V and Const. Q, both with a standard deviation of 0.02318.

A three-phase short circuit fault was introduced on the HV bus bar at 3.2 seconds and cleared at 3.4 seconds to analyze the system response during a grid fault. It was observed that all control strategies achieved voltage deviations within 5% during service restoration within 0.015 seconds. A SCADA system was developed to monitor and control the wind farm. In automatic mode, the system selects the most suitable control strategy based on wind speed and POC voltage to maintain the HV voltage

closest to the POC voltage. The SCADA evaluation results align with the findings obtained from the DigSilent PowerFactory software analysis.

5.2. Recommendations

The study was limited to operation scenarios of four different wind speeds and five points of connection voltage levels. For further research, the following are recommended:

1. Incorporating Arificial Neural Networks (ANNs): To enhance flexibility and performance, the approach of investigating ANNs'application in adaptive control strategies can enable the dynamic system's adjustment to a broader range of wind speeds and POC voltage levels.

2. Dataset Expansion: The collection and use of larger and more varied dataset for training ANNs can be explored. The data can include data from different geographical locations, seasonal variations, and different geid conditions to further investigate the control strategies robustness.

3. Real-time Implementation: The investigation into the control strategies can further be expanded to real-time systems to expore these adaptive control strategies in grid-conneceted RE Systems. Some collaboration with industry stakeholders who can assist with validation of findings in real-time applications can further be used in the expansion of research on adaptive and robust control strategies in grid-intergation of Renewable Energy Technologies.

References

[1] P. Spiru, 'Assessment of renewable energy generated by a hybrid system based on wind, hydro, solar, and biomass sources for decarbonizing the energy sector and achieving a sustainable energy transition', *Energy Reports*, vol. 9, pp. 167–174, 2023, doi: https://doi.org/10.1016/j.egyr.2023.04.316.

[2] N. F. Ngoune, B. M. K. Djousse, G. H. Djoukeng, C. G. F. Nguimeya, K. J. Tangka, and M. Tchoffo, 'Contribution of the mix renewable energy potentials in delivering parts of the electric energy needs in the west region of Cameroon', *Heliyon*, vol. 9, no. 3, p. e14554, 2023, doi: https://doi.org/10.1016/j.heliyon.2023.e14554.

[3] K. Nyarko, J. Whale, and T. Urmee, 'Drivers and challenges of off-grid renewable energy-based projects in West Africa: A review', *Heliyon*, vol. 9, no. 6, p. e16710, 2023, doi: https://doi.org/10.1016/j.heliyon.2023.e16710.

[4] K. Tanaka, C. Haga, K. Hori, and T. Matsui, 'Renewable energy Nexus: Interlinkages with biodiversity and social issues in Japan', *Energy Nexus*, vol. 6, p. 100069, 2022, doi: https://doi.org/10.1016/j.nexus.2022.100069.

[5] O. Bamisile *et al.*, 'Renewable energy and electricity incapacitation in sub-Sahara Africa: Analysis of a 100% renewable electrification in Chad', *Energy Reports*, vol. 9, pp. 1–12, 2023, doi: https://doi.org/10.1016/j.egyr.2023.05.049.

[6] X. H. Chen, K. Tee, M. Elnahass, and R. Ahmed, 'Assessing the environmental impacts of renewable energy sources: A case study on air pollution and carbon emissions in China', *Journal of Environmental Management*, vol. 345, p. 118525, 2023, doi: https://doi.org/10.1016/j.jenvman.2023.118525.

[7] N. Phuangpornpitak and S. Tia, 'Opportunities and Challenges of Integrating Renewable Energy in Smart Grid System', *Energy Procedia*, vol. 34, pp. 282–290, 2013, doi: https://doi.org/10.1016/j.egypro.2013.06.756.

[8] IRENA, 'World Energy Transitions Outlook 1-5C Pathway 2022 edition'. Accessed: Jul. 10, 2023. [Online]. Available: https://www.irena.org/Publications/2022/Mar/World-Energy-Transitions-Outlook-2022

[9] S. Fahad, A. Goudarzi, Y. Li, and J. Xiang, 'A coordination control strategy for power quality enhancement of an active distribution network', *Energy Reports*, vol. 8, pp. 5455–5471, 2022, doi: https://doi.org/10.1016/j.egyr.2022.04.014.

[10] F. Ahmed, D. A. Kez, S. McLoone, R. J. Best, C. Cameron, and A. Foley, 'Dynamic grid stability in low carbon power systems with minimum inertia', *Renewable Energy*, vol. 210, pp. 486–506, 2023, doi: https://doi.org/10.1016/j.renene.2023.03.082.

[11] N. S. Srivatchan, P. Rangarajan, and S. Rajalakshmi, 'Control Scheme for Power Quality Improvement in Islanded Microgrid Operation', *Procedia Technology*, vol. 21, pp. 212–215, 2015, doi: https://doi.org/10.1016/j.protcy.2015.10.090.

[12] M. Martínez-Lavín, R. Villena-Ruiz, A. Honrubia-Escribano, J. C. Hernández, and E. Gómez-Lázaro, 'Evaluation of the latest Spanish grid code requirements from a PV power plant perspective', *Energy Reports*, vol. 8, pp. 8589–8604, 2022, doi: https://doi.org/10.1016/j.egyr.2022.06.078.

[13] A. B. Attya, O. Anaya-Lara, P. Ledesma, and H. G. Svendsen, 'Fulfilment of Grid Code Obligations by Large Offshore Wind Farms Clusters Connected via HVDC Corridors', *Energy Procedia*, vol. 94, pp. 20–28, 2016, doi: https://doi.org/10.1016/j.egypro.2016.09.183.

[14] I. A. Irazabal, E. Ciapessoni, D. Cirio, J. Glasdam, P. Lund, and A. Pitto, 'Grid code compliant controllers for Multi-terminal HVDC grids aimed to integrate wind power: assessing their impact on the operational security of a real-world system', *Energy Procedia*, vol. 142, pp. 2165–2170, 2017, doi: https://doi.org/10.1016/j.egypro.2017.12.583.

[15] H. Wang, J. D. Watson, and N. R. Watson, 'A Lyapunov-based nonlinear direct power control for grid-side converters interfacing renewable energy in weak grids', *Electric Power Systems Research*, vol. 221, p. 109408, 2023, doi: https://doi.org/10.1016/j.epsr.2023.109408.

[16] A. ur Rehman *et al.*, 'Transition towards a sustainable power system: MA-DA&DC framework based voltage control in high PV penetration networks', *Energy Reports*, vol. 9, pp. 5922–5936, 2023, doi: https://doi.org/10.1016/j.egyr.2023.05.035.
[17] D. Zheng, K. Yuan, W. Wang, and L. Qian, 'Optimal frequency control for wind power-integrated power system based on parameter identification', *Energy Reports*, vol. 9, pp. 58–70, 2023, doi: https://doi.org/10.1016/j.egyr.2023.04.077.
[18] T. Jin, Y. Chen, J. Guo, M. Wang, and M. A. Mohamed, 'An effective compensation control strategy for power quality enhancement of unified power quality conditioner', *Energy Reports*, vol. 6, pp. 2167–2179, 2020, doi: https://doi.org/10.1016/j.egyr.2020.07.027.
[19] S. Vinnakoti and V. R. Kota, 'ANN based control scheme for a three-level converter based unified power quality conditioner', *Journal of Electrical Systems and Information Technology*, vol. 5, no. 3, pp. 526–541, 2018, doi: https://doi.org/10.1016/j.jesit.2017.11.001.
[20] LEWA, 'Annual Report 2022/23', Lesotho Electricity and Water Authority, Maseru, 2023. [Online]. Available: https://www.lewa.org.ls/download/lewa-annual-report-2020-21/
[21] M. Senatla, M. Nchake, B. M. Taele, and I. Hapazari, 'Electricity capacity expansion plan for Lesotho – implications on energy policy', *Energy Policy*, vol. 120, pp. 622–634, Sep. 2018, doi: 10.1016/j.enpol.2018.06.003.
[22] M. D'Isidoro *et al.*, 'Estimation of solar and wind energy resources over Lesotho and their complementarity by means of WRF yearly simulation at high resolution', *Renewable Energy*, vol. 158, pp. 114–129, Oct. 2020, doi: 10.1016/j.renene.2020.05.106.
[23] F. Pasanisi *et al.*, 'A Cooperation Project in Lesotho: Renewable Energy Potential Maps Embedded in a WebGIS Tool', *Sustainability*, vol. 13, no. 18, p. 10132, Sep. 2021, doi: 10.3390/su131810132.
[24] M. Mpholo, T. Mathaba, and M. Letuma, 'Wind profile assessment at Masitise and Sani in Lesotho for potential off-grid electricity generation', *Energy Conversion and Management*, vol. 53, no. 1, pp. 118–127, Jan. 2012, doi: 10.1016/j.enconman.2011.07.015.
[25] T. Mathaba, M. Mpholo, and M. Letuma, 'Velocity and power density analysis of the wind at Letšeng-la-terae in Lesotho', *Renewable Energy*, vol. 46, pp. 210–217, Oct. 2012, doi: 10.1016/j.renene.2012.04.003.
[26] S. Tsoeu-Ntokoane, M. Kali, and X. Lemaire, 'Energy democracy in Lesotho: Prioritising the participation of rural citizens', *Cogent Social Sciences*, vol. 8, no. 1, p. 2012973, Dec. 2022, doi: 10.1080/23311886.2021.2012973.
[27] LEWA, 'LEWA Annual Report 2021-22', Lesotho Electricity and Water Authority, Maseru, 2022.
[28] Y. Lavi and J. Apt, 'Inverter fast frequency response is a low-cost alternative to system inertia', *Electric Power Systems Research*, vol. 221, p. 109422, 2023, doi: https://doi.org/10.1016/j.epsr.2023.109422.
[29] Q. Hong, M. A. U. Khan, C. Henderson, A. Egea-Àlvarez, D. Tzelepis, and C. Booth, 'Addressing Frequency Control Challenges in Future Low-Inertia Power Systems: A Great Britain Perspective', *Engineering*, vol. 7, no. 8, pp. 1057–1063, 2021, doi: https://doi.org/10.1016/j.eng.2021.06.005.
[30] Q. Li, B. Ren, W. Tang, D. Wang, C. Wang, and Z. Lv, 'Analyzing the inertia of power grid systems comprising diverse conventional and renewable energy sources', *Energy Reports*, vol. 8, pp. 15095–15105, 2022, doi: https://doi.org/10.1016/j.egyr.2022.11.022.
[31] B. B. Adetokun and C. M. Muriithi, 'Application and control of flexible alternating current transmission system devices for voltage stability enhancement of renewable-integrated power grid: A comprehensive review', *Heliyon*, vol. 7, no. 3, p. e06461, 2021, doi: https://doi.org/10.1016/j.heliyon.2021.e06461.
[32] A. Salah Saidi, 'Impact of grid-tied photovoltaic systems on voltage stability of tunisian distribution networks using dynamic reactive power control', *Ain Shams Engineering Journal*, p. S2090447921002884, Jul. 2021, doi: 10.1016/j.asej.2021.06.023.
[33] Scatec, 'Scatec signs agreement for the first IPP solar project in Lesotho totalling 20 MW'. Accessed: Jul. 10, 2023. [Online]. Available: www.scatec.com

[34] Hirundo Energy, 'Lesotho: Towards sustainable enegy'. Accessed: Jul. 10, 2023. [Online]. Available: www.hirundo.energy
[35] T. N. Rateele and L. Z. Thamae, 'An optimization approach for the economic dispatch incorporating renewable energy resources into Lesotho power sources portfolio', *Heliyon*, vol. 9, no. 4, p. e14748, Apr. 2023, doi: 10.1016/j.heliyon.2023.e14748.
[36] P. A. Capó-Lugo and P. M. Bainum, 'Continuous and digital control systems', in *Orbital Mechanics and Formation Flying*, Elsevier, 2011, pp. 155–246. doi: 10.1533/9780857093875.155.
[37] A. Gupta and D. S. Yan, 'Process Control', in *Mineral Processing Design and Operation*, Elsevier, 2006, pp. 622–671. doi: 10.1016/B978-044451636-7/50019-X.
[38] P. Zhang, 'Industrial control engineering', in *Advanced Industrial Control Technology*, Elsevier, 2010, pp. 41–70. doi: 10.1016/B978-1-4377-7807-6.10002-6.
[39] N. T. Nguyen, *Model-Reference Adaptive Control*. in Advanced Textbooks in Control and Signal Processing. Cham: Springer International Publishing, 2018. doi: 10.1007/978-3-319-56393-0.
[40] K. Ogata, *Modern control engineering*, 5th ed. in Prentice-Hall electrical engineering series. Instrumentation and controls series. Boston: Prentice-Hall, 2010.
[41] X. A. Sun and A. J. Conejo, *Robust Optimization in Electric Energy Systems*, vol. 313. in International Series in Operations Research & Management Science, vol. 313. Cham: Springer International Publishing, 2021. doi: 10.1007/978-3-030-85128-6.
[42] K. Halbaoui, D. Boukhetala, and F. Boudjem, 'Introduction to Robust Control Techniques', in *Robust Control, Theory and Applications*, A. Bartoszewicz, Ed., InTech, 2011. doi: 10.5772/15213.
[43] E. Hill, A. Newton, S. A. Gadsden, and M. Biglarbegian, 'Tube-based robust model predictive control for fault tolerance', *Mechatronics*, vol. 95, p. 103051, 2023, doi: https://doi-org.nul.remotexs.co/10.1016/j.mechatronics.2023.103051.
[44] R. C. Shekhar and J. M. Maciejowski, 'Robust Predictive Control with Feasible Contingencies for Fault Tolerance', *IFAC Proceedings Volumes*, vol. 44, no. 1, pp. 4666–4671, 2011, doi: https://doi-org.nul.remotexs.co/10.3182/20110828-6-IT-1002.01683.
[45] K. Michail, A. C. Zolotas, and R. M. Goodall, 'Optimised sensor selection for control and fault tolerance of electromagnetic suspension systems: A robust loop shaping approach', *ISA Transactions*, vol. 53, no. 1, pp. 97–109, 2014, doi: https://doi-org.nul.remotexs.co/10.1016/j.isatra.2013.08.006.
[46] J.-M. Yang, 'Efficient static corrective control for model matching and fault tolerance of asynchronous sequential machines', *Journal of the Franklin Institute*, vol. 357, no. 7, pp. 3975–3992, 2020, doi: https://doi-org.nul.remotexs.co/10.1016/j.jfranklin.2020.01.009.
[47] X. Zhao, S. Garg, C. Queiroz, and R. Buyya, 'Chapter 11 - A Taxonomy and Survey of Stream Processing Systems', in *Software Architecture for Big Data and the Cloud*, I. Mistrik, R. Bahsoon, N. Ali, M. Heisel, and B. Maxim, Eds., Boston: Morgan Kaufmann, 2017, pp. 183–206. doi: https://doi.org/10.1016/B978-0-12-805467-3.00011-9.
[48] J. Faircloth, 'Chapter 6 - Architecture', in *Enterprise Applications Administration*, J. Faircloth, Ed., Boston: Morgan Kaufmann, 2014, pp. 221–271. doi: https://doi.org/10.1016/B978-0-12-407773-7.00006-5.
[49] L. Xiang, X. Yang, A. Hu, H. Su, and P. Wang, 'Condition monitoring and anomaly detection of wind turbine based on cascaded and bidirectional deep learning networks', *Applied Energy*, vol. 305, p. 117925, 2022, doi: https://doi-org.nul.remotexs.co/10.1016/j.apenergy.2021.117925.
[50] X. Jia, Y. Han, Y. Li, Y. Sang, and G. Zhang, 'Condition monitoring and performance forecasting of wind turbines based on denoising autoencoder and novel convolutional neural networks', *Energy Reports*, vol. 7, pp. 6354–6365, 2021, doi: https://doi-org.nul.remotexs.co/10.1016/j.egyr.2021.09.080.
[51] A. Zhu, Q. Zhao, T. Yang, L. Zhou, and B. Zeng, 'Condition monitoring of wind turbine based on deep learning networks and kernel principal component analysis', *Computers and Electrical Engineering*, vol. 105, p. 108538, 2023, doi: https://doi.org/10.1016/j.compeleceng.2022.108538.

[52] H. H. Hansen, N. MacDougall, C. D. Jensen, M. Kulahci, and B. F. Nielsen, 'Condition monitoring of wind turbine faults: Modeling and savings', *Applied Mathematical Modelling*, vol. 130, pp. 160–174, 2024, doi: https://doi-org.nul.remotexs.co/10.1016/j.apm.2024.02.036.
[53] M. J. Neale, Ed., 'B2 - Condition monitoring', in *Lubrication and Reliability Handbook*, Woburn: Butterworth-Heinemann, 2001, pp. 1–4. doi: https://doi.org/10.1016/B978-075065154-7/50096-6.
[54] A. Davies, Ed., *Handbook of Condition Monitoring: Techniques and Methodology*. Dordrecht: Springer Netherlands, 1998. doi: 10.1007/978-94-011-4924-2.
[55] Andy Page, 'Condition Based Maintenance and Condition Monitoring', Allied Reliability Group, Charleston, 2018. [Online]. Available: https://cdn2.assets-servd.host/wild-grenadier/production/media/resources/AR_WP_Condition-Based-Maintenance.pdf
[56] A. M. Vassallo, 'Applications of batteries for grid-scale energy storage', in *Advances in Batteries for Medium and Large-Scale Energy Storage*, Elsevier, 2015, pp. 587–607. doi: 10.1016/B978-1-78242-013-2.00017-0.
[57] E. C. Okonkwo, I. Wole-Osho, O. Bamisile, M. Abid, and T. Al-Ansari, 'Grid integration of renewable energy in Qatar: Potentials and limitations', *Energy*, vol. 235, p. 121310, Nov. 2021, doi: 10.1016/j.energy.2021.121310.
[58] E. Acha, V. G. Agelidis, O. Anaya-Lara, and T. J. E. Miller, '1 - Electrical power systems — an overview', in *Power Electronic Control in Electrical Systems*, E. Acha, V. G. Agelidis, O. Anaya-Lara, and T. J. E. Miller, Eds., in Newnes Power Engineering Series. , Oxford: Newnes, 2002, pp. 1–30. doi: https://doi-org.nul.remotexs.co/10.1016/B978-075065126-4/50001-8.
[59] S. Dhundhara, M. Sharma, F. Guéniat, and Y. Arya, 'Chapter 1 - Overview of the renewable-dominated power systems and their frequency regulation issues', in *Advanced Frequency Regulation Strategies in Renewable-Dominated Power Systems*, S. Dhundhara, Y. Arya, and R. C. Bansal, Eds., Academic Press, 2024, pp. 1–19. doi: https://doi-org.nul.remotexs.co/10.1016/B978-0-323-95054-1.00015-9.
[60] P. Moulema, S. Mallapuram, W. Yu, D. Griffith, and N. Golmie, 'Chapter 24 - Integrating Renewable Energy Resources in Smart Grid Toward Energy-Based Cyber-Physical Systems', in *Cyber-Physical Systems*, H. Song, D. B. Rawat, S. Jeschke, and C. Brecher, Eds., in Intelligent Data-Centric Systems. , Boston: Academic Press, 2017, pp. 377–398. doi: https://doi-org.nul.remotexs.co/10.1016/B978-0-12-803801-7.00024-9.
[61] M. Sechilariu and F. Locment, 'Chapter 1 - Connecting and Integrating Variable Renewable Electricity in Utility Grid', in *Urban DC Microgrid*, M. Sechilariu and F. Locment, Eds., Butterworth-Heinemann, 2016, pp. 1–33. doi: https://doi-org.nul.remotexs.co/10.1016/B978-0-12-803736-2.00001-3.
[62] 'Smart Electrical Grid', Clean Energy Institute. Accessed: Sep. 17, 2023. [Online]. Available: https://www.cei.washington.edu/education/science-of-solar/smart-electrical-grid/
[63] J. D. Glover, T. J. Overbye, and M. S. Sarma, 'Power system analysis & design', Cengage Learning, Boston, MA, 2017.
[64] C. J. Khare, H. K. Verma, and V. Khare, 'Chapter 28 - Optimal power generation and power flow control using artificial intelligence techniques', in *Renewable Energy Systems*, A. T. Azar and N. A. Kamal, Eds., in Advances in Nonlinear Dynamics and Chaos (ANDC). , Academic Press, 2021, pp. 607–631. doi: https://doi-org.nul.remotexs.co/10.1016/B978-0-12-820004-9.00028-0.
[65] M. Kamran, 'Chapter 3 - Power grids', in *Fundamentals of Smart Grid Systems*, M. Kamran, Ed., Academic Press, 2023, pp. 71–131. doi: https://doi-org.nul.remotexs.co/10.1016/B978-0-323-99560-3.00005-3.
[66] M. H. Rashid, N. Y. Abed, Z. F. Hussien, A. A. Rahim, and N. Abdullah, 'Chapter 24 - Electric Power System', in *Power Electronics Handbook (Fifth Edition)*, Fifth Edition., M. H. Rashid, Ed., Butterworth-Heinemann, 2024, pp. 845–863. doi: https://doi-org.nul.remotexs.co/10.1016/B978-0-323-99216-9.00009-3.

[67] G. V. S. Raj Kumar, A. V. H. Sai Prasad, B. Padma, and B. Raj Koti, 'Smart Grid communication and information technologies for cyber security, data privacy, and policy issues', in *Sustainable Networks in Smart Grid*, Elsevier, 2022, pp. 1–29. doi: 10.1016/B978-0-323-85626-3.00008-9.
[68] J. de Kock and K. Strauss, Eds., '1 - Introduction to power distribution', in *Practical Power Distribution for Industry*, Oxford: Newnes, 2004, pp. 1–4. doi: https://doi-org.nul.remotexs.co/10.1016/B978-075066396-0/50001-3.
[69] M. E. El-Hawary, *Electrical energy systems*. in The power engineering series. Boca Raton: CRC Press, 2000.
[70] G. Nikitas, S. Bhattacharya, and N. Vimalan, 'Wind Energy', in *Future Energy*, Elsevier, 2020, pp. 331–355. doi: 10.1016/B978-0-08-102886-5.00016-5.
[71] K. S. R. Murthy and O. P. Rahi, 'A comprehensive review of wind resource assessment', *Renewable and Sustainable Energy Reviews*, vol. 72, pp. 1320–1342, May 2017, doi: 10.1016/j.rser.2016.10.038.
[72] P. Breeze, 'Wind Power', in *Power Generation Technologies*, Elsevier, 2019, pp. 251–273. doi: 10.1016/B978-0-08-102631-1.00011-0.
[73] Z. Aqachmar *et al.*, 'Electrification of Africa through CPV installations in small-scale industrial applications: Energetic, economic, and environmental analysis', *Renewable Energy*, vol. 197, pp. 723–746, Sep. 2022, doi: 10.1016/j.renene.2022.07.106.
[74] B. Emdadi and R. Moradi, 'Wind Climates and Annual Energy Production', in *Reference Module in Earth Systems and Environmental Sciences*, Elsevier, 2023, p. B9780323939409001018. doi: 10.1016/B978-0-323-93940-9.00101-8.
[75] D. Elliott, M. Schwartz, and G. Scott, 'Wind Resource Base', in *Encyclopedia of Energy*, Elsevier, 2004, pp. 465–479. doi: 10.1016/B0-12-176480-X/00335-1.
[76] T. Wizelius, 'Design and Implementation of a Wind Power Project', in *Comprehensive Renewable Energy*, Elsevier, 2012, pp. 391–430. doi: 10.1016/B978-0-08-087872-0.00215-8.
[77] S. K. Soonee, K. V. S. Baba, S. R. Narasimhan, S. C. Saxena, M. Joshi, and K. V. N. P. Kumar, 'Chapter 16 - Grid Integration of Renewables in India', in *Renewable Energy Integration (Second Edition)*, Second Edition., L. E. Jones, Ed., Boston: Academic Press, 2017, pp. 217–229. doi: https://doi-org.nul.remotexs.co/10.1016/B978-0-12-809592-8.00016-0.
[78] Lesotho Electricity Company (LEC), 'Wind Power Generation Option', LEC/GEN/1-2009, 2009.
[79] S. M. A. Aljeddani and M. A. Mohammed, 'A novel approach to Weibull distribution for the assessment of wind energy speed', *Alexandria Engineering Journal*, vol. 78, pp. 56–64, 2023, doi: https://doi-org.nul.remotexs.co/10.1016/j.aej.2023.07.027.
[80] K. K. Dayal, J. E. Cater, M. J. Kingan, G. D. Bellon, and R. N. Sharma, 'Wind resource assessment and energy potential of selected locations in Fiji', *Renewable Energy*, vol. 172, pp. 219–237, Jul. 2021, doi: 10.1016/j.renene.2021.03.034.
[81] A. K. Azad, M. G. Rasul, M. M. Alam, S. M. A. Uddin, and S. K. Mondal, 'Analysis of Wind Energy Conversion System Using Weibull Distribution', *Procedia Engineering*, vol. 90, pp. 725–732, 2014, doi: https://doi-org.nul.remotexs.co/10.1016/j.proeng.2014.11.803.
[82] L. Wang, J. Yuan, M. E. Cholette, Y. Fu, Y. Zhou, and A. C. Tan, 'Comparative study of discretization method and Monte Carlo method for wind farm layout optimization under Weibull distribution', *Journal of Wind Engineering and Industrial Aerodynamics*, vol. 180, pp. 148–155, 2018, doi: https://doi-org.nul.remotexs.co/10.1016/j.jweia.2018.07.021.
[83] P. Breeze, 'The Anatomy of a Wind Turbine', in *Wind Power Generation*, Elsevier, 2016, pp. 19–27. doi: 10.1016/B978-0-12-804038-6.00003-7.
[84] A. D. Hansen, 'Wind turbine technologies', in *Wind Energy Engineering*, Elsevier, 2023, pp. 89–98. doi: 10.1016/B978-0-323-99353-1.00020-7.
[85] D. Zhao, N. Han, E. Goh, J. Cater, and A. Reinecke, 'Aerodynamics of horizontal axis wind turbines and wind farms', in *Wind Turbines and Aerodynamics Energy Harvesters*, Elsevier, 2019, pp. 431–461. doi: 10.1016/B978-0-12-817135-6.00007-7.

[86] N. Bagalkot, J. Jose, and A. Keprate, 'Key components of the horizontal axis wind turbine', in *Multiphysics of Wind Turbines in Extreme Loading Conditions*, Elsevier, 2024, pp. 17–31. doi: 10.1016/B978-0-323-91852-7.00006-4.
[87] R. Wang, T. Han, W. Wang, Y. Xue, and D. Fu, 'Fracture analysis and improvement of the main shaft of wind turbine based on finite element method', *Advances in Mechanical Engineering*, vol. 10, no. 4, p. 168781401876900, Apr. 2018, doi: 10.1177/1687814018769003.
[88] S. McFadden and B. Basu, 'Wind turbine gearbox design with drivetrain dynamic analysis', in *Offshore Wind Farms*, Elsevier, 2016, pp. 137–158. doi: 10.1016/B978-0-08-100779-2.00007-6.
[89] A. V. Da Rosa and J. C. Ordóñez, 'Wind Energy', in *Fundamentals of Renewable Energy Processes*, Elsevier, 2022, pp. 721–794. doi: 10.1016/B978-0-12-816036-7.00028-2.
[90] W. Jiang, J. Wu, C. Wang, H. Zhu, and X. Wang, 'Health assessment of wind turbine gearbox via parallel ensemble and fuzzy derivation collaboration approach', *Advanced Engineering Informatics*, vol. 62, p. 102576, Oct. 2024, doi: 10.1016/j.aei.2024.102576.
[91] P. Breeze, 'Drive Trains, Gearboxes, and Generators', in *Wind Power Generation*, Elsevier, 2016, pp. 41–48. doi: 10.1016/B978-0-12-804038-6.00005-0.
[92] H. Hou, W. Shi, Y. Xu, and Y. Song, 'Actuator disk theory and blade element momentum theory for the force-driven turbine', *Ocean Engineering*, vol. 285, p. 115488, Oct. 2023, doi: 10.1016/j.oceaneng.2023.115488.
[93] P. Coelho, 'The Betz limit and the corresponding thermodynamic limit', *Wind Engineering*, vol. 47, no. 2, pp. 491–496, Apr. 2023, doi: 10.1177/0309524X221130109.
[94] J. R. West and S. K. Lele, 'Wind Turbine Performance in Very Large Wind Farms: Betz Analysis Revisited', *Energies*, vol. 13, no. 5, p. 1078, Mar. 2020, doi: 10.3390/en13051078.
[95] M. T. Qaiser, J. Ejaz, O. Osen, and A. Hasan, 'Digital twin-driven energy modeling of Hywind Tampen floating wind farm', *Energy Reports*, vol. 9, pp. 284–289, Oct. 2023, doi: 10.1016/j.egyr.2023.09.023.
[96] M. Mehrjoo, M. Jafari Jozani, and M. Pawlak, 'Wind turbine power curve modeling for reliable power prediction using monotonic regression', *Renewable Energy*, vol. 147, pp. 214–222, Mar. 2020, doi: 10.1016/j.renene.2019.08.060.
[97] M. Capelletti, D. M. Raimondo, and G. De Nicolao, 'Wind power curve modeling: A probabilistic Beta regression approach', *Renewable Energy*, vol. 223, p. 119970, Mar. 2024, doi: 10.1016/j.renene.2024.119970.
[98] N. I. Alhusein, 'Asynchronous Wind Turbine Generator: Output Power Evaluation', *Brilliance*, vol. 1, no. 2, pp. 75–80, Jun. 2022, doi: 10.47709/brilliance.v1i2.1565.
[99] N. V. Lakshmi, P. S. Mayurappriyan, A. T. Mathew, M. Saravana Mohan, C. Ganesh, and R. Shanmugasundaram, 'A brief review on control strategies for hydrostatic transmission-based wind turbines', in *Next-Generation Cyber-Physical Microgrid Systems*, Elsevier, 2024, pp. 77–89. doi: 10.1016/B978-0-443-22187-3.00003-5.
[100] A. Jassal, K. Versteegh, and H. Polinder, '7 - Case study of the permanent magnet direct drive generator in the Zephyros wind turbine', in *Electrical Drives for Direct Drive Renewable Energy Systems*, M. Mueller and H. Polinder, Eds., in Woodhead Publishing Series in Energy. , Woodhead Publishing, 2013, pp. 158–174. doi: https://doi-org.nul.remotexs.co/10.1533/9780857097491.2.158.
[101] D.-D. Dang, X.-T. Pham, P. Labbe, F. Torriano, J.-F. Morissette, and C. Hudon, 'CFD analysis of turbulent convective heat transfer in a hydro-generator rotor-stator system', *Applied Thermal Engineering*, vol. 130, pp. 17–28, 2018, doi: https://doi-org.nul.remotexs.co/10.1016/j.applthermaleng.2017.11.034.
[102] P. Mthethwa, T. S. Workneh, and A. Kassim, 'Renewable energy integration into a low-cost evaporative cooling system for fresh produce storage', in *Engineering Principles, Modeling and Economics of Evaporative Coolers*, Elsevier, 2023, pp. 219–243. doi: 10.1016/B978-0-323-90039-3.00008-6.

[103] Z. Chen, 'Wind turbine drive train systems', in *Wind Energy Systems*, Elsevier, 2011, pp. 208–246. doi: 10.1533/9780857090638.2.208.
[104] S. Bhattacharjee, 'Wind power technology', in *Sustainable Fuel Technologies Handbook*, Elsevier, 2021, pp. 123–170. doi: 10.1016/B978-0-12-822989-7.00006-8.
[105] A. Khaligh and O. C. Onar, 'Energy Sources', in *Power Electronics Handbook*, Elsevier, 2018, pp. 725–765. doi: 10.1016/B978-0-12-811407-0.00025-8.
[106] P. N. Rajnarayanan and K. Kathiravan, 'Volt/var control and optimization', in *Power Systems Operation with 100% Renewable Energy Sources*, Elsevier, 2024, pp. 65–84. doi: 10.1016/B978-0-443-15578-9.00017-0.
[107] A. Sagna, G. Mansour, S. Clenet, and N. Perry, 'Non destructive control of permanent magnet rotors in a perspective of electric motor circularity', *Procedia CIRP*, vol. 122, pp. 754–759, 2024, doi: 10.1016/j.procir.2024.02.024.
[108] M. O. L. Hansen, 'Aerodynamics and the design of horizontal axis wind turbine', in *Wind Energy Engineering*, Elsevier, 2023, pp. 137–153. doi: 10.1016/B978-0-323-99353-1.00019-0.
[109] R. F. Conchas, E. N. Sanchez, L. J. Ricalde, J. G. Alvarez, and A. Y. Alanis, 'Sensor fault-tolerant control for a doubly fed induction generator in a smart grid', *Engineering Applications of Artificial Intelligence*, vol. 117, p. 105527, Jan. 2023, doi: 10.1016/j.engappai.2022.105527.
[110] T. Gu, P. Wang, D. Liu, A. Sun, D. Yang, and G. Yan, 'Modeling and small-signal stability analysis of doubly-fed induction generator integrated system', *Global Energy Interconnection*, vol. 6, no. 4, pp. 438–449, Aug. 2023, doi: 10.1016/j.gloei.2023.08.005.
[111] J. Zhang, P. Wei, and X. Gao, 'Impact of inertia response control strategy based doubly fed induction generator on frequency stability of power system', *Energy Reports*, vol. 9, pp. 577–583, 2023, doi: https://doi.org/10.1016/j.egyr.2022.11.084.
[112] J. C. Martínez, J. L. R. Amenedo, S. A. Gómez, and J. Alonso-Martínez, 'Grid-forming control of doubly-fed induction generators based on the rotor flux orientation', *Renewable Energy*, vol. 207, pp. 162–176, 2023, doi: https://doi-org.nul.remotexs.co/10.1016/j.renene.2023.02.133.
[113] P. Singh, K. Arora, U. C. Rathore, G. P. Joshi, and W. Cho, 'Comparative study of controllers in battery energy storage system integrated with doubly fed induction generator-based wind energy conversion system for power quality improvement', *Energy Reports*, vol. 11, pp. 4587–4600, Jun. 2024, doi: 10.1016/j.egyr.2024.04.020.
[114] Z. Lu, H. Li, Y. Qiao, L. Xie, and C. Singh, 'Chapter 7 - Active power balance control based on flexibility theory', in *Power System Flexibility*, Z. Lu, H. Li, Y. Qiao, L. Xie, and C. Singh, Eds., Academic Press, 2024, pp. 81–104. doi: https://doi-org.nul.remotexs.co/10.1016/B978-0-323-99517-7.00023-3.
[115] E. Santi, B. Tian, and K. Peng, 'Chapter 5 - Power Electronic Modules', in *Power Electronics Handbook (Fifth Edition)*, Fifth Edition., M. H. Rashid, Ed., Butterworth-Heinemann, 2024, pp. 151–170. doi: https://doi-org.nul.remotexs.co/10.1016/B978-0-323-99216-9.00002-0.
[116] H. Bai, C. Liu, D. Majstorovic, and F. Gao, '1 - Roles and challenges of power electronics real-time simulation', in *Real-Time Simulation Technology for Modern Power Electronics*, H. Bai, C. Liu, D. Majstorovic, and F. Gao, Eds., Academic Press, 2023, pp. 1–11. doi: https://doi-org.nul.remotexs.co/10.1016/B978-0-323-99541-2.00003-X.
[117] E. Kabalci, 'Chapter 31 - Power Electronics Applications in Smart Grid', in *Power Electronics Handbook (Fifth Edition)*, Fifth Edition., M. H. Rashid, Ed., Butterworth-Heinemann, 2024, pp. 993–1013. doi: https://doi-org.nul.remotexs.co/10.1016/B978-0-323-99216-9.00006-8.
[118] R. Saidur, S. Mekhilef, M. B. Ali, A. Safari, and H. A. Mohammed, 'Applications of variable speed drive (VSD) in electrical motors energy savings', *Renewable and Sustainable Energy Reviews*, vol. 16, no. 1, pp. 543–550, Jan. 2012, doi: 10.1016/j.rser.2011.08.020.
[119] J. Sun *et al.*, 'Realizing self-powered mechanical transmission control system via triboelectric nanogenerator and electrorheological fluid composed soft starter', *Nano Research Energy*, vol. 2, p. e9120066, Sep. 2023, doi: 10.26599/NRE.2023.9120066.

[120] P. Jang, B. J. Hyon, D. Y. Hwang, J. S. Park, J.-H. Choi, and J.-H. Kim, 'The Seamless Transition From Discrete Frequency Control to Phase Control Method Using Soft Starter', *IEEE Access*, vol. 12, pp. 13469–13476, 2024, doi: 10.1109/ACCESS.2024.3352635.
[121] B. D. Nugraha, S. Safaruddin, and A. D. Andre, 'ANALISIS SISTEM STARTING SOFT STARTER MOTOR LISTRIK PT.SEMEN BATURAJA', *Kapalamada*, vol. 1, no. 03, pp. 412–419, Sep. 2022, doi: 10.62668/kapalamada.v1i03.280.
[122] M. Yengane, S. Mokeke, and M. Mpholo, 'Design and Economic Analysis of a Solar Thermal Pre-Cooling System for Agro-Cold Chain in Lesotho', *Int Sustain Ener Conf Proc*, vol. 1, Apr. 2024, doi: 10.52825/isec.v1i.1168.
[123] G. M. Vargas Gil, R. Bittencourt Aguiar Cunha, S. Giuseppe Di Santo, R. Machado Monaro, F. Fragoso Costa, and A. J. Sguarezi Filho, 'Photovoltaic energy in South America: Current state and grid regulation for large-scale and distributed photovoltaic systems', *Renewable Energy*, vol. 162, pp. 1307–1320, Dec. 2020, doi: 10.1016/j.renene.2020.08.022.
[124] M. R. Maghami, J. Pasupuleti, and J. Ekanayake, 'Energy storage and demand response as hybrid mitigation technique for photovoltaic grid connection: Challenges and future trends', *Journal of Energy Storage*, vol. 88, p. 111680, May 2024, doi: 10.1016/j.est.2024.111680.
[125] V. Boscaino *et al.*, 'Grid-connected photovoltaic inverters: Grid codes, topologies and control techniques', *Renewable and Sustainable Energy Reviews*, vol. 189, p. 113903, Jan. 2024, doi: 10.1016/j.rser.2023.113903.
[126] N. Vázquez and J. Vázquez, 'Photovoltaic System Conversion', in *Power Electronics Handbook*, Elsevier, 2024, pp. 781–795. doi: 10.1016/B978-0-323-99216-9.00023-8.
[127] F. Wang, R. Li, G. Zhao, D. Xia, and W. Wang, 'Simulation test of 50 MW grid-connected "Photovoltaic+Energy storage" system based on pvsyst software', *Results in Engineering*, vol. 22, p. 102331, Jun. 2024, doi: 10.1016/j.rineng.2024.102331.
[128] L. Tian, C. Dong, Y. Mu, and H. Jia, 'DPGS: Data-driven photovoltaic grid-connected system exploiting deep learning and two-stage single-phase inverter', *Energy Reports*, vol. 11, pp. 1910–1924, Jun. 2024, doi: 10.1016/j.egyr.2024.01.038.
[129] M. Nkambule, A. Hasan, A. Ali, and T. Shongwe, 'A Novel Control Strategy in Grid-Integrated Photovoltaic System for Power Quality Enhancement', *Energies*, vol. 15, no. 15, p. 5645, Aug. 2022, doi: 10.3390/en15155645.
[130] W. Guo and W. Xu, 'Research on optimization strategy of harmonic suppression and reactive power compensation of photovoltaic multifunctional grid connected inverter', *International Journal of Electrical Power & Energy Systems*, vol. 145, p. 108649, Feb. 2023, doi: 10.1016/j.ijepes.2022.108649.
[131] L. Willis, 'Introduction to transmission and distribution (T&D) networks: T&D infrastructure, reliability and engineering, regulation and planning', in *Electricity Transmission, Distribution and Storage Systems*, Elsevier, 2013, pp. 3–38. doi: 10.1533/9780857097378.1.3.
[132] C. Decker, 'Energy transportation', in *Handbook of Energy Economics and Policy*, Elsevier, 2021, pp. 193–238. doi: 10.1016/B978-0-12-814712-2.00005-1.
[133] M. Ayalew and D. Gebregziabher, 'Mitigating the effects of PEV fast charging on grids with renewable and storage systems', in *Active Electrical Distribution Network*, Elsevier, 2022, pp. 145–162. doi: 10.1016/B978-0-323-85169-5.00006-X.
[134] M. H. Rashid, Z. F. Hussien, A. A. Rahim, and N. Abdullah, 'Electric Power Transmission', in *Power Electronics Handbook*, Elsevier, 2018, pp. 829–846. doi: 10.1016/B978-0-12-811407-0.00029-5.
[135] C. R. Bayliss and B. J. Hardy, Eds., '3 - Substation Layouts', in *Transmission and Distribution Electrical Engineering (Third Edition)*, Third Edition., Oxford: Newnes, 2007, pp. 92–114. doi: https://doi-org.nul.remotexs.co/10.1016/B978-075066673-2/50007-0.
[136] T. Docquier, Y.-Q. Song, V. Chevrier, L. Pontnau, and A. Ahmed-Nacer, 'Performance evaluation methodologies for Smart Grid Substation Communication Networks: A survey', *Computer Communications*, vol. 198, pp. 228–246, Jan. 2023, doi: 10.1016/j.comcom.2022.11.005.

[137] P. Neis, M. A. Wehrmeister, M. F. Mendes, and J. R. Pesente, 'Applying a model-driven approach to the development of power plant SCADA/EMS software', *International Journal of Electrical Power & Energy Systems*, vol. 153, p. 109336, 2023, doi: https://doi-org.nul.remotexs.co/10.1016/j.ijepes.2023.109336.
[138] G. Yadav and K. Paul, 'Architecture and security of SCADA systems: A review', *International Journal of Critical Infrastructure Protection*, vol. 34, p. 100433, 2021, doi: https://doi-org.nul.remotexs.co/10.1016/j.ijcip.2021.100433.
[139] H. Polat, M. Türkoğlu, O. Polat, and A. Şengür, 'A novel approach for accurate detection of the DDoS attacks in SDN-based SCADA systems based on deep recurrent neural networks', *Expert Systems with Applications*, vol. 197, p. 116748, 2022, doi: https://doi-org.nul.remotexs.co/10.1016/j.eswa.2022.116748.
[140] C. Rohmingtluanga, S. Datta, N. Sinha, and T. S. Ustun, 'SCADA based intake monitoring for improving energy management plan: Case study', *Energy Reports*, vol. 9, pp. 402–410, 2023, doi: https://doi-org.nul.remotexs.co/10.1016/j.egyr.2022.11.037.
[141] M. Alanazi, A. Mahmood, and M. J. M. Chowdhury, 'SCADA vulnerabilities and attacks: A review of the state-of-the-art and open issues', *Computers & Security*, vol. 125, p. 103028, 2023, doi: https://doi-org.nul.remotexs.co/10.1016/j.cose.2022.103028.
[142] K. O. Yoro, M. O. Daramola, P. T. Sekoai, U. N. Wilson, and O. Eterigho-Ikelegbe, 'Update on current approaches, challenges, and prospects of modeling and simulation in renewable and sustainable energy systems', *Renewable and Sustainable Energy Reviews*, vol. 150, p. 111506, 2021, doi: https://doi.org/10.1016/j.rser.2021.111506.
[143] Jan Machowski, Janusz W. Bialek, and James R. Bumby, *Power System Dynamics: Stability and Control*, 2nd ed. New Delhi: John Wiley & Sons, 2008.
[144] K. Padmanandam, S. Thangaraj, and R. Khilar, 'Smart power systems: an eyeview', in *Smart Energy and Electric Power Systems*, Elsevier, 2023, pp. 1–18. doi: 10.1016/B978-0-323-91664-6.00006-1.
[145] M. Nazir, A. Ahmad, and I. Hussain, 'Operational and environmental aspects of standalone microgrids', in *Control of Standalone Microgrid*, Elsevier, 2021, pp. 25–59. doi: 10.1016/B978-0-12-823022-0.00008-8.
[146] Sebota Mokeke, 'The Impact of Intermittent Renewable Generators on Lesotho National Electricity Grid', Masters Dissertation, National University of Lesotho, Roma, 2020. [Online]. Available: erc.nul/dissertations
[147] A. Vaccaro and A. Pepiciello, 'Uncertain voltage stability analysis by affine arithmetic', in *Affine Arithmetic-based Methods for Uncertain Power System Analysis*, Elsevier, 2022, pp. 123–133. doi: 10.1016/B978-0-32-390502-2.00016-8.
[148] H. Alsharif, M. Jalili, and K. N. Hasan, 'Fast frequency response services in low inertia power systems—A review', *Energy Reports*, vol. 9, pp. 228–237, 2023, doi: https://doi.org/10.1016/j.egyr.2023.05.193.
[149] Y. Jia, T. Zuo, Y. Li, W. Bi, L. Xue, and C. Li, 'Finite-time economic model predictive control for optimal load dispatch and frequency regulation in interconnected power systems', *Global Energy Interconnection*, vol. 6, no. 3, pp. 355–362, 2023, doi: https://doi.org/10.1016/j.gloei.2023.06.009.
[150] G. B. Yosef *et al.*, 'Frequency stability of the Israeli power grid with high penetration of renewable sources and energy storage systems', *Energy Reports*, vol. 7, pp. 6148–6161, 2021, doi: https://doi.org/10.1016/j.egyr.2021.09.057.
[151] T. Skrjanc, R. Mihalic, and U. Rudez, 'A systematic literature review on under-frequency load shedding protection using clustering methods', *Renewable and Sustainable Energy Reviews*, vol. 180, p. 113294, 2023, doi: https://doi.org/10.1016/j.rser.2023.113294.
[152] H. Gao, F. Zhang, L. Ding, B. Cornélusse, G. Zhang, and A. Salimu, 'Multi-segment droop control and optimal parameter setting strategy of wind turbine for frequency regulation', *International*

Journal of Electrical Power & Energy Systems, vol. 158, p. 109968, 2024, doi: https://doi-org.nul.remotexs.co/10.1016/j.ijepes.2024.109968.
[153] H. Lai, K. Xiong, Z. Zhang, and Z. Chen, 'Droop control strategy for microgrid inverters: A deep reinforcement learning enhanced approach', *Energy Reports*, vol. 9, pp. 567–575, 2023, doi: https://doi-org.nul.remotexs.co/10.1016/j.egyr.2023.04.263.
[154] B. Zhang and X. Fu, 'Improved droop control strategy based on voltage feedforward current compensation', *Energy Reports*, vol. 7, pp. 434–441, 2021, doi: https://doi-org.nul.remotexs.co/10.1016/j.egyr.2021.08.021.
[155] M. S. Nkambule, 'Improving Power Quality for a Grid Connected Photovoltaic System using Artificial Intelligence Techniques', PhD Thesis, University of Johannesburg, Johannesburg, 2023. [Online]. Available: https://hdl.handle.net/10210/505365
[156] H. Akagi, E. H. Watanabe, and M. Aredes, *Instantaneous power theory and applications to power conditioning*, Second edition. in IEEE Press series on power engineering, no. 62. Piscataway, NJ: IEEE Press, 2017.
[157] N. B. Roy and D. Das, 'Optimal allocation of active and reactive power of dispatchable distributed generators in a droop controlled islanded microgrid considering renewable generation and load demand uncertainties', *Sustainable Energy, Grids and Networks*, vol. 27, p. 100482, 2021, doi: https://doi-org.nul.remotexs.co/10.1016/j.segan.2021.100482.
[158] Chengshan Wang, Jianzhong Wu, Janaka Ekanayake, and Nick Jenkins, *Smart Electricity Distribution Networks*. Boca Raton, FL: Taylor & Francis Group, 2017. [Online]. Available: https://lccn.loc.gov/2016049431
[159] PowerFactory 2023, 'Technical Reference "WECC Wind Turbine Templates"'. DIgSILENT GmbH, Sep. 2023.
[160] IEC, 'IEC 62749: 2020; Assessment of Power Quality—Characteristics of Electricity Supplied by Public Networks', *International Electrotechnical Commission: Geneva, Switzerland*, 2020.
[161] J. S. Arora, 'Robust design and optimization: an introduction', in *Introduction to Optimum Design*, Elsevier, 2025, pp. 923–947. doi: 10.1016/B978-0-12-818320-5.00021-X.

Appendix A

Table A2: Bus voltages for steady state load flow analysis at wind speed=14 m/s

	LV BB1	LV BB2	LV BB3	LV BB4	MV BB1	MV BB2	MV BB3	MV BB4	Sub BB 11kV	U_{POC} BB	HV BB	HV Match
0.90 p.u.												
Const. V	0.38	0.38	0.38	0.38	10.79	10.73	10.85	10.91	10.48	79.20	78.91	0.996338
cos_phi	0.33	0.33	0.34	0.34	9.67	9.64	9.72	9.75	9.53	79.20	72.21	0.911742
Iq-Droop	0.38	0.38	0.38	0.38	10.93	10.81	10.98	11.10	10.25	79.20	82.01	1.03548
Q-Droop	0.38	0.38	0.38	0.38	10.77	10.71	10.82	10.88	10.46	79.20	78.78	0.994697
Const. Q	0.37	0.36	0.37	0.38	10.63	10.53	10.82	10.97	10.04	79.20	80.43	1.01553
0.95 p.u.												
Const. V	0.38	0.38	0.38	0.38	10.91	10.87	10.92	10.96	10.65	83.60	80.41	0.961842
cos_phi	0.35	0.35	0.35	0.35	10.17	10.14	10.22	10.25	10.03	83.60	76.05	0.909689
Iq-Droop	0.38	0.38	0.38	0.38	11.01	10.91	11.04	11.15	10.40	83.60	83.39	0.997488
Q-Droop	0.38	0.38	0.38	0.38	10.88	10.84	10.90	10.95	10.63	83.60	80.25	0.959928
Const. Q	0.38	0.38	0.39	0.39	11.11	11.01	11.30	11.43	10.55	83.60	84.46	1.010287
1.00 p.u.												
Const. V	0.38	0.38	0.38	0.38	11.07	10.98	11.10	11.21	10.54	88.00	84.64	0.961818
cos_phi	0.40	0.40	0.41	0.41	11.59	11.49	11.77	11.90	11.04	88.00	88.44	1.005
Iq-Droop	0.38	0.38	0.38	0.38	11.08	10.99	11.12	11.23	10.55	88.00	84.73	0.962841
Q-Droop	0.38	0.38	0.38	0.38	10.95	10.92	10.97	11.00	10.77	88.00	81.51	0.92625
Const. Q	0.40	0.40	0.41	0.41	11.59	11.49	11.77	11.90	11.04	88.00	88.44	1.005
1.05 p.u.												
Const. V	0.38	0.38	0.38	0.38	11.02	11.00	11.02	11.04	10.91	92.40	82.79	0.895996
cos_phi	0.39	0.39	0.39	0.39	11.17	11.15	11.22	11.25	11.05	92.40	83.73	0.906169
Iq-Droop	0.38	0.38	0.39	0.39	11.18	11.10	11.28	11.38	10.73	92.40	86.39	0.934957
Q-Droop	0.38	0.38	0.38	0.38	11.02	11.00	11.03	11.05	10.91	92.40	82.75	0.895563
Const. Q	0.42	0.41	0.42	0.43	12.07	11.97	12.24	12.37	11.54	92.40	92.10	1
1.10 p.u.												
Const. V	0.38	0.38	0.38	0.38	11.07	11.06	11.07	11.08	11.03	96.80	83.85	0.866219
cos_phi	0.40	0.40	0.40	0.41	11.68	11.66	11.72	11.75	11.56	96.80	87.60	0.904959
Iq-Droop	0.39	0.39	0.40	0.40	11.50	11.43	11.61	11.71	11.10	96.80	89.38	0.923347
Q-Droop	0.38	0.38	0.38	0.38	11.09	11.08	11.09	11.10	11.05	96.80	83.97	0.867459
Const. Q	0.43	0.43	0.44	0.44	12.54	12.45	12.71	12.83	12.03	96.80	96.34	0.995248

Table A3: Bus voltages for steady state load flow analysis at wind speed =12 m/s

	LV BB1	LV BB2	LV BB3	LV BB4	MV BB1	MV BB2	MV BB3	MV BB4	Sub BB 11kV	U_{POC} BB	HV BB	HV Match
0.90 p.u.												
Const. V	0.38	0.38	0.38	0.38	10.91	10.81	10.94	11.03	10.35	79.20	82.54	1.042172
cos_phi	0.36	0.35	0.36	0.36	10.29	10.21	10.43	10.54	9.85	79.20	78.83	0.995328
Iq-Droop	0.38	0.38	0.38	0.38	10.89	10.80	10.93	11.03	10.33	79.20	82.45	1.041035
Q-Droop	0.38	0.38	0.38	0.38	10.89	10.80	10.93	11.03	10.33	79.20	82.45	1.041035
Const. Q	0.36	0.35	0.36	0.36	10.29	10.21	10.43	10.54	9.85	79.20	78.83	0.995328
0.95 p.u.												
Const. V	0.38	0.38	0.38	0.38	10.98	10.89	10.99	11.07	10.48	83.60	83.82	1.002632
cos_phi	0.37	0.37	0.38	0.38	10.76	10.68	10.90	11.00	10.34	83.60	82.75	0.989833
Iq-Droop	0.38	0.38	0.38	0.38	10.96	10.88	10.99	11.08	10.47	83.60	83.76	1.001914
Q-Droop	0.38	0.38	0.38	0.38	10.96	10.88	10.99	11.08	10.47	83.60	83.77	1.002033
Const. Q	0.37	0.37	0.38	0.38	10.76	10.68	10.90	11.00	10.34	83.60	82.75	0.989833
1.00 p.u.												
Const. V	0.38	0.38	0.38	0.38	11.03	10.96	11.04	11.11	10.61	88.00	85.01	0.966023
cos_phi	0.39	0.39	0.39	0.40	11.23	11.16	11.37	11.47	10.83	88.00	86.67	0.984886
Iq-Droop	0.38	0.38	0.38	0.38	11.03	10.96	11.05	11.12	10.61	88.00	85.05	0.966477
Q-Droop	0.38	0.38	0.38	0.38	11.03	10.96	11.05	11.12	10.61	88.00	85.05	0.966477
Const. Q	0.39	0.39	0.39	0.40	11.23	11.16	11.37	11.47	10.61	88.00	86.67	0.984886
1.05 p.u.												
Const. V	0.38	0.38	0.38	0.38	11.08	11.02	11.08	11.14	10.73	92.40	86.20	0.9329
cos_phi	0.40	0.40	0.41	0.41	11.71	11.64	11.84	11.94	11.32	92.40	90.58	0.980303
Iq-Droop	0.38	0.38	0.38	0.38	11.09	11.03	11.11	11.17	10.73	92.40	86.34	0.934416
Q-Droop	0.38	0.38	0.38	0.38	11.09	11.03	11.11	11.17	10.75	92.40	86.33	0.934307
Const. Q	0.40	0.40	0.41	0.41	11.71	11.64	11.84	11.94	11.32	92.40	90.58	0.980303
1.10 p.u.												
Const. V	0.38	0.38	0.38	0.38	11.13	11.08	11.14	11.20	11.86	96.80	87.44	0.903306
cos_phi	0.42	0.42	0.43	0.43	12.18	12.12	12.31	12.40	11.81	96.80	94.50	0.97624
Iq-Droop	0.38	0.38	0.38	0.38	11.16	11.11	11.18	11.24	10.89	96.80	87.67	0.905682
Q-Droop	0.38	0.38	0.38	0.38	11.16	11.11	11.18	11.24	10.89	96.80	87.66	0.905579
Const. Q	0.42	0.42	0.43	0.43	12.18	12.12	12.31	12.40	11.81	96.80	94.50	0.97624

Table A4: Bus voltages for steady state load flow analysis at wind speed =7.0 m/s

	LV BB1	LV BB2	LV BB3	LV BB4	MV BB1	MV BB2	MV BB3	MV BB4	Sub BB 11kV	U_{POC} BB	HV BB	HV Match
0.90 p.u.												
Const. V	0.37	0.37	0.37	0.38	10.56	10.50	10.67	10.75	10.25	79.20	81.37	1.027399
cos_phi	0.33	0.32	0.33	0.33	9.42	9.40	9.47	9.51	9.28	79.20	74.23	0.937247
Iq-Droop	0.37	0.37	0.37	0.38	10.56	10.50	10.67	10.75	10.25	79.20	81.37	1.027399
Q-Droop	0.37	0.37	0.37	0.38	10.56	10.50	10.67	10.75	9.28	79.20	74.23	0.937247
Const. Q	0.33	0.32	0.33	0.33	9.42	9.40	9.47	9.51	10.04	79.20	80.43	1.01553
0.95 p.u.												
Const. V	0.38	0.38	0.38	0.38	10.86	10.80	10.88	10.93	10.55	83.60	83.95	1.004187
cos_phi	0.34	0.34	0.34	0.35	9.91	9.88	9.96	9.99	9.77	83.60	78.18	0.935167
Iq-Droop	0.38	0.38	0.38	0.38	10.82	10.77	10.85	10.91	10.53	83.60	83.76	1.001914
Q-Droop	0.38	0.38	0.38	0.38	10.83	10.77	10.85	10.91	10.53	83.60	83.77	1.002033
Const. Q	0.34	0.34	0.34	0.35	9.91	9.88	9.96	9.99	9.77	83.60	78.18	0.935167
1.00 p.u.												
Const. V	0.38	0.38	0.38	0.38	10.93	10.89	10.94	10.98	10.70	88.00	85.34	0.969773
cos_phi	0.36	0.36	0.36	0.36	10.40	10.37	10.44	10.48	10.27	88.00	82.14	0.933409
Iq-Droop	0.38	0.38	0.38	0.38	10.91	10.87	10.92	10.96	10.68	88.00	85.22	0.968409
Q-Droop	0.38	0.38	0.38	0.38	10.91	10.87	10.93	10.96	10.68	88.00	85.22	0.968409
Const. Q	0.36	0.36	0.36	0.36	10.40	10.37	10.44	10.48	10.27	88.00	82.14	0.933409
1.05 p.u.												
Const. V	0.38	0.38	0.38	0.38	10.99	10.96	10.99	11.02	10.83	92.40	86.63	0.937554
cos_phi	0.38	0.38	0.38	0.38	10.89	10.87	10.93	10.96	10.76	92.40	86.11	0.931926
Iq-Droop	0.38	0.38	0.38	0.38	10.98	10.96	10.99	11.02	10.83	92.40	86.60	0.937229
Q-Droop	0.38	0.38	0.38	0.38	10.98	10.96	10.99	11.02	10.83	92.40	86.60	0.937229
Const. Q	0.38	0.38	0.38	0.38	10.89	10.87	10.93	10.96	10.76	92.40	86.11	0.931926
1.10 p.u.												
Const. V	0.38	0.38	0.38	0.38	11.04	11.03	11.04	11.06	10.96	96.80	87.89	0.907955
cos_phi	0.39	0.39	0.39	0.40	11.38	11.36	11.42	11.45	11.26	96.80	90.09	0.930682
Iq-Droop	0.38	0.38	0.38	0.38	11.05	11.04	11.06	11.07	10.97	96.80	87.97	0.908781
Q-Droop	0.38	0.38	0.38	0.38	11.05	11.04	11.06	11.07	10.97	96.80	87.96	0.908678
Const. Q	0.39	0.39	0.39	0.40	11.38	11.36	11.42	11.45	11.26	96.80	90.09	0.930682

Table A5: Bus voltages for steady state load flow analysis at wind speed = 4.5 m/s

	LV BB1	LV BB2	LV BB3	LV BB4	MV BB1	MV BB2	MV BB3	MV BB4	Sub BB 11kV	U_{POC} BB	HV BB	HV Match
0.90 p.u.												
Const. V	0.33	0.33	0.33	0.33	9.44	9.42	9.48	9.50	9.34	79.20	74.55	0.941288
cos_phi	0.31	0.31	0.31	0.31	9.08	9.07	9.10	9.11	9.04	79.20	72.30	0.912879
Iq-Droop	0.33	0.33	0.33	0.33	9.44	9.42	9.48	9.50	9.34	79.20	74.55	0.941288
Q-Droop	0.33	0.33	0.33	0.33	9.44	9.42	9.48	9.50	9.34	79.20	74.55	0.941288
Const. Q	0.31	0.31	0.31	0.31	9.08	9.07	9.10	9.11	9.04	79.20	72.30	0.912879
0.95 p.u.												
Const. V	0.34	0.34	0.35	0.35	9.93	9.91	9.96	9.99	9.83	83.60	78.50	0.938995
cos_phi	0.33	0.33	0.33	0.33	9.58	9.57	9.60	9.61	9.54	83.60	76.32	0.912919
Iq-Droop	0.34	0.34	0.35	0.35	9.93	9.91	9.96	9.99	9.83	83.60	78.50	0.938995
Q-Droop	0.34	0.34	0.35	0.35	9.93	9.91	9.96	9.99	9.83	83.60	78.50	0.938995
Const. Q	0.33	0.33	0.33	0.33	9.58	9.57	9.60	9.61	9.54	83.60	76.32	0.912919
1.00 p.u.												
Const. V	0.36	0.36	0.36	0.36	10.44	10.42	10.47	10.49	10.34	88.00	82.55	0.938068
cos_phi	0.35	0.35	0.35	0.35	10.08	10.08	10.10	10.11	10.04	88.00	80.35	0.913068
Iq-Droop	0.36	0.36	0.36	0.36	10.44	10.42	10.47	10.49	10.34	88.00	82.55	0.938068
Q-Droop	0.36	0.36	0.36	0.36	10.44	10.42	10.47	10.49	10.34	88.00	82.55	0.938068
Const. Q	0.35	0.35	0.35	0.35	10.08	10.08	10.10	10.11	10.04	88.00	80.35	0.913068
1.05 p.u.												
Const. V	0.38	0.38	0.38	0.38	10.91	10.90	10.94	10.96	10.82	92.40	86.43	0.93539
cos_phi	0.37	0.37	0.37	0.37	10.59	10.58	10.60	10.61	10.55	92.40	84.39	0.913312
Iq-Droop	0.38	0.38	0.38	0.38	10.91	10.89	10.93	10.95	10.82	92.40	86.39	0.934957
Q-Droop	0.38	0.38	0.38	0.38	10.91	10.89	10.94	10.96	10.82	92.40	86.39	0.934957
Const. Q	0.37	0.37	0.37	0.37	10.59	10.58	10.60	10.61	10.55	92.40	84.39	0.913312
1.10 p.u.												
Const. V	0.38	0.38	0.38	0.38	11.01	11.01	11.01	11.02	10.98	96.80	87.91	0.908161
cos_phi	0.38	0.38	0.38	0.38	11.09	11.08	11.10	11.11	11,05	96.80	88.44	0.913636
Iq-Droop	0.38	0.38	0.38	0.38	11.01	11.01	11.01	11.02	10.99	96.80	87.93	0.908368
Q-Droop	0.38	0.38	0.38	0.38	11.01	11.01	11.01	11.02	10.99	96.80	87.93	0.908368
Const. Q	0.38	0.38	0.38	0.38	11.09	11.08	11.10	11.11	11.05	96.80	88.44	0.913636